A Three-Dimensional Mathematical Model of Directional Drilling

A DISSERTATION

SUBMITTED TO THE FACULTY OF THE GRADUATE SCHOOL

OF THE UNIVERSITY OF MINNESOTA

BY

Luc Perneder

IN PARTIAL FULFILLMENT OF THE REQUIREMENTS

FOR THE DEGREE OF

Doctor of Philosophy

ADVISER

Emmanuel Detournay

January, 2013

© Luc Perneder 2013
ALL RIGHTS RESERVED

Acknowledgements

Life is dictated by the people we encounter along the journey. I find myself incredibly lucky with the persons I had the opportunity to meet and interact with during these past five years spent in Minnesota and Perth.

The main contributor to those successful years is of course Emmanuel, whose guidance as an adviser but also as a paternal figure went way beyond what a student can expect from an adviser. He often jokingly said: "I received you as a young teenager, but let you go as a young man". In a way, I have to agree with that, although I am not entirely sure of the second part of the statement.

This experience would have been entirely different without the support and in particular the patience of Catalina. She is the dulce de leche of everyday life.

An especially affectionate thought goes to my parents, who were alongside this adventure despite the distance.

Being away from home and from my own roots also showed how friendship can take another dimension. I am particularly thankful to Vincent and Catherine, Alex and Julien (who has an incredible eye for typos), Amir, Thomas, Yevhen, Meghan, Jorge, Arvind and Jessica, Vassilis and Alissa, and so many others.

I am finally grateful to CSIRO Australia for granting me three fellowships in drilling mechanics to work in the laboratory of the Australian Resources Research Centre and for covering the travel and living expenses.

à Gros Papa

ABSTRACT

The dynamical model governing the 3D kinematics of a drill bit is constructed for rotary drilling applications for which the bit is guided by a push-the-bit rotary steerable system. The evolution of the bit trajectory, and thus of the borehole geometry, is a consequence of the interaction between the borehole, a geometric object, and the drilling structure, a mechanical object. In this respect, the model describing this evolution consists of the association between (i) a model of the near-bit region of the drillstring, (ii) a model of the bit/rock interaction, and (iii) kinematic relationships relating the motion of the bit into the rock to geometric variables for the borehole evolution. The mathematical formulation of these three elements yields a set of functional differential equations with secular terms accounting for a delayed influence of the borehole geometry on the bit trajectory. The parameters entering these relations account for the loads and properties of the drilling structure and for the properties of the bit and rock formation.

Three length scales are identified in the response of the directional drilling system; they correspond to short-, intermediate-, and long-range behaviors. The short-range response is associated with the dimensions of the bit, the small scale of the problem. It corresponds to fast variations of the bit orientation. On the intermediate-range, the wellbore trajectory converges to a quasi-constant curvature solution, if it is stable. On the long-range, the borehole curvature slowly varies and for appropriate set of drilling parameters the borehole converges toward a stationary helical path. Finally, the stability and rate of convergence on the intermediate and long range are investigated.

Contents

List of Tables

List of Figures

Nomenclature

Latin

a	Bit radius
b	Bit half height
$\mathcal{B}$	Borehole axis
$\hat{\boldsymbol{C}}$	Averaged torque on bit
$\mathcal{C}_1, \mathcal{C}_2, \ldots, \mathcal{C}_n$	Chords associated with each segment of BHA
$\boldsymbol{d}$	Penetration vector
d_1	Axial penetration
d_2, d_3	Lateral penetrations
$\mathcal{D}$	BHA axis
$(\boldsymbol{e}_x, \boldsymbol{e}_y, \boldsymbol{e}_z)$	Fixed basis
$\mathcal{E}$	Cutting edge
$\boldsymbol{f}$	Distributed force along the equivalent blade
$\hat{\boldsymbol{F}}$	Averaged force on bit
$\breve{\boldsymbol{F}}$	RSS force
$\mathcal{F}$, $\mathcal{M}$	Influence coefficients for the BHA
G_1	Saturated contact forces transmitted at the cutters wearflats
H_0, H_1, H_2, H_3	Coefficients of bit/rock interaction
$(\boldsymbol{i}_1, \boldsymbol{i}_2, \boldsymbol{i}_3)$	Local BHA basis
$(\hat{\boldsymbol{i}}_1, \hat{\boldsymbol{i}}_2, \hat{\boldsymbol{i}}_3)$	Bit basis
$(\boldsymbol{I}_1, \boldsymbol{I}_2, \boldsymbol{I}_3)$	Local borehole basis

$\boldsymbol{K}$	Curvature vector of the borehole
K_2, K_3	Components of $\boldsymbol{K}$ along $\boldsymbol{I}_2$ and $\boldsymbol{I}_3$
L	Borehole length
$\hat{\boldsymbol{M}}$	Averaged moment on bit
p	Local depth of cut of the equivalent blade
$\boldsymbol{q}$	Position vector of a point of the bit cutting profile
$\boldsymbol{r}(s;L)$	Vectorial function describing the BHA axis
$\boldsymbol{R}(S)$	Vectorial function describing the borehole axis
(r,ω,z)	Cylindrical coordinates of the bit
s	BHA curvilinear coordinate
S	Borehole curvilinear coordinate
$\mathcal{S}$	Bit cutting profile
$\boldsymbol{v}$	Velocity vector of the bit
w	Distributed weight of the BHA

Greek

β_2, β_3	Penetration angles
$\boldsymbol{\Gamma}$	Dimensionless RSS force
δ	Delta operator
ε	Intrinsic specific energy of drilling
ζ, ζ', ζ''	Single cutter interaction coefficients
η	Lateral steering resistance
θ	Inclination of the BHA tangent vector $\boldsymbol{i}_1$
$\hat{\theta}$, $\hat{\phi}$	Bit inclination and azimuth
Θ	Inclination of the borehole tangent vector $\boldsymbol{I}_1$
$\hat{\Theta}$, $\hat{\Phi}$	Borehole inclination and azimuth at the bit
$\langle\Theta\rangle_1, \langle\Theta\rangle_2, \ldots, \langle\Theta\rangle_n$	Inclinations of the chords $\mathcal{C}_1, \mathcal{C}_2, \ldots, \mathcal{C}_n$
$\boldsymbol{\kappa}$	Dimensionless curvature vector of the borehole
κ_2, κ_3	Components of $\boldsymbol{\kappa}$ along $\boldsymbol{I}_2$ and $\boldsymbol{I}_3$
$\varkappa_1, \varkappa_2, \ldots, \varkappa_n$	Dimensionless lengths of the segments of BHA

λ	Wearflat length distribution along the equivalent blade
$\lambda_1, \lambda_2, \ldots, \lambda_n$	Lengths of the segments of BHA
Λ	Position of the RSS
μ	Coefficient of friction at the wearflat
ν	Bit slenderness
ξ	Dimensionless length of the borehole
$\xi_1, \xi_2, \ldots, \xi_n$	Positions of the stabilizers along the borehole axis
ϖ	Walk angle
Π	Dimensionless active weight on bit
σ	Maximum contact pressure at the interface wearflat/rock
τ	Orientation of the RSS force
Υ	Dimensionless distributed weight of the BHA
ϕ	Azimuth of the BHA tangent vector $\boldsymbol{i}_1$
$\boldsymbol{\varphi}$	Angular penetration vector
φ_2, φ_3	Angular penetrations
Φ	Azimuth of the borehole tangent vector $\boldsymbol{I}_1$
$\langle\Phi\rangle_1, \langle\Phi\rangle_2, \ldots, \langle\Phi\rangle_n$	Azimuths of the chords $\mathcal{C}_1, \mathcal{C}_2, \ldots, \mathcal{C}_n$
χ	Angular steering resistance
ψ_2, ψ_3	Bit tilt angles
$\boldsymbol{\omega}$	Spin vector of the bit
$\boldsymbol{\Omega}$	Angular velocity vector of the bit

Chapter 1

Introduction

1.1 Background

Drilling deep boreholes weaving along complex trajectories has been made possible by the development of directional drilling techniques. The oil and gas industry takes advantage of this ability to direct the well path in order to drill multiple wells from the same rig, avoid hard-to-drill rock formations such as salt domes, drill beneath obstacles, or improve the drainage by maximizing the intersection of the well with the reservoir (Inglis, 1987). Directional drilling is also vital when rescuing an out-of-control well. For example, in 2010, BP drilled two relief wells with the objective of sealing the Macondo well responsible for the massive oil spill in the Gulf of Mexico after the explosion of the Deepwater Horizon platform. Drillers had to control, from floating platforms, the trajectories of the relief wells so as to intersect a 30 cm wide target 5500 m under the sea level. Directional drilling is also used in the geothermal and mining industry or for the recovery of shale gas.

Figure 1.1a sketches a modern rotary drilling system. The *drillstring* is a hollow slender tube that can be typically several kilometers in length. It is suspended at the rig where the rotary speed and the axial force (the *hookload*) are imposed. The lower part of the drillstring is the *bottomhole assembly* (BHA), which is generally a couple hundred meters long. It consists of heavy pipes, called drill collars, and short elements of a larger diameter, called *stabilizers*,

that center the BHA in the borehole (Fig. 1.2a). The BHA is usually equipped with 3 to 5 stabilizers. While the main part of the drillstring is in tension due to its own weight, the BHA is in compression in order to induce a sufficient *weight on bit*, the axial force transmitted to the drill bit. The main families of bit are the roller-cone bits and the fixed cutter bits, also called PDC (polycrystalline diamond compact) bits (Figs. 1.2b and 1.2c). For directional applications, PDC bits are usually favored, with their diameters ranging from about 6 in (15.2 cm) to 17 in (43.2 cm). At the rig, drilling mud is injected in the drillstring. It then flows out at the bit and back to the surface through the annular space between the string and the borehole.

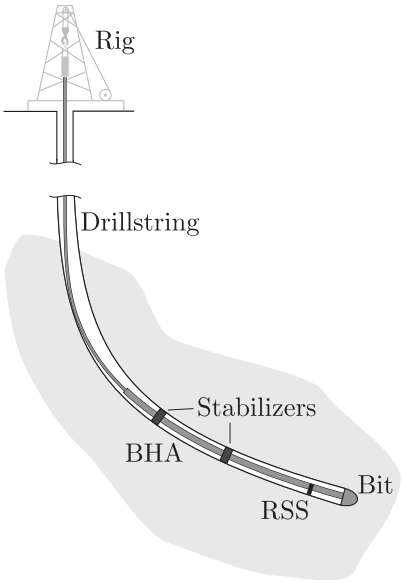

(a)

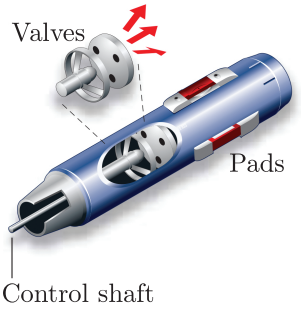

(b) Push-the-bit RSS (Kashikar, 2005).

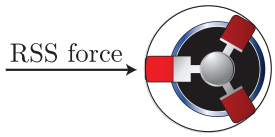

(c) Cross section of a RSS (Kashikar, 2005).

Figure 1.1: Sketch of a typical directional drilling apparatus equipped with a push-the-bit RSS.

Rotary steerable systems (RSS) are semi-automated tools that allow to steer the borehole while the drillstring is rotating (Figs. 1.1b and 1.1c). They work in association with sensors and a downhole control unit, and are actuated by the mud flowing through a system of valves (Kashikar, 2005). This work is restricted to the family of tools called *push-the-bit RSS*. They are placed between the bit and the first stabilizer and use a set of extensible pads to induce a lateral force on the side of the borehole.

The directional drilling operations aim at efficiently tracking a predefined well path, but also at limiting the tortuosity of the borehole, that is, reducing the borehole oscillations about the intended path. An excessively tortuous well complicates the drilling operations and compromises the proper completion of the well.

Studying the dynamical system of a propagating borehole is motivated by issues such as selecting a drill bit or designing the BHA. In particular, the stabilizers need to be carefully positioned on the BHA since they strongly affect the behavior of the system. The development of a mathematical formulation of the directional drilling model can also benefit the design of a controller for the RSS. Finally, drilling data collected from the surface and from down-the-hole sensors can be analyzed via a model of directional drilling to monitor the drilling operation, e.g., evaluate the wear of the bit or the properties of the rock formation.

(a) Stabilizer (Barton et al., 2007).

(b) Roller-cone bit (www.Halliburton.com).

(c) PDC bit (www.northbasinenergy.com).

Figure 1.2: Stabilizer and drill bits.

1.2 Directional Drilling Model

The directional drilling process results from the interaction between the BHA and the borehole. The evolution of the borehole geometry is a consequence of the bit kinematics. Meanwhile, the penetration of the bit into the rock formation depends on the forces transmitted by the BHA to the bit, which themselves are related to the behavior of the BHA constrained to deform within the borehole. In this respect, the model is built around three elements (Fig. 1.3) (Detournay,

2007, 2010).

- The kinematic relationships make the link between the kinematics of the bit and the evolution of the borehole, that is, the propagation of the lower boundary of the borehole defined as the surface of interaction between the bit and the rock.
- The bit/rock interface laws relate the kinematics of the bit as it penetrates the rock formation to the interaction forces at the bit/rock interface.
- The BHA is an elastic object constrained by the stabilizers to conform with the geometry of the borehole. Its lower boundary condition is controlled by the bit/rock interaction. The model of the BHA can thus be solved to provide relations between the bit forces and orientation, the geometry of the borehole, and the external loads on the BHA.

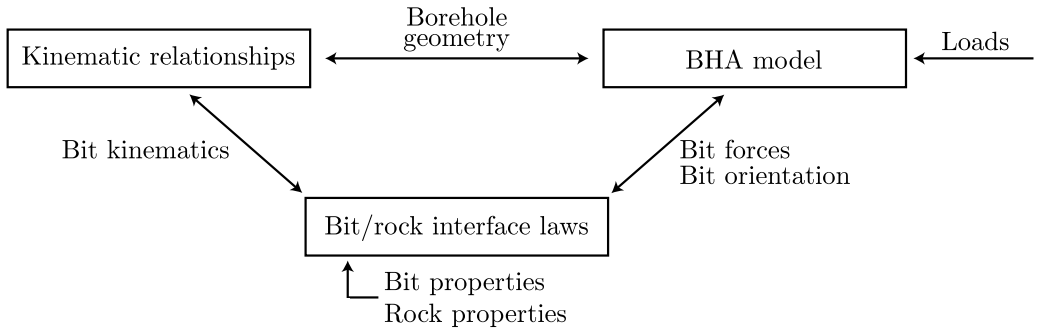

Figure 1.3: Three elements of the model.

The borehole is a slender geometric object with a moving boundary at the interface between the bit and the rock. At the scale of the borehole length, of order $O\left(10^3\,\mathrm{m}\right)$, it is viewed as a lengthening spatial curve. At this scale, the bit is collapsed to a representative point whose trajectory defines the axis of the borehole. A second length scale, of order $O\left(10^{-1}\,\mathrm{m}\right)$, is associated with the dimensions of the bit or equivalently with the dimensions of the borehole cross section. At this scale the bit is regarded as a three-dimensional object interacting with the rock formation.

The directional drilling model is constructed at the scale associated with the model of the BHA and of order $O\left(10\,\mathrm{m}\right)$. At this intermediate scale, the bit/rock interaction is embodied by

interface laws acting at a reference point of the bit. This also means that the spatial resolution of the model will be of the order of the dimensions of the bit, $O\left(10^{-1}\,\mathrm{m}\right)$.

The following hypotheses are made when formulating the model.

Hypothesis 1

The drilling process can be averaged over several revolutions of the drilling structure. This assumption is justified by the time scale associated with directional drilling being larger than the period of revolution of the drilling structure. As a matter of fact, the bit penetration per revolution, which is the incremental increase of borehole length, is generally of the order of $O\left(1\,\mathrm{mm/rev}\right)$, while the model resolution is of order $O\left(10^{-1}\,\mathrm{m}\right)$. Hence, it is reasonable to average the process over at least 100 revolutions.

This assumption also implies that dynamical processes generally occurring on a time scale of the order of the bit revolution can be disregarded in the sense that either they do not affect the drilling direction or they can be lumped into the parameters of the model. This is for example the case for the vibrations of the BHA and the bit.

Hypothesis 2

The process is rate-independent for the typical range of bit rotations per minute (RPM), of the order of $O(10 \sim 100\,\mathrm{rev/min})$. In other words, the drilling direction does not depend on the drilling rate. For the BHA, this hypothesis is justified to a limited extend by the averaging assumption (Hypothesis 1); it implies that the model of the BHA is a (quasi-)static model. This hypothesis also stems from the nature of the bit/rock interaction: the dominant variables that affect the interface laws measure the amount of rock removed by the bit over one revolution, while the rate of removal has a negligible effect.

An important consequence of this assumption is that time is not the appropriate variable to track the evolution of the system and that it should be substituted by the length of the borehole.

Hypothesis 3

In the context of directional drilling, it is sufficient to study the BHA with the rest of the drillstring lumped into contact forces at the upper boundary of the BHA. The lateral forces and moments transmitted to the bit are responsible for the directional tendency of the system. This simplification is based on the observation that these forces are predominantly influenced by the first few segments of BHA delimited by the successive contact points with the borehole. (For most practical purposes, taking into account the 3 or 4 stabilizers closest to the bit is sufficiently accurate). The rest of the drillstring, running from the upper boundary of the BHA model to the rig, impacts the transmission of axial force and torque to the bit, but does not significantly influence the lateral forces and moments on the bit.

The angular position of the drilling structure, and thus of the bit, is unimportant as the process is averaged over several revolutions. Hence, four variables function of the borehole length are sufficient to track the motion of the bit along its trajectory. They are chosen to be the inclination and azimuth of the bit drilling direction, and two tilt angles that measure the relative orientation of the bit with respect to the borehole.

The knowledge of the past history and current values of these four variables is sufficient to uniquely define the state of the system, that is, to define the geometry of the borehole and the deformed configuration of the BHA. The inclination and azimuth of the bit drilling direction describe the trajectory of the reference point of the bit, which also defines the axis of the borehole. If the bit is tilted on the borehole axis, it drills a borehole slightly overgauged with respect to the bit diameter. Hence, the borehole cross-sectional area is in principle related to the tilt angles. For the BHA, the knowledge of the geometry of the borehole and of the bit tilt is sufficient to uniquely solve for the deformed configuration of the BHA within the borehole.

1.3 Scope and Organization

Prior to any theoretical development, Chapter 2 gives a historical account and examines the specialized literature on directional drilling.

The model is then constructed for a BHA equipped with a push-the-bit RSS and a PDC bit drilling in a homogeneous isotropic rock formation. The mathematical formulation is conducted in two steps. First, Chapter 3 studies the three elements of the model independently and derives mathematical expressions for the kinematic relationships, the bit/rock interaction, and the model of the BHA. Chapter 4 scales and combines these results in order to derive the evolution equations for the bit trajectory and for the borehole geometry. These equations, written in terms of the borehole length, are functional differential equations. The secular nature of these equations is a consequence of the delayed influence of the borehole geometry on the bit drilling direction. That chapter concludes with a set of simulations that are used to motivate the subsequent analysis.

The qualitative behavior of the response is investigated in Chapter 5. A short-range response is observed and corresponds to a fast variation in the bit orientation. It is associated with a small parameter that singularly perturbs the evolution equations. On an intermediate-range, the borehole generally converges toward solutions corresponding to boreholes with quasi-constant curvatures. Finally, on a long-range, stationary solutions can be observed; they are helical boreholes with a constant inclination with respect to gravity.

Chapter 6 studies the asymptotic behaviors of the system and gives a stability analysis of the response on the intermediate and long range. Finally, Chapter 7 provides examples that illustrates some particular behaviors of the system.

Chapter 2

State of the Art

2.1 History

Two dominant techniques were used across history when drilling for natural resources: percussion drilling and rotary drilling. The first consists in periodically hitting the bottom of the borehole with a drilling tool. In China, brine wells were drilled as far back as 1000 BC using this technique (Kopey, 2007); some of these early wells are believed to have also produced asphalt, oil, and gas (Moor, 1977). Around 1200 AD, the world record depth for a percussive well was already set in China to about 450 m (Brantly, 1971). Although used nowadays to drill shallow wells, percussive drilling gradually disappeared from the oil and gas industry at the beginning of the 20^{th} century, replaced by rotary drilling.

The idea of using a rotating tool to drill a borehole had already been proposed by Leonardo da Vinci (Moon, 2007)[1]. The first well used for the sole purpose of recovering oil is believed to have been drilled in 1745 in northern France using tools similar to da Vinci's prototype (Moor, 1977). But it is only at the middle of the 19^{th} century that rotary drilling became increasingly popular in the oil industry.

At the beginning of the 20^{th} century, it was discovered that some rotary boreholes that were expected to be vertical were actually "crooked". Although the deviation of a borehole

[1] A sketch is found in the Codex Atlanticus, reference number f. 34 r.

from verticality was first seen as a complication (Muller, 1924; Lahee, 1929), engineers quickly understood that controlling the well deviation can actually be an asset (Hughes, 1935; Eastman, 1937; Close, 1939; Weaver, 1946). This motivated the invention of early directional survey tools, which measured the inclination and sometimes the azimuth at a given location of the borehole (Brantly, 1971). Taking these measurements was time consuming and was often done after the borehole had reached its desired length; nevertheless it enlightened the industry as to the problem of deviated wells. The decisive development that triggered the beginning of directional drilling was the use in the 1910s and 20s of efficient gyroscopic and magnetic survey tools able to quickly measure the inclination and azimuth at multiple locations along the borehole (Muller, 1924; Lahee, 1929; Eastman, 1937).

As early as 1895, whipstock tools were used to side-track a broken tool left at the bottom of the hole (Brantly, 1971). They are metallic wedges lowered in the hole that deflect the trajectory of the bit. But it was only with the development of surveying tools that whipstocks were used as a mean to deliberately control the well path. In 1932, although told by engineers that it was not possible, H. John Eastman deliberately drilled deviated wells using whipstocks and cutting-edge surveying tools (Close, 1939)[2]. In 1934, Eastman's greatest feat was to drill as close as 2 meters away from an out-of-control well more than a kilometer and a half underground in order to kill it by injecting pressurized water in the reservoir. Other early deviation techniques are the knuckle joint tools, which are devices with a universal joint, or jetting, which uses a spudding drill bit that washes out the rock formation in the desired drilling direction (Hughes, 1935; Weaver, 1946). Rotary steerable systems are the last generation of tools and made their appearance in the 90s (Downton et al., 2000).

The buckling of drillpipes was believed to be a major cause of borehole deviation; it was presumed to change the orientation of the bit and thus its drilling direction (Muller, 1924; Capelushnikov, 1930). On this ground, stabilizers where introduced as a mean to reduce the tendency of the drillstring to buckle (MacDonald and Lubinski, 1951). It was also understood that careful placement of the stabilizers along the BHA could advantageously influence the directional drilling tendency in inclined boreholes (Lubinski and Woods, 1953; Woods and Lubinski,

[2] Close (1939) also states that, thanks to the new possibilities brought by directional drilling, "American oil geologists, according to whose past estimates we ran out of oil in 1924, in 1928, and again in 1932, will once more have to revise their predictions."

1955). Stabilizers are now systematically used in directional drilling.

In the 70s, measurement while drilling (MWD) techniques have been developed. They enable to communicate with down-the-hole tools or convey measurements to the surface during the drilling operations. Today, MWD systems generally use mud pulse telemetry, which sends pressure waves up and down the mud column. This system is inefficient as it transmits information at a rate of the order of 10 bits per second.

The current world record depth of $12,262\,\mathrm{m}$ achieved by a borehole was set in Russia in 1989 for scientific purposes (Kozlovsky, 1984; Brochure, 2012). But, the longest well ever drilled is an extended reach well with a length of $12,345\,\mathrm{m}$ and a record horizontal reach of $11,475\,\mathrm{m}$ (ExxonMobil, 2011).

2.2 Literature Review

The groundbreaking publication of Lubinski and Woods (1953) is maybe the first theoretical work on directional drilling and is certainly the most influential one. This work and other early publications (Murphey and Cheatham, 1966) derived analytical models for the bit/rock interaction and BHA model, but did not provide a general formulation of the system kinematics. Nevertheless, they gave kinematic relationships for the system propagating along straight and circular trajectories. In the 70s and 80s, most publications on directional drilling focused on modeling the mechanics of the BHA, as it was believed to be the key element affecting the drilling direction. In this respect, the significance of the directional interaction of the bit with the rock formation has been overshadowed until the mid-80s. The contribution of Cheatham and Ho (1981) is maybe the first (unpublished) theoretical work on this subject and the work of Ho (1987, 1989, 1995, 1997) is definitely the most influential one. Almost systematically, the problem of predicting the directional borehole evolution is tackled numerically. Only few publications derive the equations governing the evolution of the directional drilling system for some particular cases: the contributions of Neubert and Heisig (1996) and Neubert (1997), which did not really reach the community, Downton (2007), Detournay and Perneder (2011), and Perneder and Detournay (2013b).

The remaining of this section details the major contributions toward modeling the bit/rock

interaction, the BHA, and the whole directional drilling problem regrouping the different elements.

2.2.1 Bit/Rock Interaction

The directional behavior of a bit penetrating the rock was first attributed to the anisotropy and inhomogeneity of the rock formation. The first publications by Lubinski and Woods (1953) and by Murphey and Cheatham (1966) considered that in an isotropic and homogeneous rock, the bit drills in the direction of the force transmitted by the BHA, with deviation from coaxiality caused by the rock anisotropy or by a change in rock properties. Later, this assumption of coaxiality for isotropic rock formations was relaxed and an angle between the bit drilling direction and the bit force was allowed since the bit ability to drill along its axis of revolution is greater than its side cutting ability (Bradley, 1975; Millheim and Warren, 1978; Callas, 1981). The concept of bit/rock interface laws within the context of directional drilling appears to have been first introduced by Cheatham and Ho (1981). They provide linear relations between the components of the bit force and drilling rate vector, in which explicit distinction is made between the separate contributions of the rock anisotropy and the "bit anisotropy", the factor that contrasts the bit axial and lateral drilling abilities. This model was later refined by Ho (1987, 1989, 1995, 1997), who proposed a general linear bit/rock interaction model that also accounts for moments acting on the bit and for a turning rate vector of the bit.

The nature of the interface laws is still a matter of debate, in particular regarding the following two points. First, it is generally assumed that the bit/rock interaction does not induce any moment at the bit. In other words, the forces at the bit/rock interface are reduced to a torque and a force vector only, while the moments orthogonal to the bit axis of revolution are supposed to vanish. Only a handful of contributions contemplate the possibility for such moments (Voinov and Reutov, 1991; Simon, 1996; Neubert, 1997; Maouche, 1999), which are incorporated in the interface laws in rare cases (Chen and Geradin, 1993; Ho, 1995; Neubert, 1997; Menand, 2001; Perneder et al., 2012). Voinov and Reutov (1991) justify the no-moment condition as a consequence of the overgauging of the borehole with respect to the bit diameter, while Simon (1996) considers the possibility of the bit being blocked in rotation.

Second, the nature of the kinematic variables entering the interface laws is not universally accepted. In some instances, they are defined as drilling rates, which have dimensions of a velocity (Cheatham and Ho, 1981; Ho, 1995). In other cases, they are selected to be penetration variables per revolution, with dimensions of a length per revolution (Teale, 1965; Detournay and Defourny, 1992; Menand, 2001; Palmov and Vetyukov, 2002; Detournay et al., 2008; Franca, 2010; Perneder et al., 2012). The latter choice is adopted hereafter and is justified as a consequence of the nature of the interface laws.

Two approaches are followed in the literature when deriving the directional interface laws: numerical and experimental. The numerical approach uses interaction laws for a single cutter of the bit to derive the interface laws for the bit (Chen and Geradin, 1993). Typically, the kinematics of the bit is imposed, from which the depth of cut of each cutter can be computed. The single cutter laws are then used to compute the resultant forces on each cutter, which are finally integrated and averaged over one revolution. Experimental setups usually impose axial and angular velocities to the bit while a constant side force or constant lateral velocity of the bit relative to the rock sample is imposed (Millheim and Warren, 1978; Brown et al., 1981; Clark and Walker, 1985; Pastusek et al., 1992; Norris et al., 1998; Ernst et al., 2007). Also, it seems that the influence of the rate of change of the bit orientation on the bit/rock interaction has never been investigated experimentally.

Additional investigations are concerned with the interaction of a bit with anisotropic or interbedded rock formations (Bradley, 1975; Voinov and Reutov, 1991; Simon, 1996; Boualleg et al., 2006) or with the evolution of the bit wear while drilling (Cheatham and Loeb, 1985; Faÿ, 1993; Waughman et al., 2002; Rashidi et al., 2008).

2.2.2 BHA Model

When studying the directional drilling process, the BHA is generally modeled from the bit to the "point of tangency", which is, the first contact point with the borehole not being located at a stabilizer (at that point, the BHA is tangent to the borehole). The rest of the drillstring is systematically replaced by forces at the upper boundary of the BHA. The computation of these forces requires a model of the complete drillstring, called a torque and drag model (Ho,

1988; Aarrestad and Blikra, 1994; Aadnoy and Andersen, 1998; Menand et al., 2006; Denoël and Detournay, 2011).

The lower boundary reflects the bit/rock interaction; it is almost systematically assumed to be a no moment boundary condition.

In many cases, the drilling direction is supposed to be only related to the lateral force transmitted to the bit; Millheim et al. (1978), Millheim (1979), and Birades and Fenoul (1986, 1988) exclusively concentrate on computing this lateral force. But the current trend usually considers that the relative orientation of the bit with respect to the borehole is also important, which can also be computed from a model of the BHA (Callas and Callas, 1980; Brett et al., 1986; Williamson and Lubinski, 1986; Menand et al., 2012).

Models of the BHA take multiple forms whether they are analytical or numerical, static or dynamic, and allowing for 3D or 2D deformations. The majority of the contributions tackle the problem numerically (generally finite element or finite difference) (Fischer, 1974; Millheim, 1977; Millheim et al., 1978; Callas and Callas, 1980; Amara, 1985; Birades and Fenoul, 1986; Rafie et al., 1986; Birades and Fenoul, 1988; Chen and Wu, 2008), while only a handful of works proposes analytical models of the BHA (Lubinski and Woods, 1953; Murphey and Cheatham, 1966; Bai, 1986; Chandra, 1986; Ho, 1986; Miska et al., 1988; Aadnoy and Huusgaard, 2002). Finally, Birades (1986) suggests that dynamical effects in the BHA model do not have a strong influence on the borehole propagation when averaged over several revolutions.

2.2.3 Borehole Propagation Model

Many numerical solutions without any explicit description of the underlying mathematical model have been proposed (Callas, 1981; Millheim, 1982; Brett et al., 1986; Rafie, 1988; Maouche, 1999; Boualleg et al., 2006; Studer et al., 2007). Typically, the scheme solves at each step the BHA model and the bit/rock interface laws to estimate the direction of propagation of the bit; the borehole is then propagated over an incremental length in this direction. Only a few contributions aim at deriving the equations governing the evolution of the borehole and BHA (Neubert and Heisig, 1996; Downton, 2007; Detournay and Perneder, 2011; Perneder and Detournay, 2013b).

So-called equilibrium solutions corresponding to straight boreholes (Lubinski and Woods, 1953; Bradley, 1975; Perneder and Detournay, 2013a) and circular boreholes in a vertical plane (Murphey and Cheatham, 1966; Fischer, 1974; Birades and Fenoul, 1986; Jogi et al., 1988; Pastusek et al., 2005; Downton, 2007; Studer et al., 2007) have been derived. The motivation to study these solutions is simply to determine and identify the equilibrium points toward which the dynamical system is expected to converge as the controlling parameters are maintained constant.

Chapter 3

Elements of the Model

This section formulates the elements of the model, namely, (i) the bit/rock interface laws, (ii) the kinematic relationships, and (iii) the model of the BHA (Fig. 1.3). But first, the assumptions and the 3D geometrical formalism used to describe the system are introduced.

3.1 Assumptions

In addition to the hypotheses on the intrinsic nature of the problem postulated in Section 1.2 (averaging over a revolution, rate-independency, and reduced problem of the BHA), the following assumptions are adopted.

A first set of assumptions specifies an idealized directional drilling system.

- The bit/rock interface laws are derived for drag bits interacting with a homogeneous and isotropic rock formation.
- The BHA has uniform flexural rigidity and distributed weight. It is modeled from the bit to the last stabilizer. More precisely, the upper boundary of the BHA model is just above the last stabilizer.
- The stabilizers perfectly fit the borehole and do not transmit any moment between the borehole wall and the BHA. They are thus modeled as point supports of the BHA located

on the axis of the borehole. Also, with the exception of the bit and stabilizers, there is no additional contact between the BHA and the borehole wall. This last condition introduces some restrictions on the deformation of the BHA, which needs to be small enough to avoid having additional contacts.

- The RSS is a push-the-bit system, which is conceptualized as inducing a lateral force on the BHA between the bit and the first stabilizer. This assumption is valid as long as the pads of the RSS are not fully extended; otherwise the force condition at the RSS would become a displacement constraint.

A second set of assumptions is used to simplify and linearize the mathematical formulation.

- The radius of curvature of the borehole is large with respect to the considered length of BHA. As a matter of fact, the length of the BHA is generally of the order of 100 m, from which only the first $20 \sim 30$ meters significantly influence the directional tendency of the system. The industry measures the borehole curvature by the so-called build rate, which is the increase of borehole inclination over a length of 100 ft ($\sim$ 30 m) of borehole. For a push-the-bit RSS, the maximum build rate is usually of the order of $6\,^\circ/100$ft, which corresponds roughly to a radius of curvature of 280 m.

- At the length scale of the BHA, its axis is a small perturbation of the borehole axis. This assumption is justified by the small clearance, of the order of $1 \sim 10$ cm, between the BHA and the borehole wall compared to the length of the BHA.

- The axial force and torque on the BHA are at least an order of magnitude smaller than the loads that would induce buckling of the BHA. The typical axial strains of the BHA are of the order of $O(10^{-4})$ so that it is considered to be inextensible. Finally, the Euler-Bernoulli hypotheses for the bending of a rod are adopted.

3.2 Geometry

Figure 3.1 sketches the borehole and the BHA.

The fixed basis $(\boldsymbol{e}_x, \boldsymbol{e}_y, \boldsymbol{e}_z)$ is defined with its origin at the rig and the $\boldsymbol{e}_z$-axis points in the direction of gravity.

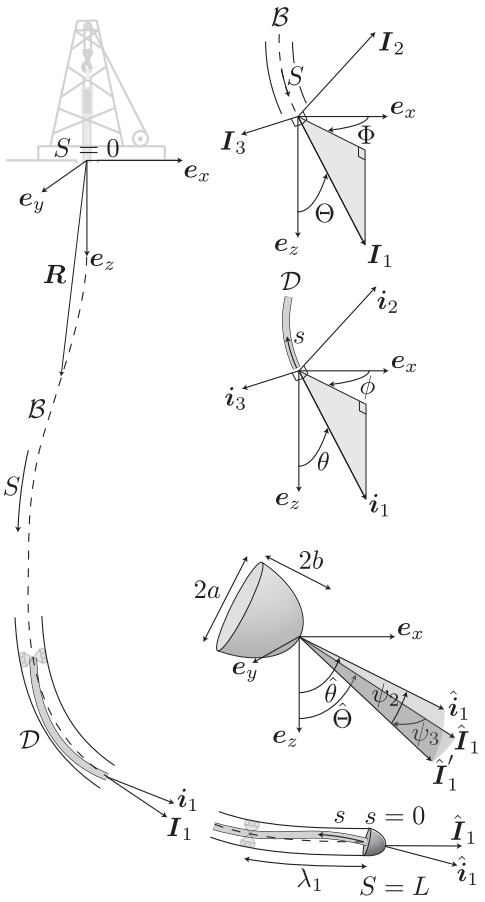

Figure 3.1: Geometric description of the borehole and BHA.

The borehole is a cylindrical object defined by its central axis $\mathcal{B}$ and its varying cross section. It is parametrized by the curvilinear coordinate S with $0 \leq S \leq L$, where $S = 0$ at the surface and L is the increasing length of the borehole. Its axis $\mathcal{B}$ is formally defined as the trajectory of the bit reference point. It is described by $\boldsymbol{R}(S)$, a vectorial function of the coordinate S, which is continuous in S but only piecewise continuously differentiable as sudden changes in

orientation can occur.

At a point where $\boldsymbol{R}$ is differentiable, the tangent unit vector to the borehole is locally defined by

$$\boldsymbol{I}_1 = \frac{\mathrm{d}\boldsymbol{R}}{\mathrm{d}S}. \tag{3.1}$$

The axis $\mathcal{B}$ is completely defined by the inclination $\Theta(S)$ and the azimuth $\Phi(S)$ of $\boldsymbol{I}_1$, two piecewise continuous functions of S with $\Theta(S) \in [0, \pi]$ measured with respect to the vertical axis $\boldsymbol{e}_z$ and $\Phi(S) \in [0, 2\pi]$ being the horizontal angle from $\boldsymbol{e}_x$. The local borehole basis $(\boldsymbol{I}_1, \boldsymbol{I}_2, \boldsymbol{I}_3)$ is defined in such a way that $\boldsymbol{I}_2$ is in the same vertical plane as $\boldsymbol{I}_1$, and $\boldsymbol{I}_3 = \boldsymbol{I}_1 \times \boldsymbol{I}_2$ is horizontal.

The curvature vector $\boldsymbol{K}$ of the borehole axis is given by

$$\boldsymbol{K} = \frac{\mathrm{d}\boldsymbol{I}_1}{\mathrm{d}S} \tag{3.2}$$

and is orthogonal to the tangent vector $\boldsymbol{I}_1$. It can be expressed in terms of the inclination Θ and azimuth Φ of the borehole and its components along $\boldsymbol{I}_2$ and $\boldsymbol{I}_3$ are respectively given by

$$K_2 = \frac{\mathrm{d}\Theta}{\mathrm{d}S}, \qquad K_3 = \frac{\mathrm{d}\Phi}{\mathrm{d}S}\sin\Theta. \tag{3.3}$$

The axis $\mathcal{D}$ of the BHA is a small perturbation of the borehole axis $\mathcal{B}$. It is parametrized by the curvilinear coordinate s with origin at the bit, and is described by the vectorial function $\boldsymbol{r}(s; L)$ measured from the origin of $(\boldsymbol{e}_x, \boldsymbol{e}_y, \boldsymbol{e}_z)$. Here, the length L of the borehole needs to be understood as the evolution variable, which enables the tracking of the BHA motion. Hence, $\boldsymbol{r}$ is a continuously differentiable function of s but is only piecewise continuously differentiable with respect to L. The tangent unit vector $\boldsymbol{i}_1$ to $\mathcal{D}$ points in the direction of decreasing s; it is thus itself a small perturbation of the borehole tangent vector $\boldsymbol{I}_1$. The inclination $\theta(s; L) \in [0, \pi]$ and azimuth $\phi(s; L) \in [0, 2\pi]$ of $\boldsymbol{i}_1$ express the deformed configuration of the BHA for a given length L of the borehole. As for $(\boldsymbol{I}_1, \boldsymbol{I}_2, \boldsymbol{I}_3)$, the local BHA basis $(\boldsymbol{i}_1, \boldsymbol{i}_2, \boldsymbol{i}_3)$ is defined in such a way that $\boldsymbol{i}_2$ is in the same vertical plane as $\boldsymbol{i}_1$, and that $\boldsymbol{i}_3 = \boldsymbol{i}_1 \times \boldsymbol{i}_2$ is horizontal.

The bit has a diameter $2a$ and a height $2b$. Hereafter, a hat is attributed to variables evaluated at the bit, e.g., $\hat{\Theta} = \Theta(L)$ is the borehole inclination at the bit, $\hat{\theta} = \theta(0; L)$ and $\hat{\phi} = \phi(0; L)$ are the inclination and azimuth of the bit axis, and $(\hat{\boldsymbol{i}}_1, \hat{\boldsymbol{i}}_2, \hat{\boldsymbol{i}}_3)$ is the bit basis. The relative orientation of the bit with respect to the borehole is measured by two small angles ψ_2

and ψ_3 defined as

$$\psi_2 = \hat{\theta} - \hat{\Theta}, \qquad \psi_3 = \left(\hat{\phi} - \hat{\Phi}\right) \sin \hat{\Theta}. \tag{3.4}$$

Under normal drilling conditions, they are of the order of $O(1^\circ)$ (Ernst et al., 2007). The angle ψ_2 is measured from $\hat{\boldsymbol{I}}_1'$ to $\hat{\boldsymbol{i}}_1$, while ψ_3 is measured from $\hat{\boldsymbol{I}}_1$ to $\hat{\boldsymbol{I}}_1'$, with the unit vector $\hat{\boldsymbol{I}}_1'$ being defined in the vertical plane $(\hat{\boldsymbol{i}}_1, \hat{\boldsymbol{i}}_2)$ as the vector of inclination $\hat{\Theta}$. The tilt angles ψ_2, ψ_3 and the bit inclination $\hat{\theta}$ and azimuth $\hat{\phi}$ are piecewise continuous functions of L.

Although describing the geometry of the problem by means of angles appears to be natural, some complications are inherited from this formulation. In particular, large variations in azimuthal direction are encountered when the borehole is close to verticality. In the limit, the azimuth Φ of a vertical borehole is not well-defined.

3.3 Bit/Rock Interface Laws

The interaction of the bit with the rock formation is characterized by interface laws that embody information about the rock fragmentation and other dissipative processes induced at the bit/rock interface during drilling. It typically depends on the properties of the rock formation and the bit, in particular, on the disposition of the cutters on the bit body and their characteristics. Ultimately, the interaction relationships serve as lower boundary condition for the BHA.

The interface laws relate generalized forces at the bit/rock interface with variables describing the kinematics of the bit as it penetrates the rock formation. The dynamic and kinematic variables in these relationships are averaged quantities over several revolutions of the bit and are measured at a reference point of the bit.

The derivation of the interface laws for PDC bits is based on the publication by Perneder et al. (2012), itself a generalization of the work by Detournay and Defourny (1992).

This section starts with a discussion about the nature of the interface laws; specifically, the kinematic and dynamic variables entering these relations are identified. The methodology used to derive the interface laws is then exposed. A whole section is dedicated to the interaction of a single cutter of a PDC bit with the rock and provides laws governing this interaction. Finally, the expressions for the bit/rock interface laws are given.

3.3.1 Nature of the Interface Laws

The dynamic and kinematic variables in the interface laws can be identified via the hypotheses postulated in Section 1.2. First, Hypothesis 1 justifies the use of averaged variables over a revolution. As a consequence, the interface laws, as proposed here, are inadequate when studying dynamical phenomena evolving on time scales smaller or of the same order as the period of revolution; for example stick-slip or whirl vibrations (Richard et al., 2007; Germay et al., 2009). Second, the rate-independency of the interface laws, as stated in Hypothesis 2, is supported by single cutter experiments suggesting that the interaction of a cutter with the rock formation does not depend on its cutting velocity for the range of velocities encountered in drilling applications (Deliac, 1986). Experimental results with roller-cone bits indicate that this assumption also seems to hold for this type of bit. In particular, drilling tests show an independency of the torque on bit with respect to the rotary speed, provided that the penetration per revolution remains constant (Franca, 2010).

The interface laws are collapsed on a point, the reference point of the bit, which also defines the lower boundary of the BHA model. This point is naturally defined on the bit axis $\hat{\boldsymbol{i}}_1$ but its position on this axis is arbitrary. The reference point will be chosen in such a way to simplify the final expressions of the interface laws.

The bit/rock interaction forces are reduced to generalized forces averaged over a revolution: a force $\hat{\boldsymbol{F}}$, a moment $\hat{\boldsymbol{M}}$ orthogonal to the bit axis $\hat{\boldsymbol{i}}_1$, and a torque $\hat{\boldsymbol{C}}$ acting along $\hat{\boldsymbol{i}}_1$; they act at the reference point (Fig. 3.2). The torque $\hat{\boldsymbol{C}}$ hardly influences the directional behavior of the system and is thus not included in the interface laws. The components of $\hat{\boldsymbol{F}}$ and $\hat{\boldsymbol{M}}$ in the bit basis $(\hat{\boldsymbol{i}}_1, \hat{\boldsymbol{i}}_2, \hat{\boldsymbol{i}}_3)$ are collectively represented by the vector of generalized forces $\boldsymbol{\mathcal{F}} = \{\hat{F}_1, \hat{F}_2, \hat{F}_3, \hat{M}_2, \hat{M}_3\}^T$.

Similarly, the kinematics of the bit is defined by its velocity vector $\boldsymbol{v}$, its spin vector $\boldsymbol{\omega}$ orthogonal to the bit axis $\hat{\boldsymbol{i}}_1$, and its angular velocity vector $\boldsymbol{\Omega}$ aligned with $\hat{\boldsymbol{i}}_1$. The rate independency assumption implies, through a dimensional analysis argument, that the appropriate kinematic variables entering the interface laws are penetrations per revolution. A more general argument is based on the observation that, after averaging, the energy dissipated by the rock removal process is predominantly controlled by the volume of rock removed by the bit, while the

rate of removal only seems to have a secondary effect. The penetrations per revolution indirectly measure this volume of rock removed over a revolution of the bit.

The penetration vector $\boldsymbol{d}$ and angular penetration vector $\boldsymbol{\varphi}$ are thus defined as

$$\boldsymbol{d} = \frac{2\pi \boldsymbol{v}}{\Omega}, \qquad \boldsymbol{\varphi} = \frac{2\pi \boldsymbol{\omega}}{\Omega}, \tag{3.5}$$

where Ω is the magnitude of the angular velocity vector. In the bit basis $(\hat{\boldsymbol{i}}_1, \hat{\boldsymbol{i}}_2, \hat{\boldsymbol{i}}_3)$, they reduce to an axial penetration d_1, lateral penetrations d_2, d_3, and angular penetrations φ_2, φ_3. The generalized penetrations are thus represented by $\boldsymbol{\mathcal{P}} = \{d_1, d_2, d_3, \varphi_2, \varphi_3\}^T$.

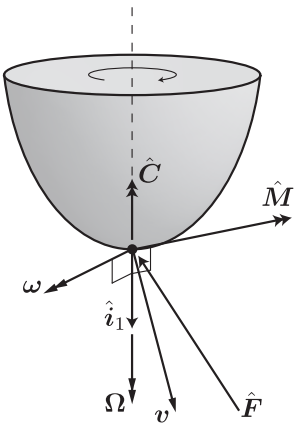

Figure 3.2: The generalized forces $\{\hat{\boldsymbol{F}}, \hat{\boldsymbol{M}}, \hat{\boldsymbol{C}}\}$ and the kinematics $\{\boldsymbol{v}, \boldsymbol{\omega}, \boldsymbol{\Omega}\}$ of the bit. The torque $\hat{\boldsymbol{C}}$ and angular velocity vector $\boldsymbol{\Omega}$ are aligned with the bit axis $\hat{\boldsymbol{i}}_1$, while the moment $\hat{\boldsymbol{M}}$ and spin vector $\boldsymbol{\omega}$ are orthogonal to $\hat{\boldsymbol{i}}_1$.

The bit/rock interaction laws are thus condensed into the relationship

$$\boldsymbol{\mathcal{F}} = \boldsymbol{\mathcal{L}}\left(\boldsymbol{\mathcal{P}}\right), \tag{3.6}$$

where the tensorial operator $\boldsymbol{\mathcal{L}}$ embodies properties of the bit and the rock formation. If the hypothesis of rate-independency is not valid, $\boldsymbol{\mathcal{L}}$ also depends on the angular velocity Ω.

The interface laws are similar to force/velocity relationships, that is, similar in nature to a dashpot. The difference lies in the definition of the kinematic quantities; although, strictly speaking, they are not velocities, they can be viewed as such in a scaled time-space that uses the period of revolution as unit of time. The dissipation D over a revolution associated with

directional drilling can be defined as

$$D = -\boldsymbol{\mathcal{F}} \cdot \boldsymbol{\mathcal{P}}. \tag{3.7}$$

It is relevant in the context of directional drilling and is different from the total energy P dissipated at the bit over a revolution, which is given by

$$P = D + 2\pi\hat{C}, \tag{3.8}$$

where $\hat{C}$ is the torque on bit. Under normal drilling conditions the term $2\pi\hat{C}$ is the main contribution to P.

For isotropic and homogeneous rock formations, the interface laws present some symmetries inherited from the averaging over a revolution. They are not endowed with a preferential lateral direction so that a rotation of the interaction laws around the axis of symmetry $\hat{\boldsymbol{i}}$ leaves the bitmetric operator $\boldsymbol{\mathcal{L}}$ unchanged. Formally, this constraint is expressed as

$$\boldsymbol{\mathcal{R}} \cdot \boldsymbol{\mathcal{L}}\left(\boldsymbol{\mathcal{P}}\right) = \boldsymbol{\mathcal{L}}\left(\boldsymbol{\mathcal{R}} \cdot \boldsymbol{\mathcal{P}}\right), \tag{3.9}$$

for any $\boldsymbol{\mathcal{P}}$ and for any ω-rotation tensor $\boldsymbol{\mathcal{R}}$ given by

$$\boldsymbol{\mathcal{R}} = \begin{bmatrix} 1 & 0 & 0 & 0 & 0 \\ 0 & \cos\omega & -\sin\omega & 0 & 0 \\ 0 & \sin\omega & \cos\omega & 0 & 0 \\ 0 & 0 & 0 & \cos\omega & -\sin\omega \\ 0 & 0 & 0 & \sin\omega & \cos\omega \end{bmatrix}. \tag{3.10}$$

3.3.2 Derivation of the Interface Laws

In principle, a theoretical derivation of the bit/rock interface laws can be conducted from a three-dimensional description of the bit geometry, involving the position and characteristics of all the cutters. Given a prescribed steady motion of the bit while drilling, the penetration of each cutter into the rock can be computed, from which the individual cutter forces can be determined using local cutter/rock interaction laws. Force and moment balances can then be used to calculate the statically equivalent global forces and moments acting on the bit.

Rather than accounting for the interaction of each individual cutter with the rock, we proceed here by replacing all the cutters by an equivalent blade. This approach greatly simplifies the derivation of the interface laws, as it enables to avoid a detailed description of the bit geometry. The geometrical reduction of a bit to an equivalent blade is permissible because only forces and moments averaged over one revolution are of interest here and the motion of the bit is assumed to be stationary. More precisely, the bit kinematics is considered stationary over a propagation distance of the order of the dimensions of the bit.

The bit cutting profile $\mathcal{S}$ is defined as the surface of revolution outlined by the cutter edges as the bit is rotated around its axis $\hat{\boldsymbol{i}}_1$ (Fig. 3.3a). A point P of $\mathcal{S}$ is characterized by its position vector $\boldsymbol{q}$; in a cylindrical system of coordinates (r, ω, z), it is given by $\boldsymbol{q} = -z\,\hat{\boldsymbol{i}}_1 + r\cos\omega\,\hat{\boldsymbol{i}}_2 + r\sin\omega\,\hat{\boldsymbol{i}}_3$. The cutting edge $\mathcal{E}$ is the envelope of the intersection of the cutter edges with a fixed plane containing the axis of rotation $\hat{\boldsymbol{i}}_1$. It is thus the two-dimensional curve that generates, by rotation, the cutting profile $\mathcal{S}$. The position of a point P on the cutting edge is measured by the curvilinear coordinate ρ. The vector $\boldsymbol{n}$ is the local outward normal to the cutting profile and $\boldsymbol{e}_\omega$ is orthogonal to $\boldsymbol{n}$ and to the cutting edge.

The equivalent blade is a fictitious blade geometrically identical to the cutting edge $\mathcal{E}$. Its properties are such that the forces on the equivalent blade are the same as those acting on the bit cutters, after averaging over a revolution. For example, the wearflat length distribution λ along the blade reflects the state of wear of the bit cutters.

The local depth of cut p of the equivalent blade for a given angular position ω of the blade can be computed from the global kinematics as follows. The incremental displacement $\delta\boldsymbol{u}$ of a point P is the displacement of P after a 2π-rotation of the equivalent blade (Fig. 3.3b). It is given by

$$\delta\boldsymbol{u} = \boldsymbol{d} + \boldsymbol{\varphi} \times \boldsymbol{q}. \tag{3.11}$$

The incremental normal displacement δu_n of P is the projection of $\delta\boldsymbol{u}$ on $\boldsymbol{n}$:

$$\delta u_n = \delta\boldsymbol{u} \cdot \boldsymbol{n}. \tag{3.12}$$

The local depth of cut p at P equals the incremental normal displacement δu_n if P is penetrating

the rock; that is,

$$p = \begin{cases} \delta u_n & \text{if} \quad \delta u_n > 0 \\ 0 & \text{if} \quad \delta u_n \leq 0 \end{cases} . \tag{3.13}$$

The volume of rock removed by the bit over a revolution can be obtained by integrating the depth of cut p over the cutting surface $\mathcal{S}$.

The force $\boldsymbol{f}$ per unit length of equivalent blade can be computed from the penetration p using cutter/rock interaction laws. Formally it is defined as $\boldsymbol{f} = \mathrm{d}\boldsymbol{F}/\mathrm{d}\rho$ where $\boldsymbol{F}$ is the total force acting on the segment $[0, \rho]$ of the equivalent blade. This force is finally integrated on the length of the equivalent blade and then averaged on a revolution to yield the averaged forces and moments on the bit, $\boldsymbol{\mathcal{F}} = \{\hat{F}_1, \hat{F}_2, \hat{F}_3, \hat{M}_2, \hat{M}_3\}^T$. This derivation is illustrated in Appendix A for a cylindrical bit.

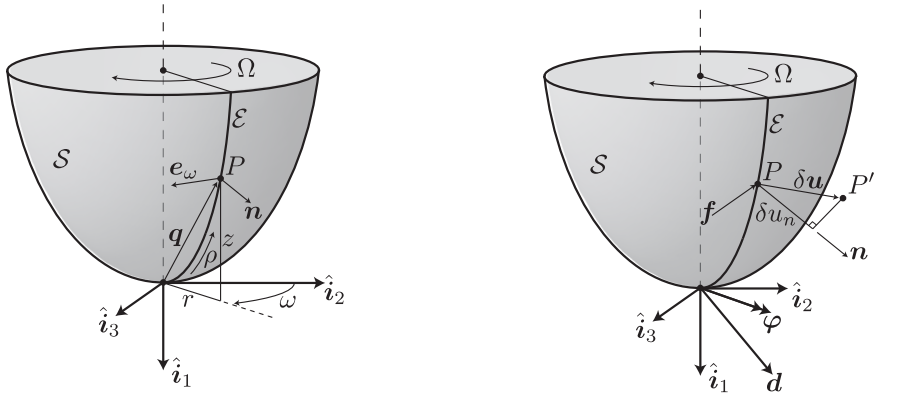

(a) Definition of the equivalent blade and the cylindrical coordinates (r, ω, z).

(b) After one revolution, the point P of the cutting edge is at P'; its incremental displacement is $\delta\boldsymbol{u}$.

Figure 3.3: From the global kinematics of the bit to the local depth of cut p of the equivalent blade.

3.3.3 Cutter/Rock Interaction

A simple model that captures the main features of the interaction between a cutter and the rock is outlined here (Detournay and Defourny, 1992; Perneder et al., 2012).

The interaction of a single cutter with the rock has been investigated experimentally (Gray et al., 1962; Cheatham and Daniels, 1979; Glowka, 1989; Sellami et al., 1989; Almenara and

Detournay, 1992; Detournay and Defourny, 1992; Lasserre, 1994; Dagrain et al., 2001; Detournay and Atkinson, 2000; Gerbaud et al., 2006; Boualleg et al., 2006) and numerically (Kou et al., 1999; Liu, 2002; Huang and Detournay, 2008; Huang et al., 2012). Observations suggest that the interaction of a single cutter with the rock is characterized by a bilinear relationship between the forces and the cross-sectional area of the cut, provided that cutting takes place in a ductile mode, that is, if the rock removal proceeds as a continuous diffuse fragmentation of the rock (Fig. 3.4). In sedimentary rocks, this ductile mode usually occurs for depths of cut ranging from 0.1 to 2 mm, which typically covers the depths of cut met in drilling applications (Detournay and Defourny, 1992). For larger depths of cut, the cutting process enters in a brittle mode called chipping.

The bilinear relationship is justified by the coexistence of two different processes: cutting that takes place at the cutting face, and frictional contact along the cutter wearflat, which is subparallel to the velocity $\boldsymbol{V}$ (Fairhurst and Lacabanne, 1957; Glowka, 1989; Detournay and Defourny, 1992; Sinor et al., 1998; Detournay et al., 2008). Experimental investigations suggest that the resultant force on the cutting face is proportional to the area of the cut, or equivalently to the depth of cut p for a rectangular cutter (Fig. 3.4). The contact forces on the wearflat also seem to be proportional to p but only for depths of cut smaller than a threshold p_*; for $p > p_*$, these contact forces saturate and are proportional to the length λ of the wearflat.

Hence, the presence of these two surfaces leads to the existence of two main regimes of interaction: regime I, where the forces are dominated by the frictional contact between the wearflat and rock ($p < p_*$), and regime II, where the forces on the cutting face dominate since the forces on the wearflat have reached saturation ($p > p_*$).

The force density $\boldsymbol{f}$ on a single cutter is defined similarly as for the equivalent blade; it is a function of the curvilinear coordinate ρ running along the width of the cutter. The components of $\boldsymbol{f}$ in the $\boldsymbol{n}$ and $\boldsymbol{e}_\omega$ directions are given by

$$\begin{aligned} &f_n = \zeta' \varepsilon p, && f_\omega = \zeta'' \varepsilon p, && \text{if } p < p_* \text{ (regime I)}, \\ &f_n = \sigma\lambda + \zeta\varepsilon p, && f_\omega = \mu\sigma\lambda + \varepsilon p, && \text{if } p > p_* \text{ (regime II)}. \end{aligned} \tag{3.14}$$

The parameters of this model are (1) the intrinsic specific energy of drilling ε; (2) the maximum contact pressure σ on the interface wearflat/rock; (3) a coefficient of friction μ at the wearflat,

and (4) three interaction numbers ζ, ζ', and ζ'', which essentially depend on the inclination of the wearflat and of the cutting face on the cutter velocity (Detournay and Defourny, 1992; Detournay et al., 2008).

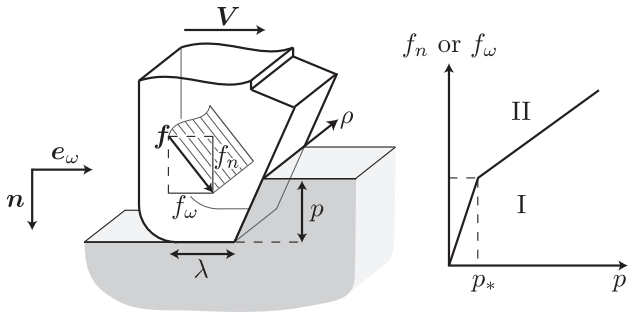

Figure 3.4: The interaction of a blunt cutter with the rock formation is modeled by bilinear laws between the depth of cut p and the force $\boldsymbol{f}$ per unit width of the cutter.

3.3.4 Results and Simplifications

It is assumed that the axial interaction of the bit with the rock takes place in regime II, while the lateral interaction is governed by regime I. This assumption is valid as long as the axial penetration is larger than the threshold penetration p_* and if the depth of cut p, associated with the lateral interaction of the bit with the rock, remains small. Also, it is assumed that the surface of the bit interacting with the rock does not change significantly. These additional assumptions ensure that the interface laws can be reduced to a linear relationship

$$\boldsymbol{\mathcal{F}} = -\boldsymbol{\mathcal{G}} - \boldsymbol{\mathcal{H}} \cdot \boldsymbol{\mathcal{P}}. \tag{3.15}$$

The vector $\boldsymbol{\mathcal{G}}$ is related to the saturated contact forces transmitted at the cutters wearflats and is in this respect a measure of the bit bluntness. The matrix $\boldsymbol{\mathcal{H}}$ presents some symmetries inherited from the constraint (3.9) on the interface laws;

$$\boldsymbol{\mathcal{H}} = \begin{bmatrix} H_{11} & 0 & 0 & 0 & 0 \\ 0 & H_{22} & H_{23} & H_{24} & H_{25} \\ 0 & -H_{23} & H_{22} & -H_{25} & H_{24} \\ 0 & H_{42} & H_{43} & H_{44} & H_{45} \\ 0 & -H_{43} & H_{42} & -H_{45} & H_{44} \end{bmatrix}. \tag{3.16}$$

As a consequence of the general form of $\boldsymbol{\mathcal{H}}$ and of the linearity of the interface laws, the coefficients H in $\boldsymbol{\mathcal{H}}$ can be computed considering a planar trajectory of the bit (that is, with $d_3 = 0$ and $\varphi_2 = 0$).

Finally, the bit/rock interface laws are reduced to

$$\begin{Bmatrix} \hat{F}_1 \\ \hat{F}_2 \\ \hat{F}_3 \\ \hat{M}_2 \\ \hat{M}_3 \end{Bmatrix} = - \begin{Bmatrix} G_1 \\ 0 \\ 0 \\ 0 \\ 0 \end{Bmatrix} - \begin{bmatrix} H_1 & 0 & 0 & 0 & 0 \\ 0 & H_2 & H_3 & 0 & 0 \\ 0 & -H_3 & H_2 & 0 & 0 \\ 0 & 0 & 0 & H_0 & 0 \\ 0 & 0 & 0 & 0 & H_0 \end{bmatrix} \begin{Bmatrix} d_1 \\ d_2 \\ d_3 \\ \varphi_2 \\ \varphi_3 \end{Bmatrix}. \tag{3.17}$$

The vanishing terms in the $\boldsymbol{\mathcal{H}}$ matrix appear to be negligible, in particular if the reference point of the bit is appropriately selected (see Appendix A). The parameters H_1, H_2, and H_0 are positive. The parameter H_3 is positive or negative; it measures the walk tendency of the bit, a natural phenomenon induced by the rotation of the bit (Voinov and Reutov, 1991; Ho, 1995; Menand et al., 2002): in a plane orthogonal to the bit axis $\hat{\boldsymbol{i}}_1$, the lateral penetration (d_2, d_3) is not necessarily coaxial with the lateral force $(\hat{F}_2, \hat{F}_3)$. The walk angle ϖ measured between the lateral force and penetration is given by

$$\varpi = \arctan \frac{H_3}{H_2}. \tag{3.18}$$

If $\varpi = 0$, the lateral force and penetration are aligned and the bit is said to have a neutral walk tendency. Otherwise, it is said to have a left or right walk tendency depending on the relative orientation of the lateral penetration with respect to the lateral force. For PDC bits, walk angles ϖ of about $-15°$ are often observed (Menand et al., 2002). The minus sign accounts for a left tendency of the bit, meaning that, in a plane perpendicular to the bit axis, the lateral penetration is "on the left" of the lateral force, when looking in the direction of $\hat{\boldsymbol{i}}_1$.

3.4 Kinematic Relationships

The propagation of the moving boundary of the borehole, defined as the surface of interaction between the bit and the rock formation, is related to the bit kinematics, described here by the generalized penetration vector $\boldsymbol{\mathcal{P}} = \{d_1, d_2, d_3, \varphi_2, \varphi_3\}^T$. For simplicity, the δ-operator is introduced to express the incremental change of a variable over a revolution of the bit (Detournay, 2007); it is viewed as a differential operator.

The penetration vector $\boldsymbol{d}$ is the incremental lengthening of the borehole axis $\mathcal{B}$ over one revolution, that is, $\boldsymbol{d} = \delta\hat{\boldsymbol{R}}$, where $\hat{\boldsymbol{R}} = \boldsymbol{R}(L)$ gives the position of the bit relative to the origin of the fixed coordinate system. Hence, $\boldsymbol{d}$ is tangent to the borehole axis and $\boldsymbol{d} = d\hat{\boldsymbol{I}}_1$, where the penetration d is the magnitude of the penetration vector, but also the incremental increase of the borehole length over a revolution, that is, $d = \delta L$. A formal definition of the delta operator is thus given by

$$\delta = d\frac{\mathrm{d}}{\mathrm{d}L}. \tag{3.19}$$

The penetration angles β_2 and β_3 measure the relative orientation of the penetration vector $\boldsymbol{d}$ with respect to the bit (Fig. 3.5). Under normal drilling conditions, β_2 and β_3 are small as a consequence of the penetration vector $\boldsymbol{d}$ being nearly coaxial with the bit axis $\hat{\boldsymbol{i}}_1$. They are thus given by

$$\begin{aligned} \beta_2 &= \frac{d_2}{d_1}, \\ \beta_3 &= \frac{d_3}{d_1}. \end{aligned} \tag{3.20}$$

Because the penetration vector $\boldsymbol{d}$ is tangent to the borehole axis ($\boldsymbol{d} = d\hat{\boldsymbol{I}}_1$), the angles of penetration are related to the tilt angles by

$$\begin{aligned} \psi_2 &= -\beta_2, \\ \psi_3 &= -\beta_3. \end{aligned} \tag{3.21}$$

Despite these relations, the distinction between these two sets of angles is maintained. The tilt angles ψ_2, ψ_3 are geometric variables measuring the relative orientation of the bit with the borehole, while the penetration angles β_2, β_3 are kinematic variables that measure the orientation of the bit velocity with respect to the borehole.

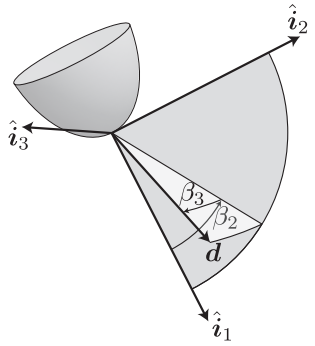

Figure 3.5: Definition of the penetration angles β_2 and β_3 of the bit, with β_2 measured in the vertical plane $(\hat{\boldsymbol{i}}_1, \hat{\boldsymbol{i}}_2)$ and β_3 measured perpendicularly to $(\hat{\boldsymbol{i}}_1, \hat{\boldsymbol{i}}_2)$.

The overgauge of the borehole with respect to the bit diameter $2a$ is affected by the tilt of the bit, as suggested by the horizontal view sketched in Figure 3.6 for a cylindrical bit. In that case, the borehole radius A measured in the vertical plane of the borehole can be approximated by

$$A = a + b\,|\beta_2| \tag{3.22}$$

if the bit is cylindrical and for idealized drilling conditions, that is if the rock formation is not being washed out and the bit is not vibrating. Hence, the penetration angles β_2 and β_3, or equivalently ψ_2 and ψ_3, can also be interpreted as a measure of the borehole overgauge.

The angular penetration vector $\boldsymbol{\varphi}$ measures the rate of change of the bit axis $\hat{\boldsymbol{i}}_1$ over a revolution: $\boldsymbol{\varphi} = \hat{\boldsymbol{i}}_1 \times \delta\hat{\boldsymbol{i}}_1$. The projection of this last expression onto the bit basis yields

$$\begin{aligned} \frac{\varphi_2}{d_1} &= -\frac{\mathrm{d}\hat{\phi}}{\mathrm{d}L}\sin\hat{\theta}, \\ \frac{\varphi_3}{d_1} &= \frac{\mathrm{d}\hat{\theta}}{\mathrm{d}L}. \end{aligned} \tag{3.23}$$

Strictly speaking, d instead of d_1 should have been used in these equations for φ_2 and φ_3. However, since both $\beta_2 \ll 1$ and $\beta_3 \ll 1$ in the expression of the penetration

$$d = d_1\sqrt{1 + \beta_2^2 + \beta_3^2}, \tag{3.24}$$

no distinction is made between d and d_1.

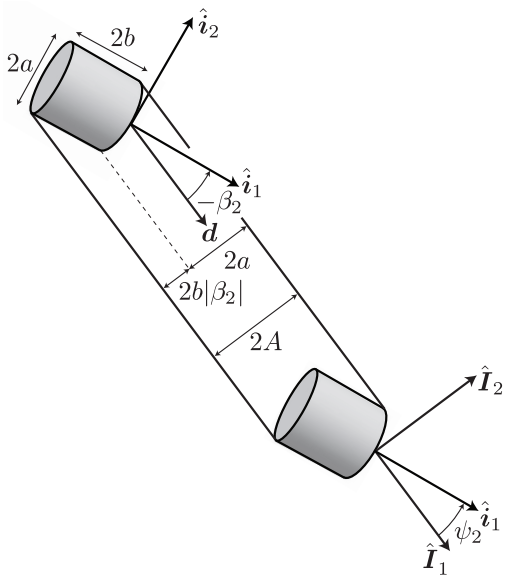

Figure 3.6: Link between the tilt angle ψ_2, the angle of penetration β_2, and the overgauging of the borehole in the vertical plane $(\hat{\boldsymbol{I}}_1, \hat{\boldsymbol{I}}_2)$. The borehole diameter $2A$ in this vertical plane is in principle related to the bit tilt ψ_2, or equivalently to the penetration angle β_2. This correspondence is illustrated here for a cylindrical bit.

3.5 BHA Model

3.5.1 Preamble

The BHA consists of a connected set of heavy pipes and stabilizers. At the intermediate scale of order $O\,(10\text{ m})$ used to construct the model of directional drilling, the BHA is a slender elastic object subject to external forces and moments. Thus, at that scale, the BHA can in principle be modeled as a rod, which is constrained by the stabilizers to conform with the borehole geometry.

The model assumes that the BHA has a uniform bending stiffness EI and a uniform distributed weight w (the weight minus the buoyancy force due to the drilling mud), and there is no contact between the BHA and the borehole wall, other than those taking place at the bit and at the stabilizers. The model of the BHA is a static model that extends from the bit to the last stabilizer. Dynamical effects are neglected in part as a result of the averaging of the directional drilling process over several revolutions.

The n stabilizers, which are numbered from 1 to n starting with the closest stabilizer to the

bit, are treated as discrete geometrical constraints (Fig. 3.7). They define n BHA segments of initial lengths $\lambda_1, \lambda_2, \ldots, \lambda_n$. On account of the assumed inextensibility of the BHA, the curvilinear coordinate s remains the arc length for the axis of the BHA after deformation. Hence, the position s_i of the i^{th} stabilizer is always given by

$$s_i = \sum_{j=1}^{i} \lambda_j, \ i = 1, \ldots, n. \tag{3.25}$$

In the following, the notation is conveniently generalized by assigning the index $i = 0$ to the bit, e.g., this last expression is also valid for $i = 0$ as $s_0 = 0$. A chord $\mathcal{C}_i$, $i = 1, \ldots, n$, is associated with the i^{th} segment of BHA. It is the straight line linking the successive contact points located at s_i and s_{i-1}. It has an inclination $\langle\theta\rangle_i$ and and azimuth $\langle\phi\rangle_i$.

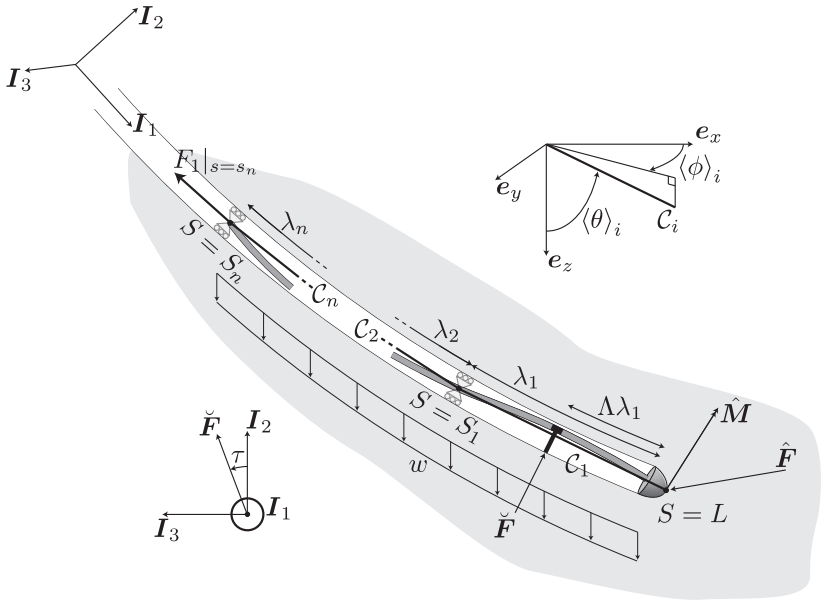

Figure 3.7: Beam model of the BHA. The RSS force is alternatively measured by its components $\breve{F}_2$ and $\breve{F}_3$ along $\boldsymbol{I}_2$ and $\boldsymbol{I}_3$, or by its magnitude $\breve{F}$ and orientation τ. The chord $\mathcal{C}_i$, $i = 1, \ldots, n$, links two successive contact points and has inclination $\langle\theta\rangle_i$ and azimuth $\langle\phi\rangle_i$.

The stabilizers are here supposed to perfectly fit the borehole and to not transmit any moment between the borehole wall and the BHA. They are thus modeled as point supports where the BHA axis $\mathcal{D}$ and the borehole axis $\mathcal{B}$ intersect. Also, since the velocity discontinuity at a borehole/stabilizer contact is essentially orthogonal to $\boldsymbol{I}_1$, the frictional forces are fully

subsumed in a frictional torque at the stabilizer and the reaction force at the contact can be assumed to be orthogonal to the borehole. In other words, the stabilizers can be assumed to slide frictionlessly along the axis of the borehole, a consequence of the rotation of the drillstring.

The RSS, located at a distance $\Lambda\lambda_1$ from the bit, applies a transversal force $\breve{\boldsymbol{F}}$ on the BHA. This force $\breve{\boldsymbol{F}}$ is also assumed to be locally orthogonal to the borehole axis $\boldsymbol{I}_1$; it is thus defined by its components $\breve{F}_2$ and $\breve{F}_3$ along the axes $\boldsymbol{I}_2$ and $\boldsymbol{I}_3$. In some instances, it will be more convenient to use the norm $\breve{F}$ and the angle τ measured from $\boldsymbol{I}_2$ (Fig. 3.7).

This section first aims at deriving the differential equations governing the deformation of the BHA. The BHA is first viewed as a Kirchhoff rod; a succession of simplifications is then introduced that ultimately allows to view the BHA as a Euler-Bernoulli beam. The purpose of such a deductive approach is to estimate the errors introduced by the beam theory when modeling the behavior of the BHA. These results are then used to derive the general expressions for the forces and moments transmitted to the bit by the BHA. Throughout this section, the dependence on the borehole length L is ignored as the problem of the BHA aims at determining its deformed configuration for a given length L of the borehole, e.g., the BHA inclination is temporarily denoted $\theta(s)$ instead of $\theta(s;L)$.

3.5.2 Characterization of the BHA Deformation

Before writing the equations governing the deformation of the BHA and bringing further simplifications to this problem, the Frenet-Serret basis $(\bar{\boldsymbol{i}}_1, \bar{\boldsymbol{i}}_2, \bar{\boldsymbol{i}}_3)$ is introduced as the natural basis for the BHA axis $\mathcal{D}$. The tangent, normal, and binormal vectors of this basis are respectively defined as

$$\bar{\boldsymbol{i}}_1 = \boldsymbol{i}_1, \quad \bar{\boldsymbol{i}}_2 = -\frac{\bar{\boldsymbol{i}}_1'}{\left\|\bar{\boldsymbol{i}}_1'\right\|}, \quad \bar{\boldsymbol{i}}_3 = \bar{\boldsymbol{i}}_1 \times \bar{\boldsymbol{i}}_2. \tag{3.26}$$

(The unconventional minus sign in this second expression is a consequence of choosing the direction of $\boldsymbol{i}_1$ to be the same as $\boldsymbol{I}_1$, i.e., in the direction of increasing S but decreasing s.) The strain associated with the curving of the axis $\mathcal{D}$ of the BHA is captured by the vector $\bar{\boldsymbol{u}}$, defined as

$$\bar{\boldsymbol{i}}_j' = -\bar{\boldsymbol{u}} \times \bar{\boldsymbol{i}}_j, \quad j = 1, 2, 3. \tag{3.27}$$

A bar over a vector is used to indicate that its components are defined in the Frenet-Serret basis. In this basis, $\bar{\boldsymbol{u}} = \{t, 0, k\}^T$; the curvature k is the rate of change of the tangent vector $\bar{\boldsymbol{i}}_1$ with s, while the torsion t measures the rate of change of the binormal vector $\bar{\boldsymbol{i}}_3$, the normal to the osculating plane $(\bar{\boldsymbol{i}}_1, \bar{\boldsymbol{i}}_2)$ to the curve. The components of $\boldsymbol{i}_1$ in the reference coordinate system are given by $\boldsymbol{i}_1 = \{\sin\theta\cos\phi, \sin\theta\sin\phi, \cos\theta\}^T$, so that the curvature $k = ||\boldsymbol{i}_1'||$ is given by

$$k = \sqrt{\theta'^2 + \phi'^2 \sin^2\theta}. \tag{3.28}$$

For any vector $\bar{\boldsymbol{a}}$ with components expressed in the basis $(\bar{\boldsymbol{i}}_1, \bar{\boldsymbol{i}}_2, \bar{\boldsymbol{i}}_3)$, its derivative $\bar{\boldsymbol{a}}'$ with respect to s can be expressed as

$$\bar{\boldsymbol{a}}' = \frac{\partial \bar{\boldsymbol{a}}}{\partial s} - \bar{\boldsymbol{u}} \times \bar{\boldsymbol{a}}, \tag{3.29}$$

where $\partial\bar{\boldsymbol{a}}/\partial s$ denotes the derivative of the components of $\boldsymbol{a}$ in the Frenet-Serret basis, i.e., $\partial\bar{\boldsymbol{a}}/\partial s = \{\partial\bar{a}_1/\partial s, \partial\bar{a}_2/\partial s, \partial\bar{a}_3/\partial s\}^T$, and where $\bar{\boldsymbol{u}} \times \bar{\boldsymbol{a}}$ accounts for the rate of change of the basis.

Similar relations can be derived for the BHA basis $(\boldsymbol{i}_1, \boldsymbol{i}_2, \boldsymbol{i}_3)$. The rate of change of this basis is given by

$$\boldsymbol{i}_j' = -\boldsymbol{v} \times \boldsymbol{i}_j, \quad j = 1, 2, 3, \quad \text{with} \quad \boldsymbol{v} = \left\{ \begin{array}{c} -\phi'\cos\theta \\ \phi'\sin\theta \\ -\theta' \end{array} \right\}. \tag{3.30}$$

Similarly to equation (3.29), the derivative of a vector $\boldsymbol{a}$ with components in the BHA basis $(\boldsymbol{i}_1, \boldsymbol{i}_2, \boldsymbol{i}_3)$ is given by

$$\boldsymbol{a}' = \frac{\partial \boldsymbol{a}}{\partial s} - \boldsymbol{v} \times \boldsymbol{a}, \tag{3.31}$$

where $\partial\boldsymbol{a}/\partial s$ now denotes the derivative of the components of $\boldsymbol{a}$ when expressed in the BHA basis.

3.5.3 Kirchhoff Rod Model

A starting point is to treat the BHA as a Kirchhoff rod, deduced from the Cosserat rod by neglecting axial and shear deformations and by adopting the classical Euler-Bernoulli hypotheses for the bending deformation (Antman, 2005). The axial strains are of the order of $O(10^{-4})$ and the inextensibility of the BHA ensures that the tangent vector $\boldsymbol{i}_1 = -\boldsymbol{r}'$ after deformation, where a prime denotes a derivative with respect to s.

The Euler-Bernoulli hypotheses entail that the bending moment is proportional to the curvature and that the moment vector is orthogonal to the local osculating plane of the BHA axis; that is,

$$\boldsymbol{M} = EIk\bar{\boldsymbol{i}}_3, \tag{3.32}$$

where EI is the flexural rigidity. The projection of this relation onto $(\boldsymbol{i}_2, \boldsymbol{i}_3)$ yields expressions for the components M_2 and M_3 of the bending moment, which are given by

$$M_2 = EI\phi' \sin\theta, \qquad M_3 = -EI\theta'. \tag{3.33}$$

The local equilibrium in translation and rotation at a point of the BHA other than the stabilizers and RSS can be written as follows (Antman, 2005):

$$\boldsymbol{F}' - \boldsymbol{w} = \boldsymbol{0}, \qquad \boldsymbol{M}' + \boldsymbol{C}' + \boldsymbol{r}' \times \boldsymbol{F} = \boldsymbol{0}, \tag{3.34}$$

where $\boldsymbol{F}$ is the contact force transmitted at the cross section with outer normal $\boldsymbol{i}_1$ located at s, $\boldsymbol{M}$ is the bending moment, $\boldsymbol{C}$ is the torque, and $\boldsymbol{w} = w\boldsymbol{e}_z$ with w denoting the uniform buoyant weight of the BHA per unit length. In the Frenet-Serret basis, $\bar{\boldsymbol{M}} = \{0, 0, M\}^T$, a consequence of the Euler-Bernoulli hypotheses, and $\bar{\boldsymbol{C}} = \{C, 0, 0\}^T$. When writing the equilibrium equations (3.34), we have neglected the equivalent body force and body couple arising from the relative velocity between the mud and the BHA.

3.5.4 Simplification into a Beam

The simplification of the Kirchhoff rod model into a beam relies on the so-called small rotation assumption. The validity of this assumption is supported by the small magnitude of borehole curvatures encountered in the field (Table 7.1). Also, it is recognized that the angle between

$\boldsymbol{i}_1$ (the tangent to the BHA axis $\mathcal{D}$) and $\boldsymbol{I}_1$ (the tangent to the borehole axis $\mathcal{B}$) is everywhere very small, as a consequence of the small clearance between the BHA and the borehole wall. In other words, at the scale of the BHA, $\mathcal{B}$ is the leading order approximation of $\mathcal{D}$. Formally, the small rotation assumption is equivalent to considering that the norm of the vector $\boldsymbol{v}$ that characterizes the deformation of the BHA is small everywhere.

An expression for the shear force $\boldsymbol{F}_s = -\boldsymbol{i}_1 \times (\boldsymbol{i}_1 \times \boldsymbol{F})$ can readily be derived from the rotational equilibrium in (3.34) and using the differentiation rules (3.29) for $\bar{\boldsymbol{C}}'$ and (3.31) for $\boldsymbol{M}'$ yields

$$\boldsymbol{F}_s = -M_2'\boldsymbol{i}_3 + M_3'\boldsymbol{i}_2 + \boldsymbol{i}_1 \times (\boldsymbol{v} \times \boldsymbol{M}) + kC\bar{\boldsymbol{i}}_3. \tag{3.35}$$

The small rotation approximation allows to neglect the terms $\boldsymbol{v} \times \boldsymbol{M}$ and kC in this last expression. Using the quantities listed in Table 7.1, the curvature k and the torsion t are recognized to be at most of the same order of magnitude as the maximum curvature of the borehole. Hence, both $|kC|$ and $||\boldsymbol{v} \times \boldsymbol{M}||$ are about two orders of magnitude smaller than the magnitude of the shear force $||\boldsymbol{F}_s||$. The components of $\boldsymbol{F}_s$ expressed in the BHA basis are thus approximated by

$$F_2 = M_3' = -EI\theta'', \qquad F_3 = -M_2' = -EI\left(\theta'\phi'\cos\theta + \phi''\sin\theta\right). \tag{3.36}$$

Using the same argument of small rotations, the expression of the component F_3 of the shear force can further be simplified into

$$F_3 = -EI\left(\phi''\sin\theta\right). \tag{3.37}$$

Indeed, the term $EI\theta'\phi'\cos\theta$ is a component of the vector $\boldsymbol{v} \times \boldsymbol{M}$ and is suitably neglected.

We also note that $C' = 0$ (except at the stabilizers and at the RSS) since C' is the only component in the direction $\boldsymbol{i}_1$ in the left-hand side of (3.34b). In other words, the calculation of the torque is uncoupled from that of the contact force $\boldsymbol{F}$ and bending moment $\boldsymbol{M}$.

The translational equilibrium equations in (3.34) can also be expressed in terms of the force components in the BHA basis. Rewriting (3.34a) in that basis and using (3.31) yields

$$\frac{\partial \boldsymbol{F}}{\partial s} - \boldsymbol{v} \times \boldsymbol{F} - \boldsymbol{w} = \boldsymbol{0}. \tag{3.38}$$

Similarly, it can be argued that the norm $||\boldsymbol{v} \times \boldsymbol{F}||$ is generally one order of magnitude smaller than $\|\boldsymbol{w}\|$. In fact, the term $||\boldsymbol{v} \times \boldsymbol{F}||$ is of the order of $|kF_1|$, itself of order $O(10^{-1}\,\mathrm{kN/m})$ under

normal drilling conditions. The magnitude of $\|\boldsymbol{w}\|$ can be found in Table 7.1 and is of order $O(1\,\mathrm{kN/m})$. Thus, the equilibrium equation (3.38) is simplified to

$$\frac{\partial \boldsymbol{F}}{\partial s} - \boldsymbol{w} = \boldsymbol{0}. \tag{3.39}$$

The initial undeformed configuration of the BHA is chosen to be aligned with the chord $\mathcal{C}_1$ linking the bit to the first stabilizer. Consequently, the inclination θ of the BHA is approximated by $\langle\theta\rangle_1$, the inclination of $\mathcal{C}_1$, when it is appropriate to do so in the expressions governing the deformation of the BHA.

These simplifications have reduced the model of the BHA to an elastic beam. They can be tested a posteriori by checking if $|kC| \ll M'$, $||\boldsymbol{v} \times \boldsymbol{M}|| \ll M'$, and $||\boldsymbol{v} \times \boldsymbol{F}|| \ll ||\boldsymbol{w}||$. If these inequalities do not hold, the results obtained from the linear beam theory are not reliable and further investigations are required.

The beam equations and the expressions for the components of the bending moment and shear force in the BHA basis are summarized here:

$$EI\theta''' = w \sin\langle\theta\rangle_1, \qquad EI \sin\langle\theta\rangle_1 \, \phi''' = 0, \tag{3.40a}$$

$$M_2 = EI \sin\langle\theta\rangle_1 \, \phi', \qquad M_3 = -EI\theta', \tag{3.40b}$$

$$F_2 = -EI\theta'', \qquad F_3 = -EI \sin\langle\theta\rangle_1 \, \phi''. \tag{3.40c}$$

They can be solved together with the boundary conditions at the bit and last stabilizer, and knowing the force at the RSS and the geometric constraints at the stabilizers.

The linearization is equivalent to writing the balance equations (3.34) in an undeformed configuration of the BHA aligned with $\mathcal{C}_1$. This also means that the expressions of the bending moments (3.40b) and shear forces (3.40c) are measured according to this undeformed configuration.

The longitudinal equilibrium, given by the projection of (3.39) on the axis of the BHA, reduces to

$$F_1' = w \cos\langle\theta\rangle_1 . \tag{3.41}$$

This equation can be integrated from the last stabilizer to the bit and thus provide a relation between the imposed axial force at the last stabilizer, $F_1|_{s=s_n}$, and the axial force transmitted to the bit $\hat{F}_1$.

3.5.5 Resolution

The BHA is forced to espouse the geometry of the borehole by means of the stabilizers, which introduce n isoperimetric constraints (one per stabilizer) that can be formally expressed as

$$\int_{S_i}^{S_{i-1}} \boldsymbol{I}_1 \mathrm{d}S = \int_{s_{i-1}}^{s_i} \boldsymbol{i}_1 \mathrm{d}s, \quad i = 1, \ldots, n, \tag{3.42}$$

where S_i denotes the position of the i^{th} stabilizer on the borehole axis and $S_0 = L$ is the bit position.

The isoperimetric constraints can be simplified, however, by using the same hypotheses postulated to derive the beam equations for the BHA. First, on account that the BHA axis $\mathcal{D}$ is a perturbation of the borehole axis $\mathcal{B}$, the same curvilinear coordinate can be used as a measure of the arc length for $\mathcal{B}$ and $\mathcal{D}$ and $S = L - s$. This implies that the positions of the stabilizers along the borehole $\mathcal{B}$ are known: $S_i = L - s_i$, $i = 1, \ldots, n$. Also, the BHA and borehole inclinations θ and Θ along the i^{th} segment of BHA are at first order approximated by the inclination $\langle\Theta\rangle_i$ of the chord $\mathcal{C}_i$. Similarly, $\langle\Phi\rangle_i$ is the first order approximation for ϕ and Φ along the i^{th} segment. The isoperimetric constraints (3.42) can thus be approximated by

$$\begin{aligned}
\langle\Theta\rangle_i &= \frac{1}{\lambda_i} \int_{S_i}^{S_{i-1}} \Theta(S) \mathrm{d}S \simeq \frac{1}{\lambda_i} \int_{s_{i-1}}^{s_i} \theta(s; L) \mathrm{d}s = \langle\theta\rangle_i, \\
\langle\Phi\rangle_i &= \frac{1}{\lambda_i} \int_{S_i}^{S_{i-1}} \Phi(S) \mathrm{d}S \simeq \frac{1}{\lambda_i} \int_{s_{i-1}}^{s_i} \phi(s; L) \mathrm{d}s = \langle\phi\rangle_i .
\end{aligned} \tag{3.43}$$

Within the framework of the linear beam approximation of the BHA, the isoperimetric constraints (3.43) introduced by the n stabilizers can be enforced by initially imposing $n - 1$ known kinks at each stabilizer, with the exception of the n^{th} stabilizer. This approach has a simple physical interpretation and is illustrated in Figure 3.8 for the case of a 2-stabilizer BHA. The BHA, in its initial undeformed configuration, is aligned with the chord $\mathcal{C}_1$. Kinks are then imposed at the $n - 1$ "internal" stabilizers to bring each of them on the borehole axis. These kinks are equivalent to applying singular moment dipoles at each stabilizer with magnitude $\langle\Theta\rangle_i - \langle\Theta\rangle_{i+1}$ in the vertical plane $(\boldsymbol{I}_1, \boldsymbol{I}_2)$ and $\langle\Phi\rangle_i - \langle\Phi\rangle_{i+1}$ in the plane $(\boldsymbol{I}_1, \boldsymbol{I}_3)$. At this stage, the BHA segments are aligned with the chords $\mathcal{C}_1, \ldots, \mathcal{C}_n$, and the BHA is unstressed except at the kinks, where it is singularly loaded. Finally, the singular moment dipoles are relaxed, causing the development of transverse reaction forces at all the stabilizers and at the bit, as well

as a moment at the bit.

The lower boundary conditions of the BHA are controlled by the bit/rock interaction; hence, the model of the BHA cannot be solved independently from the interface laws. The beam equations are thus solved in terms of the a priori unknown orientation of the bit, measured by $\hat{\theta}$ and $\hat{\phi}$. A no moment boundary condition is imposed at the n^{th} stabilizer. In general, accounting for the first 3 or 4 stabilizers closest to the bit is sufficient to accurately compute the bit forces and the deformation of the BHA at the bit (see Appendix B).

The beam equations (3.40a) are uncoupled in the sense that the inclination θ and azimuth ϕ can be solved independently. They can be integrated to yield

$$\begin{aligned} EI\theta &= A_0 + A_1 s + A_2 s^2 + \tfrac{1}{6} w \sin \langle \Theta \rangle_1 \; s^3, \\ EI \sin \langle \Theta \rangle_1 \; \phi &= B_0 + B_1 s + B_2 s^2. \end{aligned} \tag{3.44}$$

Evidently, the above expressions are valid along parts of the BHA comprised between points of singular loading. Indeed, the coefficients A_2 and B_2 are discontinuous at the RSS and at the internal stabilizers $s = s_i$, $i = 1, \ldots, n-1$; the jumps in A_2 and B_2 are directly related to the RSS force $\breve{\boldsymbol{F}}$ and the reaction forces at the stabilizers. By enforcing the lower and upper boundary conditions and the orientation of the initial undeformed configuration of the BHA, the coefficients A and B can be computed.

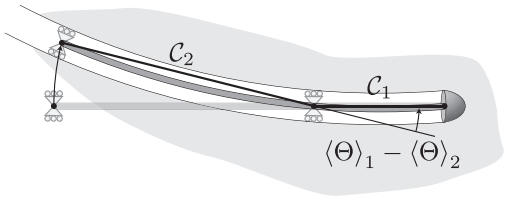

Figure 3.8: The constraints brought by the borehole on the deformation of a 2-stabilizer BHA deforming in a vertical plane is quantified by the difference in inclination $\langle \Theta \rangle_1 - \langle \Theta \rangle_2$.

3.5.6 Solution

Once the deformed configuration of the BHA is known, the moments and lateral forces on the bit can be computed from (3.40b) and (3.40c). After some algebra, they are expressed as

$$\begin{aligned}
\hat{F}_2 &= \mathcal{F}_b \frac{3EI}{\lambda_1^2}\left(\hat{\theta} - \langle\Theta\rangle_1\right) + \mathcal{F}_w w\lambda_1 \sin\langle\Theta\rangle_1 + \mathcal{F}_r \breve{F}_2 + \frac{3EI}{\lambda_1^2}\sum_{i=1}^{n-1} \mathcal{F}_i \left(\langle\Theta\rangle_i - \langle\Theta\rangle_{i+1}\right), \\
\hat{M}_3 &= \mathcal{M}_b \frac{3EI}{\lambda_1}\left(\hat{\theta} - \langle\Theta\rangle_1\right) + \mathcal{M}_w w\lambda_1^2 \sin\langle\Theta\rangle_1 + \mathcal{M}_r \lambda_1 \breve{F}_2 + \frac{3EI}{\lambda_1}\sum_{i=1}^{n-1} \mathcal{M}_i \left(\langle\Theta\rangle_i - \langle\Theta\rangle_{i+1}\right), \\
\hat{F}_3 &= \mathcal{F}_b \frac{3EI}{\lambda_1^2}\left(\hat{\phi} - \langle\Phi\rangle_1\right) \sin\langle\Theta\rangle_1 + \mathcal{F}_r \breve{F}_3 + \frac{3EI}{\lambda_1^2}\sum_{i=1}^{n-1} \mathcal{F}_i \left(\langle\Phi\rangle_i - \langle\Phi\rangle_{i+1}\right) \sin\langle\Theta\rangle_1, \\
\hat{M}_2 &= -\mathcal{M}_b \frac{3EI}{\lambda_1}\left(\hat{\phi} - \langle\Phi\rangle_1\right) \sin\langle\Theta\rangle_1 - \mathcal{M}_r \lambda_1 \breve{F}_3 - \frac{3EI}{\lambda_1}\sum_{i=1}^{n-1} \mathcal{M}_i \left(\langle\Phi\rangle_i - \langle\Phi\rangle_{i+1}\right) \sin\langle\Theta\rangle_1 .
\end{aligned} \tag{3.45}$$

The right-hand sides are linear expressions of the loads and constraints imposed on the BHA. The influence coefficients $\mathcal{F}$ and $\mathcal{M}$ are numbers that only depend on the geometry of the BHA, that is on the position of the RSS and stabilizers; see Appendix C for the expressions of $\mathcal{F}$ and $\mathcal{M}$. They are numbers of the order of $O(1)$. The terms with subscript b account for the relative orientation of the bit with respect to the chord $\mathcal{C}_1$, which is a priori unknown. (The factor $3EI/\lambda_1^2$ is introduced here for convenience and will be justified as a consequence of the scaling used in the next section.) The terms with subscript w account for the gravity loading, while the terms with subscript r express the dependence of the forces and moments at the bit on the RSS force $\breve{\boldsymbol{F}}$, with components $\breve{F}_2$ and $\breve{F}_3$. Finally, the terms with subscript i account for the constraints imposed by the geometry of the borehole.

The components of the bit lateral force and moment provided in (3.45) by the model of the BHA are measured with respect to the chord $\mathcal{C}_1$, that is, with respect to the undeformed initial configuration of the BHA. They are thus strictly speaking different from the components of the bit forces introduced in the interface laws (3.17). But, on account of the small difference in orientation between the chord $\mathcal{C}_1$ and the bit axis $\hat{\boldsymbol{i}}_1$, no distinction is made between these two sets of components (see Appendix D for a discussion on the error brought by this simplification).

Chapter 4

Evolution Equations

The equations governing the three elements of the directional drilling model form together a closed system of equations; that is, they are sufficient to describe the propagation of the borehole and the evolution of the deformed configuration of the BHA, given appropriate initial conditions.

The mathematical model can be reduced to a set of four evolution equations in terms of the inclination $\hat{\Theta}(L)$ and azimuth $\hat{\Phi}(L)$ of the borehole at the bit and the inclination $\hat{\theta}(L)$ and azimuth $\hat{\phi}(L)$ of the bit axis. An alternative set of variables substitutes $\hat{\theta}(L)$ and $\hat{\phi}(L)$ by the tilt angles $\psi_2(L)$ and $\psi_3(L)$; they are related according to (3.4). These variables are piecewise continuous functions of the length L of the borehole. At the scale of the BHA, the borehole inclination and azimuth describe the borehole axis $\mathcal{B}$ or equivalently the trajectory of the reference point of the bit. The tilt angles ψ_2 and ψ_3 are interpreted as a measure of the borehole cross-sectional area since it has been suggested that the enlargement of the borehole diameter with respect to the bit diameter is related to these tilt angles (Fig. 3.6).

The first section of this chapter scales the equations governing the elements of the model. The second one explains how the equations governing the elements of the problem can be reduced to a set of four evolution equations in $\hat{\Theta}(L)$, $\hat{\Phi}(L)$, $\hat{\theta}(L)$, and $\hat{\phi}(L)$. These evolution equations are given in the third section. Finally, a set of simulations illustrates the response of the system under typical drilling conditions.

4.1 Scaling

The problem is viewed at the scale of the BHA. Thus, it is scaled using the distance λ_1 from the bit to the first stabilizer and the bending stiffness EI of the BHA. These two quantities combine to define the characteristic force $F_* = 3EI/\lambda_1^2$, which has a simple physical interpretation: F_* is the reaction force induced at the end of a simply supported beam of length λ_1 and stiffness EI in response to a unit inclination angle imposed at that end.

The dimensionless length of the borehole $\xi = L/\lambda_1$ is the variable used to measure the lengthening of the borehole; it is the independent variable for the differential equations governing the evolution of the system. Also, scaling the borehole curvature vector yields $\boldsymbol{\kappa} = \lambda_1 \boldsymbol{K}$ with components κ_2 and κ_3 along $\boldsymbol{I}_2$ and $\boldsymbol{I}_3$.

With the introduction of the characteristic length λ_1, the geometry of the BHA reduces to n numbers: the scaled distances between the stabilizers $\varkappa_i = \lambda_i/\lambda_1$, $i = 2, \ldots, n$, and the distance Λ between the bit and the RSS. (To simplify later expressions, the scaled length of the first segment of BHA will be sometimes written $\varkappa_1$ although its value is always 1). While Λ is typically in the range [0.15, 0.35], all the numbers $\varkappa_i$ are of order $O(1)$ (see Table 7.2).

Scaling the first equation $\hat{F}_1 = -G_1 - H_1 d_1$ of the bit/rock interface laws (3.17) yields a linear relationship between the axial penetration d_1 and the scaled component of the weight on bit associated with penetration $\Pi = -(\hat{F}_1 + G_1)/F_*$. The number Π, which is typically of order $O(10^{-1})$, is a measure of the active weight on bit, that is the weight minus the reaction force transmitted by the cutters wearflats.

After consideration of the kinematic relationships (3.20) and (3.21), the scaled bit/rock interface laws for the lateral forces on the bit reduce to

$$\begin{Bmatrix} \hat{F}_2/F_* \\ \hat{F}_3/F_* \end{Bmatrix} = \eta\Pi \begin{bmatrix} \cos\varpi & \sin\varpi \\ -\sin\varpi & \cos\varpi \end{bmatrix} \begin{Bmatrix} \psi_2 \\ \psi_3 \end{Bmatrix}. \tag{4.1}$$

The lateral steering resistance $\eta = \sqrt{H_2^2 + H_3^2}/H_1$ is a positive number that measures the relative difficulty of imposing a lateral penetration to the bit compared to an axial penetration. It usually ranges between 10 and 100 (Menand et al., 2002; Perneder et al., 2012), and mainly depends on the aggressiveness and height of the bit gauge. The force $\eta\Pi F_*$ can be interpreted as a measure of the resistance offered by the bit/rock interface to a tilt of the bit. Consequently,

the dimensionless group $\eta\Pi$ can be viewed as a relative measure of this resistance against the stiffness of the BHA.

Similarly, the expressions of the bit moments in (3.17) are scaled to yield

$$\left\{ \begin{array}{c} \hat{M}_2/F_*\lambda_1 \\ \hat{M}_3/F_*\lambda_1 \end{array} \right\} = -\chi\Pi \left\{ \begin{array}{c} \lambda_1\varphi_2/d_1 \\ \lambda_1\varphi_3/d_1 \end{array} \right\}. \tag{4.2}$$

The angular steering resistance $\chi = H_0/\lambda_1^2 H_1$ measures the difficulty of imposing an angular penetration to the bit relative to an axial penetration. It is typically one to two orders of magnitude smaller than η. It can be shown, using expressions for the coefficients of the bit/rock interface laws provided in Appendix A, that the ratio χ/η is proportional to $(b/\lambda_1)^2$. In other words, χ/η contrasts the dimensions of the bit with the length of the first segment of BHA. The dimensionless group $\chi\Pi$ measures the resistance of the system against an angular penetration.

Finally, two dimensionless quantities are introduced after scaling the RSS force $\breve{\boldsymbol{F}}$ and the weight w,

$$\boldsymbol{\Gamma} = \frac{\breve{\boldsymbol{F}}}{F_*}, \qquad \Upsilon = \frac{w\lambda_1}{F_*}. \tag{4.3}$$

In summary, the scaled directional drilling problem can be described by n geometric numbers, $\varkappa_i$, $i = 2, \ldots, n$, and Λ, two numbers, $\eta\Pi$ and $\chi\Pi$, that contrast the resistance of the bit to penetration with the stiffness of the BHA, the bit walk angle ϖ, one number Υ representing the ratio of the weight of the first segment of the BHA to the characteristic force, and finally the RSS force $\boldsymbol{\Gamma}$, which is a control parameter. The orders of magnitude of these dimensionless parameters are $\eta\Pi = O(1)$, $\chi\Pi = O(10^{-2})$, $\Gamma = O(10^{-2})$, $\Upsilon = O(10^{-3} \sim 10^{-2})$ (Table 7.2).

4.2 Derivation

Each element of the model provides a set of four equations.

The bit/rock interaction laws reduce to (4.1) and (4.2). The fifth interface equation relating the axial penetration d_1 to the axial force $\hat{F}_1$ can be used to estimate the advancement rate of the borehole given by

$$\frac{\mathrm{d}L}{\mathrm{d}t} = d_1 \frac{\Omega}{2\pi}. \tag{4.4}$$

This drilling rate does not influence the directional tendency of the system as a consequence of the assumed rate-independency of the drilling process.

The geometric relations (3.4) and kinematic relationships (3.23) are reproduced here after scaling;

$$\begin{aligned} \psi_2 &= \left(\hat{\theta} - \hat{\Theta}\right), \\ \psi_3 &= \left(\hat{\phi} - \hat{\Phi}\right) \sin\hat{\Theta}, \end{aligned} \tag{4.5a}$$

$$\begin{aligned} -\frac{\mathrm{d}\hat{\phi}}{\mathrm{d}\xi} \sin\hat{\theta} &= \frac{\lambda_1 \varphi_2}{d_1}, \\ \frac{\mathrm{d}\hat{\theta}}{\mathrm{d}\xi} &= \frac{\lambda_1 \varphi_3}{d_1}. \end{aligned} \tag{4.5b}$$

After scaling, the expressions (3.45) of the forces and moments on the bit derived from the BHA model yield

$$\begin{aligned} \frac{\hat{F}_2}{F_*} &= \mathcal{F}_b \left(\hat{\theta} - \langle\Theta\rangle_1\right) + \mathcal{F}_w \Upsilon \sin\langle\Theta\rangle_1 + \mathcal{F}_r \Gamma_2 + \sum_{i=1}^{n-1} \mathcal{F}_i \left(\langle\Theta\rangle_i - \langle\Theta\rangle_{i+1}\right), \\ \frac{\hat{M}_3}{F_* \lambda_1} &= \mathcal{M}_b \left(\hat{\theta} - \langle\Theta\rangle_1\right) + \mathcal{M}_w \Upsilon \sin\langle\Theta\rangle_1 + \mathcal{M}_r \Gamma_2 + \sum_{i=1}^{n-1} \mathcal{M}_i \left(\langle\Theta\rangle_i - \langle\Theta\rangle_{i+1}\right), \\ \frac{\hat{F}_3}{F_*} &= \mathcal{F}_b \left(\hat{\phi} - \langle\Phi\rangle_1\right) \sin\langle\Theta\rangle_1 + \mathcal{F}_r \Gamma_3 + \sum_{i=1}^{n-1} \mathcal{F}_i \left(\langle\Phi\rangle_i - \langle\Phi\rangle_{i+1}\right) \sin\langle\Theta\rangle_1, \\ \frac{\hat{M}_2}{F_* \lambda_1} &= -\mathcal{M}_b \left(\hat{\phi} - \langle\Phi\rangle_1\right) \sin\langle\Theta\rangle_1 - \mathcal{M}_r \Gamma_3 - \sum_{i=1}^{n-1} \mathcal{M}_i \left(\langle\Phi\rangle_i - \langle\Phi\rangle_{i+1}\right) \sin\langle\Theta\rangle_1. \end{aligned} \tag{4.6}$$

Equations (4.1), (4.2), (4.5), and (4.6) can be reduced to a system of four equations in the unknown functions $\hat{\Theta}$, $\hat{\Phi}$, $\hat{\theta}$, and $\hat{\phi}$.

4.3 Solutions

From now on and throughout the remainder of this dissertation, we exclusively focus on investigating the dynamical equations governing the evolution of $\hat{\Theta}$, $\hat{\Phi}$, $\hat{\theta}$, and $\hat{\phi}$. The notation is hereafter simplified by first dropping the hat used to suggest that a variable is evaluated at the bit. Also, all the variables are functions of the scaled length ξ of the borehole and the notation $'$ denotes a derivative with respect to ξ.

The general evolution equations are derived and two particular cases are then considered. The first particular case pertains to a borehole constrained to evolve in a vertical plane on the assumption that $\varpi = 0$ and $\Gamma_3 = 0$. The evolution equations then reduce to two equations in the borehole and bit inclinations, Θ and θ. This simpler 2D problem will be extensively used as its behavior is qualitatively similar to the more general 3D case. The second particular case corresponds to the degenerated problem of an infinitely stiff BHA, $EI \to \infty$. In this case, the nature of the evolution equations changes.

4.3.1 General Solution

The general evolution equations are given by

$$\begin{aligned}
&\eta\Pi\left[(\theta-\Theta)\cos\varpi + (\phi-\Phi)\sin\Theta\,\sin\varpi\right] \\
&\qquad = \mathcal{F}_b\left(\theta - \langle\Theta\rangle_1\right) + \mathcal{F}_w\Upsilon\sin\langle\Theta\rangle_1 + \mathcal{F}_r\Gamma_2 + \sum_{i=1}^{n-1}\mathcal{F}_i\left(\langle\Theta\rangle_i - \langle\Theta\rangle_{i+1}\right), \qquad (4.7a)\\
&-\chi\Pi\theta' \\
&\qquad = \mathcal{M}_b\left(\theta - \langle\Theta\rangle_1\right) + \mathcal{M}_w\Upsilon\sin\langle\Theta\rangle_1 + \mathcal{M}_r\Gamma_2 + \sum_{i=1}^{n-1}\mathcal{M}_i\left(\langle\Theta\rangle_i - \langle\Theta\rangle_{i+1}\right), \qquad (4.7b)\\
&\eta\Pi\left[-(\theta-\Theta)\sin\varpi + (\phi-\Phi)\sin\Theta\,\cos\varpi\right] \\
&\qquad = \mathcal{F}_b\left(\phi - \langle\Phi\rangle_1\right)\sin\langle\Theta\rangle_1 + \mathcal{F}_r\Gamma_3 + \sum_{i=1}^{n-1}\mathcal{F}_i\left(\langle\Phi\rangle_i - \langle\Phi\rangle_{i+1}\right)\sin\langle\Theta\rangle_1, \qquad (4.7c)\\
&-\chi\Pi\phi'\sin\theta \\
&\qquad = \mathcal{M}_b\left(\phi - \langle\Phi\rangle_1\right)\sin\langle\Theta\rangle_1 + \mathcal{M}_r\Gamma_3 + \sum_{i=1}^{n-1}\mathcal{M}_i\left(\langle\Phi\rangle_i - \langle\Phi\rangle_{i+1}\right)\sin\langle\Theta\rangle_1. \qquad (4.7d)
\end{aligned}$$

where the integral terms read

$$\begin{aligned}
\langle\Theta\rangle_i &= \frac{1}{\varkappa_i}\int_{\xi_i}^{\xi_{i-1}}\Theta(\zeta)\mathrm{d}\zeta, \\
\langle\Phi\rangle_i &= \frac{1}{\varkappa_i}\int_{\xi_i}^{\xi_{i-1}}\Phi(\zeta)\mathrm{d}\zeta,
\end{aligned}
\qquad \text{with} \qquad
\begin{aligned}
\xi_{i-1} &= \xi - \sum_{j=1}^{i-1}\varkappa_j, \\
\xi_i &= \xi - \sum_{j=1}^{i}\varkappa_j,
\end{aligned}
\qquad i = 1,\ldots,n. \qquad (4.8)$$

The position ξ_i is the curvilinear coordinate of the i^{th} stabilizer on the borehole axis when the borehole has length ξ. Physically, these terms are used to account for the constraints

imposed by the borehole on the deformation of the BHA, which ultimately influence the borehole propagation.

The system (4.7) can further be reduced to two equations in Θ and Φ of the form

$$\begin{aligned}\Theta'(\xi) = F_\Theta\big(&\Theta(\xi),\Phi(\xi),\Theta(\xi_1),\ldots,\Theta(\xi_n),\Phi(\xi_1),\ldots,\Phi(\xi_n),\\ &\langle\Theta\rangle_1,\ldots,\langle\Theta\rangle_n,\langle\Phi\rangle_1,\ldots,\langle\Phi\rangle_n;\Pi,\Gamma_2,\Gamma_3,\Pi',\Gamma_2',\Gamma_3'\big),\\ \Phi'(\xi) = F_\Phi\big(&\Theta(\xi),\Phi(\xi),\Theta(\xi_1),\ldots,\Theta(\xi_n),\Phi(\xi_1),\ldots,\Phi(\xi_n),\\ &\langle\Theta\rangle_1,\ldots,\langle\Theta\rangle_n,\langle\Phi\rangle_1,\ldots,\langle\Phi\rangle_n;\Pi,\Gamma_2,\Gamma_3,\Pi',\Gamma_2',\Gamma_3'\big).\end{aligned} \tag{4.9}$$

where the continuous functions F_Θ and F_Φ embody properties of the drilling system. The reduction of (4.7) into (4.9) uses first (4.7a) and (4.7c) to derive expressions for the bit inclination θ and azimuth ϕ in terms of Θ and Φ, which are then differentiated and introduced into (4.7b) and (4.7d) after observing that

$$\begin{aligned}\langle\Theta\rangle_i' &= \frac{1}{\varkappa_i}\left[\Theta(\xi_{i-1}) - \Theta(\xi_i)\right],\\ \langle\Phi\rangle_i' &= \frac{1}{\varkappa_i}\left[\Phi(\xi_{i-1}) - \Phi(\xi_i)\right].\end{aligned} \tag{4.10}$$

Equations (4.7), or equivalently (4.9), are a set of functional differential equations, meaning that the rate of change of the state variables is determined by the present but also the past values of these variables via the secular terms in $\langle\Theta\rangle_i$ and $\langle\Phi\rangle_i$, $i = 1,\ldots,n$. The nature of the problem is thus of an infinite dimensional system (Stepan, 1989). The maximum length of retardation is the length of the BHA, $\sum_{j=1}^{n}\varkappa_j$. It is the maximum distance from which information on the geometry of the borehole feedbacks into the system.

The system (4.7) can be brought to a system of first order delay differential equations (DDE). For this purpose, additional state variables are introduced as the averaged inclinations $\langle\Theta\rangle_1,\ldots,\langle\Theta\rangle_n$ and azimuths $\langle\Phi\rangle_1,\ldots,\langle\Phi\rangle_n$. The $2n$ additional equations are given in (4.10). This observation is of interest as the mathematical theory for DDE is better developed than the more general functional differential equation theory.

The system is said to be of a retarded type (Hale, 1977) to emphasize that the right-hand sides in (4.9) are independent of the history of Θ' and Φ'. This terminology is used to make a distinction with so-called neutral functional differential equations. This second family of

equations involves delayed evaluation of the rate of change of the unknown variables. Our system will actually appear to degenerate into a neutral type under certain conditions, in which case the right-hand sides in (4.9) will also include terms in $\Theta'(\xi_1), \ldots, \Theta'(\xi_n)$ and $\Phi'(\xi_1), \ldots, \Phi'(\xi_n)$.

Solving (4.7) requires to specify initial conditions on the interval $\xi \in [\xi_0 - \sum_{j=1}^{n} \varkappa_j, \xi_0]$, where ξ_0 is the initial length of borehole. Without loss of generality, the initial conditions are specified on the interval $\xi \in [-\sum_{j=1}^{n} \varkappa_j, 0]$, that is $\xi_0 = 0$; in that case, ξ is no longer the total length of the borehole but rather the distance from the initial point $\xi_0 = 0$. A solution to this initial condition problem is the set of functions $\{\Theta, \Phi, \theta, \phi\}$ defined on the interval $\xi \in [-\sum_{j=1}^{n} \varkappa_j, \xi_f)$ with $\xi_f > 0$ such that the initial conditions are respected on the interval $\xi \in [-\sum_{j=1}^{n} \varkappa_j, 0]$ and the evolution equations (4.7) are satisfied on the interval $\xi \in [0, \xi_f)$.

The control parameters used to guide the borehole trajectory are the axial force transmitted to the bit, indirectly measured by Π, and the RSS force $\mathbf{\Gamma}$. The system is linear in the components Γ_2 and Γ_3 of the RSS force, a consequence of the linearity of the beam equations governing the model of the BHA. The active weight on bit Π plays a rather different role as it multiplies the rate of change of the state variables.

If the input variables Π and $\mathbf{\Gamma}$ are continuous functions of ξ, a solution to the initial condition problem exists and is unique except when $\sin\Theta = 0$ (that is when the azimuthal direction Φ is no longer well defined). Also, the continuous dependence of a solution on the initial conditions and parameters of the problem is ensured for Π and $\mathbf{\Gamma}$ continuous (see Hale (1977) for a general statement of the theorem of existence, uniqueness and continuous dependence for retarded functional differential equations).

The problem is generalized by accepting the possibility of sudden variations in the values of the weight on bit and RSS force. Formally, Π and $\mathbf{\Gamma}$ are thus defined as piecewise continuous functions of ξ and jumps of amplitudes $[\![\Pi]\!]$ and $[\![\mathbf{\Gamma}]\!]$ are allowed. Such discontinuities result in jumps in the magnitudes of the state variables; their amplitudes $[\![\Theta]\!]$, $[\![\Phi]\!]$, $[\![\theta]\!]$, and $[\![\phi]\!]$ can be related to $[\![\Pi]\!]$ and $[\![\mathbf{\Gamma}]\!]$. The investigation of these discontinuities uses the framework of generalized functions.

The formulation of the problem defines a first set of variables associated with the vertical plane $(\boldsymbol{I}_1, \boldsymbol{I}_2)$ tangent to the borehole, e.g., the inclination Θ, the tilt angle ψ_2, and the RSS force Γ_2 (Figs. 3.1 and 3.7). A second set of variables can be viewed as related to the inclined

plane $(\boldsymbol{I}_1, \boldsymbol{I}_3)$, e.g., the azimuth Φ, tilt angle ψ_3, and RSS force Γ_3. It is observed that the vertical and azimuthal behaviors of the system (4.7) are coupled as a consequence of the walk tendency of the bit and the influence of the inclination on the azimuthal behavior.

4.3.2 2D Solution

If the bit has a neutral walk tendency ($\varpi = 0$), the evolution equations (4.7) yield

$$\eta\Pi\left(\theta - \Theta\right) = \mathcal{F}_b\left(\theta - \langle\Theta\rangle_1\right) + \mathcal{F}_w\Upsilon\sin\langle\Theta\rangle_1 + \mathcal{F}_r\Gamma_2 + \sum_{i=1}^{n-1}\mathcal{F}_i\left(\langle\Theta\rangle_i - \langle\Theta\rangle_{i+1}\right), \tag{4.11a}$$

$$-\chi\Pi\theta' = \mathcal{M}_b\left(\theta - \langle\Theta\rangle_1\right) + \mathcal{M}_w\Upsilon\sin\langle\Theta\rangle_1 + \mathcal{M}_r\Gamma_2 + \sum_{i=1}^{n-1}\mathcal{M}_i\left(\langle\Theta\rangle_i - \langle\Theta\rangle_{i+1}\right), \tag{4.11b}$$

$$\eta\Pi\left(\phi - \Phi\right) = \mathcal{F}_b\left(\phi - \langle\Phi\rangle_1\right) + \mathcal{F}_r\frac{\Gamma_3}{\sin\Theta} + \sum_{i=1}^{n-1}\mathcal{F}_i\left(\langle\Phi\rangle_i - \langle\Phi\rangle_{i+1}\right), \tag{4.11c}$$

$$-\chi\Pi\phi' = \mathcal{M}_b\left(\phi - \langle\Phi\rangle_1\right) + \mathcal{M}_r\frac{\Gamma_3}{\sin\Theta} + \sum_{i=1}^{n-1}\mathcal{M}_i\left(\langle\Phi\rangle_i - \langle\Phi\rangle_{i+1}\right), \tag{4.11d}$$

after making the approximation $\sin\theta \simeq \sin\langle\Theta\rangle_1 \simeq \sin\Theta$. In this case, the evolution of the inclinations Θ and θ, governed by (4.11a) and (4.11b), is decoupled from the azimuthal dynamics. Also, equations (4.11c) and (4.11d) governing the azimuthal evolution of the system are similar to (4.11a) and (4.11b); the differences are that the weight Υ has no component in the azimuthal direction and that the factor $1/\sin\Theta$ amplifies the RSS force Γ_3.

Equations (4.11a) and (4.11b) can further be reduced to a single functional differential equation governing the evolution of the borehole inclination. If the active weight on bit Π is constant,

this equation yields

$$\begin{aligned}\chi\Pi\Theta'(\xi) = &-\mathcal{M}_b\left[\Theta(\xi) - \langle\Theta\rangle_1\right] + \frac{\chi}{\eta}\mathcal{F}_b\left[\Theta(\xi) - \Theta(\xi_1)\right] \\ &+ \sum_{i=1}^{n-1}\left[\frac{\mathcal{F}_b\mathcal{M}_i - \mathcal{F}_i\mathcal{M}_b - \mathcal{M}_i\eta\Pi}{\eta\Pi}\right]\left(\langle\Theta\rangle_i - \langle\Theta\rangle_{i+1}\right) \\ &- \frac{\chi}{\eta}\sum_{i=1}^{n-1}\mathcal{F}_i\left(\frac{\Theta(\xi_{i-1}) - \Theta(\xi_i)}{\varkappa_i} - \frac{\Theta(\xi_i) - \Theta(\xi_{i+1})}{\varkappa_{i+1}}\right) \\ &+ \frac{\mathcal{F}_b\mathcal{M}_w - \mathcal{F}_w\mathcal{M}_b - \mathcal{M}_w\eta\Pi}{\eta\Pi}\Upsilon\sin\langle\Theta\rangle_1 \\ &- \frac{\chi}{\eta}\mathcal{F}_w\Upsilon\left[\Theta(\xi) - \Theta(\xi_1)\right]\cos\langle\Theta\rangle_1 \\ &+ \frac{\mathcal{F}_b\mathcal{M}_r - \mathcal{F}_r\mathcal{M}_b - \mathcal{M}_r\eta\Pi}{\eta\Pi}\Gamma_2 - \frac{\chi}{\eta}\mathcal{F}_r\Gamma_2'. \end{aligned} \tag{4.12}$$

It governs the evolution of a borehole evolving in a vertical plane, for which (i) $\varpi = 0$ and (ii) all the loads on the BHA are in this vertical plane. The rate of change of the borehole inclination Θ' (that is the borehole curvature if the azimuth Φ is constant) is impacted by (i) the borehole geometry (lines 1 to 3 in this last expression), (ii) the distributed weight Υ (lines 4 and 5), and (iii) the RSS force Γ_2 (line 6). With the exception of the terms in Υ, the right-hand side is linear in the borehole inclination.

4.3.3 Rigid BHA

The case of an infinitely rigid BHA is contemplated from an academic standpoint and is viewed as the limit case of an increasing stiffness EI of the BHA. Speaking about an infinitely rigid BHA is only relevant when the BHA has 1 or 2 stabilizers; for 3 or more stabilizers, an infinitely stiff BHA is over-constrained and the only valid solution is a straight borehole. Note that, despite its simplicity, the toy problem of a BHA with 1 stabilizer is not totally unrealistic. In practice, a flexible element is often placed in the BHA between the first and the second stabilizer, with the purpose of reducing the impact of the rest of the BHA on the directional behavior of the system. Typically, its bending stiffness is about a third of that of the other elements constituting the BHA. Ideally, this flexible element operates as a hinge and the BHA can be conceptualized as a 1-stabilizer BHA.

The model for a BHA with a large bending stiffness EI is rescaled using the alternate

characteristic force $\bar{F}_* = w\lambda_1$, which is the buoyant weight of the first segment of BHA. New dimensionless quantities are thus defined as

$$\bar{\Pi} = -\frac{\hat{F}_1 + G_1}{\bar{F}_*}, \qquad \bar{\mathbf{\Gamma}} = \frac{\breve{\boldsymbol{F}}}{\bar{F}_*}. \tag{4.13}$$

Also, for EI large,

$$\Upsilon = \frac{\bar{F}_*}{F_*} = \frac{w\lambda_1^3}{3EI} \tag{4.14}$$

is a small parameter that gives a measure of the compliance of the BHA. The infinitely stiff case thus corresponds to taking the limit $\Upsilon \to 0$.

1-Stabilizer BHA

To simplify the exposition of the one-stabilizer rigid case, the problem is discussed for a borehole propagating in a vertical plane. The generalization to 3D is straightforward. If $\varpi = 0$, the evolution equations for the bit and the borehole inclinations yield after rescaling

$$\eta\bar{\Pi}\Upsilon\left(\theta - \Theta\right) = -\left(\theta - \langle\Theta\rangle_1\right) + \frac{5}{8}\Upsilon\sin\langle\Theta\rangle_1 - \frac{2 - 3\Lambda^2 + \Lambda^3}{2}\Upsilon\bar{\Gamma}_2, \tag{4.15a}$$

$$-\chi\bar{\Pi}\Upsilon\theta' = \left(\theta - \langle\Theta\rangle_1\right) - \frac{1}{8}\Upsilon\sin\langle\Theta\rangle_1 + \frac{\Lambda\left(2 - 3\Lambda + \Lambda^2\right)}{2}\Upsilon\bar{\Gamma}_2. \tag{4.15b}$$

These equations can further be reduced to a single equation in the borehole inclination Θ, given by

$$\begin{aligned}\chi\bar{\Pi}\Upsilon\Theta'\left(\xi\right) + \left(1 + \frac{\chi}{\eta}\right)\Theta\left(\xi\right) = \frac{\chi}{\eta}\Theta\left(\xi - 1\right) + \langle\Theta\rangle_1 \\ - \frac{4 - \eta\bar{\Pi}\Upsilon}{8\eta\bar{\Pi}}\sin\langle\Theta\rangle_1 - \frac{5\chi}{8\eta}\Upsilon\left[\Theta\left(\xi\right) - \Theta\left(\xi - 1\right)\right]\cos\langle\Theta\rangle_1 \\ + \frac{\left(1 - \Lambda\right)\left[2 - \Lambda\left(2 - \Lambda\right)\eta\bar{\Pi}\Upsilon\right]}{2\eta\bar{\Pi}}\bar{\Gamma}_2 + \frac{\chi}{\eta}\frac{\left(2\Lambda - 3\Lambda^2 + \Lambda^3\right)}{2}\Upsilon\bar{\Gamma}_2'.\end{aligned} \tag{4.16}$$

The limit case of an infinitely rigid BHA with one stabilizer is sketched in Figure 4.1. After taking the limit $\Upsilon \to 0$, the evolution equations (4.15) reduce to

$$\theta = \langle\Theta\rangle_1, \tag{4.17a}$$

$$\left(1 + \frac{\chi}{\eta}\right)\Theta\left(\xi\right) = \frac{\chi}{\eta}\Theta\left(\xi - 1\right) + \langle\Theta\rangle_1 - \frac{1}{2\eta\bar{\Pi}}\sin\langle\Theta\rangle_1 + \left(1 - \Lambda\right)\frac{\bar{\Gamma}_2}{\eta\bar{\Pi}}. \tag{4.17b}$$

For an infinitely stiff BHA, the bit axis $\hat{\boldsymbol{i}}_1$ is aligned with the BHA, this is formally expressed by (4.17a). Equation (4.17b) is a functional equation of neutral type: the borehole curvature $\Theta'(\xi)$ at the bit, depends on its curvature $\Theta'(\xi-1)$ at the stabilizer. In this respect, they are of a different nature than the retarded system (4.15).

2-Stabilizer BHA

For an infinitely rigid 2-stabilizer BHA, the spatial position of the stabilizers prescribes the location of the drill bit (Fig. 4.2): the problem is purely geometric and the only relevant parameter that survives is the ratio $\varkappa_2 = \lambda_2/\lambda_1$ between the lengths of the two BHA segments. A solution of the rigid system depends on $\varkappa_2$ and the initial borehole geometry. In that sense, the rigid 2-stabilizer problem is drastically different from the 1-stabilizer case.

After rescaling, taking the limit $\Upsilon \to 0$ of the evolution equations (4.7) yields

$$\begin{aligned} \theta &= \langle \Theta \rangle_1 = \langle \Theta \rangle_2 \,, \\ \phi &= \langle \Phi \rangle_1 = \langle \Phi \rangle_2 \,. \end{aligned} \tag{4.18}$$

They express that the orientations of the bit axis $\hat{\boldsymbol{i}}_1$ and of the two segments of BHA are the same. The evolution equation for the borehole inclination can equivalently be written after differentiation as

$$\Theta(\xi) = \left(1 + \frac{1}{\varkappa_2}\right) \Theta(\xi - 1) - \frac{1}{\varkappa_2} \Theta(\xi - 1 - \varkappa_2) \,, \tag{4.19}$$

a delay difference equation. The same equation governs the azimuth Φ.

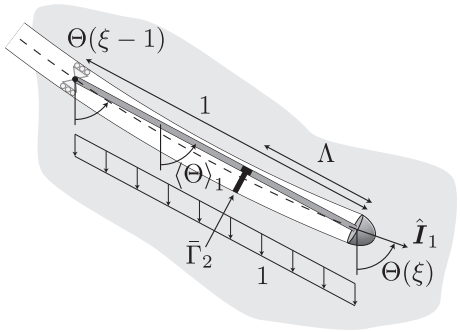

Figure 4.1: Scaled model of a 1-stabilizer stiff BHA in the vertical plane $(\boldsymbol{I}_1, \boldsymbol{I}_2)$ of the borehole.

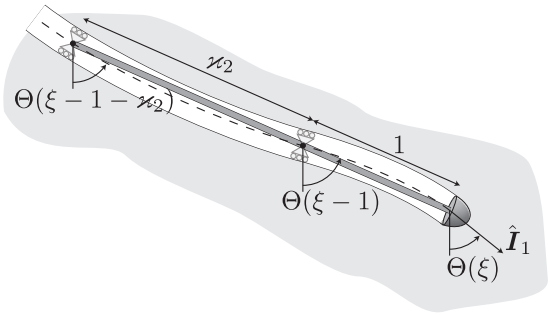

Figure 4.2: Scaled model of a 2-stabilizer stiff BHA in the vertical plane $(\boldsymbol{I}_1, \boldsymbol{I}_2)$ of the borehole.

Chapter 5

Qualitative Response: Three Length Scales

The main objective of this chapter is to describe qualitatively the behavior of the system governed by (4.7). Typically, three scales are identified in the response: a short scale $O(10^{-1})$, an intermediate scale $O(1)$, and a large scale $O(10^{2})$. The first section justifies their existence using dimensional analysis arguments applied to (4.7). After explaining how an initial condition can be numerically propagated, the second section provides a set of examples that validates these qualitative properties.

5.1 Qualitative Response

A short-range evolution is associated with a fast dynamics controlled by the small parameter $\chi\Pi = O(10^{-2})$, which multiplies the θ'- and ϕ'-terms in (4.7). This dimensionless group, $\chi\Pi$, is a measure of the resistance against a change of bit orientation; its small magnitude thus allows for fast changes in the bit and borehole orientation. Also, on this short range, the secular terms in $\langle\Theta\rangle_i$ and $\langle\Phi\rangle_i$, $i = 1, \ldots, n$, and the forcing terms in Υ and $\mathbf{\Gamma}$ are quasi-constant. In other words, this fast dynamics is at first order governed by a system of ODE obtained by freezing the magnitudes of the secular and forcing terms. It will be argued in Section 6.1 that the scale

associated with this behavior is of the order of $O[(b/\lambda_1)^2]$, where b is the half length of the bit.

The forcing parameters $\Gamma = O(10^{-2})$ and $\Upsilon = O(10^{-3})$ are small so that the borehole inclination is expected to vary slowly, that is, the borehole curvature κ is small. As a consequence, the gravity terms in Υ are quasi-constant forcing terms on a length scale that is at least an order of magnitude smaller than the radius of curvature of the borehole. The intermediate range is defined accordingly and is thus dominated by the secular influence of the borehole geometry on the deformation of the BHA, measured by the terms $\langle\Theta\rangle_i$ and $\langle\Phi\rangle_i$, $i = 1, \ldots, n$, in (4.7). In this respect, the intermediate dynamics is controlled by the position of the stabilizers along the BHA; it is intrinsically related to the dimensionless group $\eta\Pi$ and to the influence coefficients $\mathcal{F}$ and $\mathcal{M}$, all numbers of order $O(1)$.

But in many cases (see Section 6.3), it will appear that this transient behavior converges and the system evolves in such a way that the secular terms reach (quasi-)stationarity on the intermediate scale. The corresponding asymptotic solutions are characteristic of a large scale behavior, whose evolution is now dominated by the small forcing parameters $\mathbf{\Gamma}$ and Υ.

The solutions corresponding to constant secular terms are such that the deformed configuration of the BHA in the borehole is stationary; in other words, the motion of the BHA axis is a rigid body motion. The solutions allowing for such an evolution are boreholes with a constant curvature. The large scale asymptotes are thus investigated after making the assumption that the variations of borehole curvature are negligible on a length of borehole equivalent to the length of the BHA; in other words, at the scale of the BHA, the system sees a constant-curvature borehole. Formally, the ersatz

$$\begin{aligned} \Theta(\xi) &= \kappa_{2s}(\xi)\,\xi, \\ \Phi(\xi) &= \frac{\kappa_{3s}(\xi)}{\sin\Theta}\xi \end{aligned} \tag{5.1}$$

is defined with κ_{2s} and κ_{3s} being slowly-varying curvature components of the borehole, that is $\kappa'_{2s}/\kappa_{2s} \ll 1$ and $\kappa'_{3s}/\kappa_{3s} \ll 1$. It can be introduced in the evolution equation (4.7), to yield an equation of the form

$$A \left\{ \begin{array}{c} \kappa_{2s}(\xi) \\ \kappa_{3s}(\xi) \end{array} \right\} = B\Upsilon \sin\langle\Theta\rangle + C \left\{ \begin{array}{c} \Gamma_2 \\ \Gamma_3 \end{array} \right\}, \tag{5.2}$$

if the control parameters Γ_2, Γ_3, and Π are constant. This equation governs the slow dynamics

on a length scale at least an order of magnitude larger than the length of the BHA. The slowly varying inclination $\langle\Theta\rangle_1$ has been here substituted by an overall BHA, or alternatively borehole, inclination $\langle\Theta\rangle$ since the BHA is now viewed as a rigid and small object. Strictly speaking and without loss of generality, the curvature components can rather be defined in terms of this averaged BHA inclination; for example $\kappa_{2s} = \langle\Theta\rangle'$. The matrices A, B, and C depends on the drilling parameters and are of the order of $O(1)$. Equation (5.2) is an ODE as the delayed dependence on the borehole geometry to vanish at this scale of order $O(10^2)$.

Finally, the large-scale asymptotes converge to stationary solutions if the borehole inclination Θ reaches equilibrium, or equivalently, if the component κ_{2s} of the curvature vector vanishes. The corresponding borehole trajectories are helices winding around a vertical axis. These solutions are the equilibrium points of the dynamical system (4.7).

5.2 Simulations

The following numerical simulations exemplify the qualitative behavior discussed in the previous section. But first, the discontinuities generated by a sudden change in drilling parameters are investigated. Understanding how they arise and propagate along a solution path is crucial for solving the problem numerically.

Three examples are then provided. The first gives the solution for a bit with a neutral walk tendency ($\varpi = 0$); in this case we focus on the 2D behavior of the system in a vertical plane, which is governed by the inclination equation (4.12). The second example considers a left walk tendency of the bit ($\varpi = -15°$), while keeping the other drilling parameters unchanged, and solves the evolution equations (4.7). The last set of examples simulates the infinitely stiff cases with 1 and 2 stabilizers.

5.2.1 Smoothness of the Solution

The control forces applied on the system, Π and $\mathbf{\Gamma}$, are discontinuous functions of ξ since jumps of amplitudes $[\![\Pi]\!]$ and $[\![\mathbf{\Gamma}]\!]$ are allowed. In view of (4.7), such discontinuities in the forcing translate into (i) jumps in the borehole orientation measured by $[\![\Theta]\!]$ and $[\![\Phi]\!]$, meaning that the borehole is locally kinked, and (ii) jumps in the rate of change of the bit orientation, $[\![\theta']\!]$

and $[\![\phi']\!]$. An abrupt change in bit orientation is not possible if $\chi > 0$ since it would require a moment of infinitely large magnitude on the bit (a consequence of the bit/rock interface laws).

The evolution equations (4.7) are used to derive relationships between the amplitudes of the jumps in the forcing functions and in the variables Θ, Φ, θ', and ϕ'. At a point of discontinuity, the left and right-handed limits (respectively the limits for increasing and decreasing ξ) of the borehole inclination and azimuth are related according to $\Theta^+ = \Theta^- + [\![\Theta]\!]$ and $\Phi^+ = \Phi^- + [\![\Phi]\!]$. Jumps in the RSS force components $[\![\Gamma_2]\!]$ and $[\![\Gamma_3]\!]$ translate into discontinuities of magnitude

$$
\begin{aligned}
[\![\Theta]\!] &= \mathcal{F}_r \frac{\sin\varpi\,[\![\Gamma_3]\!] - \cos\varpi\,[\![\Gamma_2]\!]}{\eta\Pi},\\
[\![\Phi]\!] &= -\frac{[\mathcal{F}_r\cos\varpi\,[\![\Gamma_3]\!] + \mathcal{F}_r\sin\varpi\,[\![\Gamma_2]\!] + \eta\Pi\,(\phi-\Phi^-)\,(\sin\Theta^- - \sin\Theta^+)]\csc\Theta^+}{\eta\Pi},\\
[\![\theta']\!] &= -\mathcal{M}_r\frac{[\![\Gamma_2]\!]}{\chi\Pi},\\
[\![\phi']\!] &= -\mathcal{M}_r\frac{\csc\theta\,[\![\Gamma_3]\!]}{\chi\Pi}.
\end{aligned}
\tag{5.3}
$$

Similar expressions can be derived for a jump $[\![\Pi]\!]$ in the active weight on bit; the discontinuities are then given by

$$
\begin{aligned}
[\![\Theta]\!] &= \left(\theta-\Theta^-\right)\frac{[\![\Pi]\!]}{\Pi^+},\\
[\![\Phi]\!] &= \left(\phi-\Phi^-\right)\left[1-\frac{\Pi^-\sin\Theta^-\,\csc\Theta^+}{\Pi^+}\right],\\
[\![\theta']\!] &= -\theta^{-'}\frac{[\![\Pi]\!]}{\Pi^+},\\
[\![\phi']\!] &= -\phi^{-'}\frac{[\![\Pi]\!]}{\Pi^+},
\end{aligned}
\tag{5.4}
$$

which are independent of the bit walk angle ϖ.

Finally, the initial conditions on $[-\sum_{j=1}^n \varkappa_j, 0]$ do not necessarily verify the evolution equations, that is, they are not physical. In that case the solution is not continuous across $\xi = 0$.

The system governed by (4.7) is a retarded system. The solutions become smoother: if the initial conditions on $[-\sum_{j=1}^n \varkappa_j, 0]$ is continuous, the solution is continuously differentiable on $(0, \sum_{j=1}^n \varkappa_j]$, twice-continuously differentiable on $(\sum_{j=1}^n \varkappa_j, 2\sum_{j=1}^n \varkappa_j]$, and so on (Michiels and Niculescu, 2007). This means that a discontinuity in the borehole orientation feedbacks into the system and induces a jump discontinuity of a lesser order, e.g., a jump in the borehole inclination $[\![\Theta]\!]$ at $\xi = 0$ produces on the interval $\xi \in (0, \sum_{j=1}^n \varkappa_j]$ jumps in the borehole curvature Θ'.

The story is different for the rigid cases, governed by (4.17) and (4.18), which are of neutral type. Solutions to neutral systems do not benefit from the same smoothening property. For example, a jump in the borehole inclination $[\![\Theta]\!]$ will propagate as discontinuities of the same order, with amplified or reduced magnitude.

5.2.2 Numerical Resolution

The solutions are computed in Matlab using a simple implicit finite difference scheme of (4.7) for the general 3D problem, or of (4.11a) and (4.11b) for the degenerate 2D problem in a vertical plane. The discretization step $\Delta\xi$ is constant. The derivatives θ' and ϕ' are approximated using the Euler backward formula and the integrals in the right hand sides are evaluated using the trapezoidal rule. Alternatively, the 2D evolution equation for the inclination (4.12) has also been solved using the built-in delay differential equation solver from Mathematica 8. To this effect, equation (4.12) is first differentiated with respect to ξ. The remaining integrals $\langle\Theta\rangle_1$ in the Υ-terms are then approximated by $[\Theta(\xi) + \Theta(\xi - 1)]/2$, the averaged of the borehole inclinations at the bit and at the first stabilizer; this approximation is good only when the variations of borehole inclination on a unit length of borehole are small. This procedure yields a delay differential equation of the second order in the inclination Θ; the n spatial delays in this equation correspond to the n stabilizers. The solutions computed using these two methods are in good agreement.

5.2.3 2D Simulation

A specific set of parameters is defined that will be used in the following simulations and throughout Chapters 6 and 7. It considers a $4^3/4$" push-the-bit RSS. The BHA is equipped with three stabilizers, with the corresponding segment lengths given by $\lambda_1 = 3.5\,\mathrm{m}$, $\lambda_2 = 7\,\mathrm{m}$, $\lambda_3 = 15\,\mathrm{m}$. The actuating pads of the RSS are 1 m away from the bit. According to Table 7.1, $w = 0.88\,\mathrm{kN/m}$ and $EI = 2 \times 10^3\,\mathrm{kNm^2}$. The weight on bit is fixed to $|\hat{F}_1| = 30\,\mathrm{kN}$ and the constant RSS force has a magnitude of $\breve{F} = 2.45\,\mathrm{kN}$. The bit bluntness and rock properties are chosen so that $G_1 = 10\,\mathrm{kN}$. The lateral and angular steering resistances are respectively selected to be $\eta = 25$

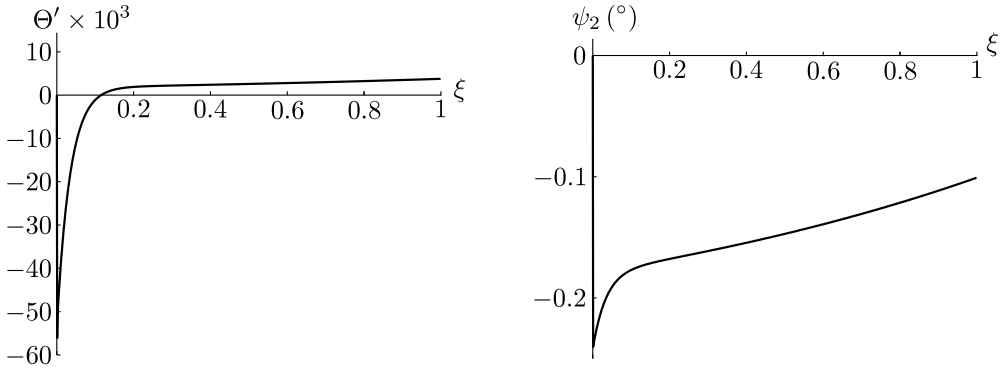

(a) Borehole curvature.

(b) Bit tilt ψ_2.

Figure 5.1: Short-range 2D simulation. The system parameters are $\varkappa_2 = 2$, $\varkappa_3 = 4.285$, $\Lambda \simeq 0.29$, $\eta = 25$, $\chi = 1$, $\varpi = 0$, $\Upsilon \simeq 6.3 \times 10^{-3}$, $\Pi = 4.08 \times 10^{-2}$, $\Gamma_2 = 5 \times 10^{-3}$, and $\Gamma_3 = 0$.

and $\chi = 1$; they correspond to a bit with a rather long passive gauge. In view of the above description, $\Upsilon \simeq 6.3 \times 10^{-3}$, $\Gamma = 5 \times 10^{-3}$, $\Pi = 4.08 \times 10^{-2}$, and $\Lambda \simeq 0.29$.

The first simulation considers a bit with a neutral walk tendency and the RSS force is in the vertical plane of the borehole, that is, $\Gamma_2 = \Gamma$ and $\Gamma_3 = 0$. The problem is thus confined to this vertical plane and the evolution of Θ and θ is computed. The initial conditions assume a straight vertical borehole and a straight undeformed BHA. At $\xi = 0$, the RSS force is applied and kept constant.

The solution initially jumps to an inclination of $\Theta^+ = 0.0042°$ and a curvature of $\Theta^{+'} = -0.054$ at $\xi = 0^+$; in this case, the kink induced by the brusque change in the RSS force is thus negligible for any practical purpose. At $\xi = 0$, the curvature is locally infinite and can be represented by a Dirac Delta function whose amplitude is equal to the initial jump in the borehole inclination. Follows a fast evolution of the curvature Θ' and bit tilt ψ_2 on the interval $\xi \in [0, 0.1]$ (Figs. 5.1a and 5.1b). These signs will be interpreted as the emergence of a boundary layer due to the small parameter $\chi\Pi$.

The intermediate-range evolution for the curvature and bit tilt is given in Figures 5.2a and 5.2b for $\xi \in [0, 10]$. At $\xi = 1$, $\xi = 1 + \varkappa_2$, and $\xi = 1 + \varkappa_2 + \varkappa_3$, the borehole curvature is discontinuous, a consequence of the discrete delay terms in (4.12). Physically, when a stabilizer passes through the inclination discontinuity at $\xi = 0$, it induces a discontinuity of lesser order

at the bit, that is, a discontinuity in the curvature. The effect of this discontinuous behavior appears to diminish quickly and the curvature seems to converge to a quasi-constant value.

The borehole inclination then varies slowly and converges toward a stationary inclination (Fig. 5.3a). The curvature of the borehole Θ' slowly decays and appears to vanish for $\xi \to \infty$ as the inclination stabilizes (Fig. 5.3b). This behavior occurs on a large range, which is several orders of magnitude bigger than the total length of the BHA.

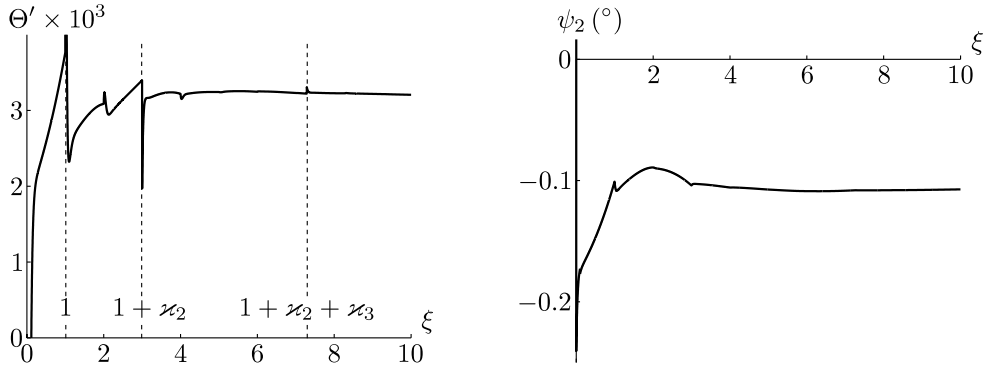

(a) Borehole curvature.

(b) Bit tilt ψ_2.

Figure 5.2: Intermediate-range 2D simulation. The system parameters are $\varkappa_2 = 2$, $\varkappa_3 = 4.285$, $\Lambda \simeq 0.29$, $\eta = 25$, $\chi = 1$, $\varpi = 0$, $\Upsilon \simeq 6.3 \times 10^{-3}$, $\Pi = 4.08 \times 10^{-2}$, $\Gamma_2 = 5 \times 10^{-3}$, and $\Gamma_3 = 0$.

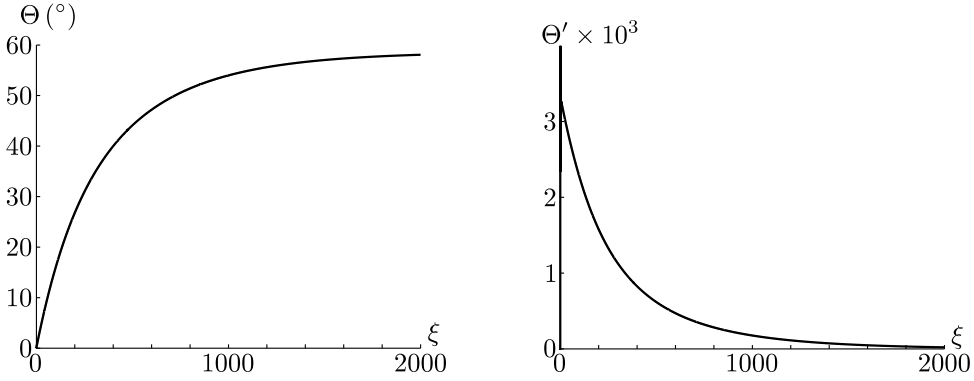

(a) Borehole inclination.

(b) Borehole curvature.

Figure 5.3: Long-range 2D simulation. The system parameters are $\varkappa_2 = 2$, $\varkappa_3 = 4.285$, $\Lambda \simeq 0.29$, $\eta = 25$, $\chi = 1$, $\varpi = 0$, $\Upsilon \simeq 6.3 \times 10^{-3}$, $\Pi = 4.08 \times 10^{-2}$, $\Gamma_2 = 5 \times 10^{-3}$, and $\Gamma_3 = 0$.

In practice, the borehole is steered at the intermediate scale. Typically, the trajectory of the borehole is sampled every 100 feet (~ 30 m) by downhole sensors and the commands controlling the RSS are adjusted at this same rate. Hence, the intermediate scale is the most important one for directional drilling applications.

5.2.4 3D Simulation

The only parameters that differ from the previous example are (i) the bit walk angle, set to $\varpi = -15°$, and (ii) the RSS force, which is tilted by an angle $\tau = 45°$ so that the RSS force is no longer in the vertical plane of the borehole and $\Gamma_2 = \Gamma_3 = \Gamma/\sqrt{2}$. The initial conditions consider a straight borehole inclined by 10° on the vertical and with azimuth $\Phi = 0$ (the initial inclination needs to be different than 0 in order to have well defined azimuthal angles). The initial configuration of the BHA is aligned with the borehole. At $\xi = 0$, a constant RSS force is applied. The solution solves for Θ, Φ, θ, and ϕ, which are governed by (4.7).

The evolutions of the borehole inclination Θ and its corresponding component $\kappa_2 = \Theta'$ of the curvature vector are qualitatively similar to the 2D case (Figs. 5.4a and 5.4c are comparable to 5.2a and 5.3a). The medium-range evolution of the azimuthal curvature $\kappa_3 = \Phi' \sin\Theta$ is similar to the component κ_2 (Fig. 5.4b). The azimuth Φ does not stabilize but appears to reach a steady rate of change Φ' for ξ large (Fig. 5.4d). The stationary borehole geometry, corresponding to a constant inclination and constant Φ', is a helical borehole with a vertical axis.

It can finally be noticed that for these examples (2D and 3D), the assumptions introduced in Section 3.1 hold. In particular, the radius of curvature of the borehole and the tilt angles ψ_2 and ψ_3 are everywhere small.

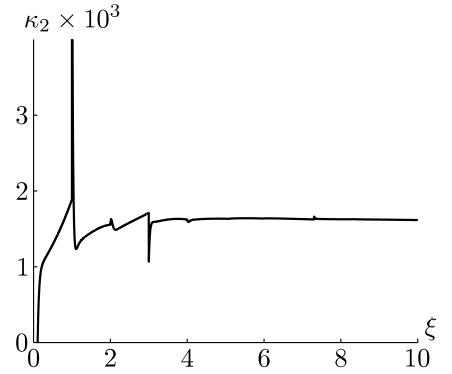

(a) Medium-range evolution of the borehole curvature $\kappa_2 = \Theta'$.

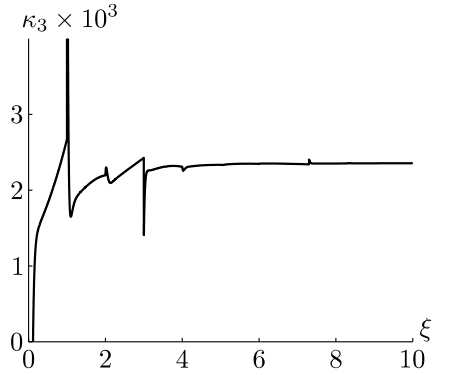

(b) Medium-range evolution of the borehole curvature $\kappa_3 = \Phi' \sin\Theta$.

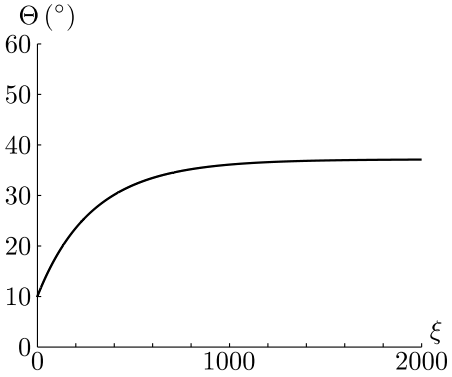

(c) Long-range evolution of the borehole inclination.

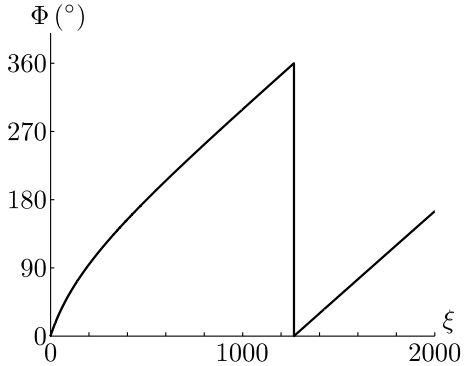

(d) Long-range evolution of the borehole azimuth.

Figure 5.4: Simulation of the 3D problem governed by (4.7). The system parameters are $\varkappa_2 = 2$, $\varkappa_3 = 4.285$, $\Lambda \simeq 0.29$, $\eta = 25$, $\chi = 1$, $\varpi = -15^\circ$, $\Upsilon \simeq 6.3 \times 10^{-3}$, $\Pi = 4.08 \times 10^{-2}$, $\Gamma_2 = 3.54 \times 10^{-3}$, and $\Gamma_3 = 3.54 \times 10^{-3}$.

5.2.5 Rigid Simulations

The infinitely stiff solutions are given for one and two stabilizers and are compared with the solutions for a BHA of finite but increasing stiffness EI.

1-Stabilizer BHA

Figure 5.5 shows the 2D evolution of the inclination for a borehole propagating in a vertical plane after setting $\varpi = 0$ and $\Gamma_3 = 0$. This example varies the stiffness of the BHA measured by Υ in (4.15). The lateral steering resistance η has been set to 1, which is unrealistic in practice

but is used here to accentuate the features of the response. The borehole and BHA are initially vertical and at $\xi = 0$ a constant RSS force is applied. A jump in the borehole inclination is induced at $\xi = 0$ whether the BHA is rigid or flexible. This initial discontinuity propagates into discontinuities of lesser order if the BHA is flexible, $\Upsilon > 0$. On the contrary, for the rigid BHA, whenever the stabilizer passes through a discontinuity, it induces a discontinuity of the same order but with an amplitude reduced by a factor $\chi/(\eta + \chi)$. Hence, the inclination for the rigid BHA is not only discontinuous at $\xi = 0$ but also at $\xi = 1, 2, \ldots$ (Fig. 5.5).

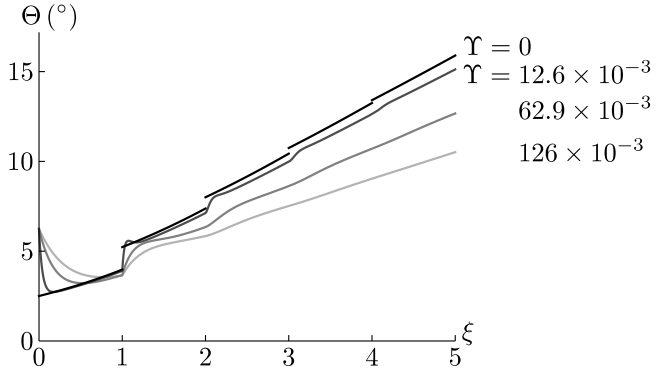

Figure 5.5: Inclination Θ of a borehole evolving in a vertical plane for various stiffnesses of the BHA. The borehole and BHA are initially vertical. The system parameters are $\Lambda \simeq 0.29$, $\eta = 1$, $\chi = 1$, $\varpi = 0$, $\bar{\Pi} = 6.49$, $\bar{\Gamma}_2 = 0.795$, and $\bar{\Gamma}_3 = 0$.

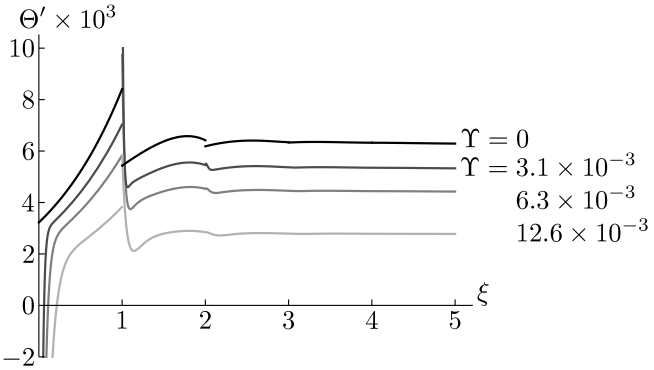

Figure 5.6: Curvature Θ' of a borehole evolving in a vertical plane for various stiffnesses of the BHA. The borehole and BHA are initially vertical. The system parameters are $\Lambda \simeq 0.29$, $\eta = 25$, $\chi = 1$, $\varpi = 0$, $\bar{\Pi} = 6.49$, $\bar{\Gamma}_2 = 0.795$, and $\bar{\Gamma}_3 = 0$.

The borehole curvature is plotted in Figure 5.6 for the more realistic case of $\eta = 25$. The system is singularly perturbed with respect to the small parameter $\chi\Pi$ and an initial layer becomes apparent at $\xi = 0$.

The intermediate- and large-range behaviors of the rigid case with 1 stabilizer are qualitatively similar to the flexible case.

2-Stabilizer BHA

Figure 5.7 illustrates the propagation of a piecewise linear initial condition by the rigid system (4.18) and compares it with the solutions for BHA of finite stiffnesses. The solution appears to quickly converge toward a quasi-constant curvature solution for a small stiffness of the BHA (Fig. 5.7a). As the rigidity increases ($\Upsilon \to 0$), the stability is lost and the solution starts to oscillate (Figs. 5.7b and 5.7c).

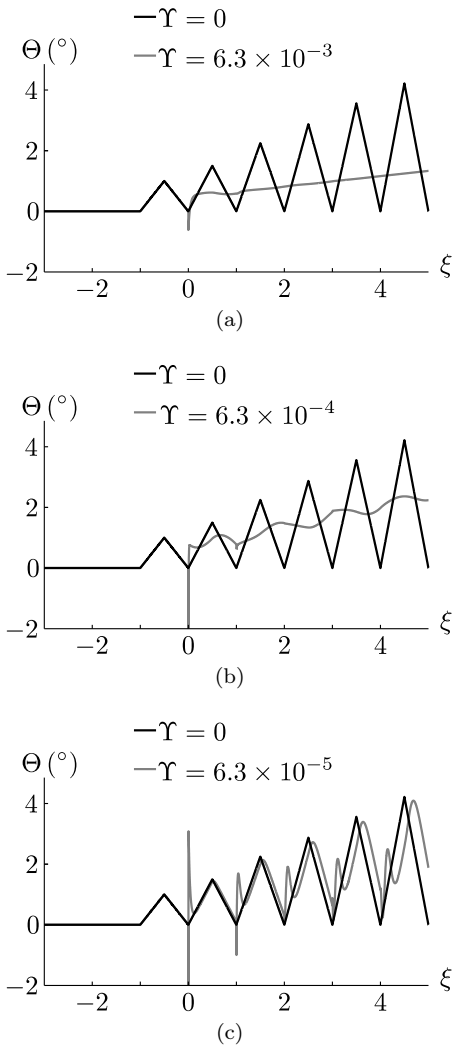

Figure 5.7: Evolution of the borehole inclination Θ for various magnitudes of Υ measuring the stiffness of the BHA. The system parameters are $\varkappa_2 = 2$, $\Lambda \simeq 0.29$, $\eta = 25$, $\chi = 1$, $\varpi = 0$, $\bar{\Pi} = 6.49$, $\bar{\Gamma}_2 = 0.795$, and $\bar{\Gamma}_3 = 0$. The initial condition is defined as a piecewise linear function on $\xi \in [-3, 0]$.

Chapter 6

Asymptotic et Stability Analyses

As argued in Section 5.1, the short-range asymptotes correspond to a fast dynamics allowed by small values of $\chi\Pi$. In Section 6.1, this behavior is interpreted as the emergence of a boundary layer and in the limit $\chi\Pi \to 0$ the system (4.7) is singularly perturbed.

Section 6.2 studies the long-range solutions. They are obtained independently of their stability; in other words, they are derived after assuming that the intermediate dynamics converges to solutions governed by (5.2).

Finally, Section 6.3 deals with a stability analysis that investigates (i) the convergence of the intermediate-range dynamics to a long-range asymptote but also (ii) the stability of equilibrium solutions.

6.1 Short-Range Asymptotes

The short-range evolution is investigated in relation to the dimensionless group $\chi\Pi$, which embodies properties of the bit, the rock, and the BHA, and the axial force transmitted to the bit. But we are here mainly interested in understanding the influence of χ on the fast dynamics.

The angular steering resistance χ measures the difficulty to change the orientation of the bit while drilling. With the exception of the contribution of Neubert (1997), other theoretical investigations consider the bit free to change its orientation, that is $\chi = 0$. The resistance of

the bit against a change in orientation has never been measured, as experimental investigations to determine the directional behavior of drill bits generally focus on determining the lateral steering resistance η only.

The ratio χ/η is proportional to $(b/\lambda_1)^2$ so that in general $\chi/\eta \ll 1$, a consequence of (A.7). It is thus legitimate to wonder whether this parameter significantly impacts the solution.

The 2D problem governed by (4.11a) and (4.11b) is considered. Figure 6.1 plots the short-range evolution of the borehole and bit inclinations for various magnitudes of χ. The borehole and BHA are initially vertical and at $\xi = 0$ a constant RSS force is imposed. For $\chi \neq 0$, the bit inclination is continuous through $\xi = 0$ and is thus given by the initial condition, $\theta(0) = 0$. A fast variation in the bit orientation follows; it is interpreted as a boundary layer (Hinch, 1991). As $\chi \to 0$, this boundary layer degenerates into a discontinuity in the bit inclination at $\xi = 0$.

The small parameter $\epsilon = \chi\Pi$ is introduced and an inner solution is derived in the stretched coordinate

$$\zeta = \frac{\xi}{\epsilon}. \tag{6.1}$$

The equation (4.11b) for the bit inclination θ thus becomes

$$-\tilde{\theta}' = \mathcal{M}_b \left(\tilde{\theta} - \langle\Theta\rangle_1\right) + \mathcal{M}_w \Upsilon \sin\langle\Theta\rangle_1 + \mathcal{M}_r \Gamma_2 + \sum_{i=1}^{n-1} \mathcal{M}_i \left(\langle\Theta\rangle_i - \langle\Theta\rangle_{i+1}\right), \tag{6.2}$$

where $\tilde{\theta}(\zeta)$ is the bit inclination as a function of ζ. At first order, the integral terms $\langle\Theta\rangle_1, \ldots, \langle\Theta\rangle_n$ are constant in the boundary layer if ϵ is small: the windows on which they are evaluated move by an incremental distance of order $O(\epsilon)$ in the unstretched coordinate ξ so that their variations are also of order $O(\epsilon)$. The inner solution is thus obtained for Γ_2 and $\langle\Theta\rangle_1, \ldots, \langle\Theta\rangle_n$ taken as constants and is given by

$$\tilde{\theta}(\zeta) = \left(e^{-\mathcal{M}_b \zeta} - 1\right) \left[-\langle\Theta\rangle_1 + \frac{\mathcal{M}_w}{\mathcal{M}_b} \Upsilon \sin\langle\Theta\rangle_1 + \frac{\mathcal{M}_r}{\mathcal{M}_b} \Gamma_2 + \sum_{i=1}^{n-1} \frac{\mathcal{M}_i}{\mathcal{M}_b} \left(\langle\Theta\rangle_i - \langle\Theta\rangle_{i+1}\right) \right], \tag{6.3}$$

with initial condition $\tilde{\theta}(0) = 0$ (Fig. 6.1a). The thickness of the layer is of the order of $O(\chi\Pi/\mathcal{M}_b) = O(\chi\Pi)$.

For ζ large, the departure between the exact and inner solutions is due to the variations in the secular terms $\langle\Theta\rangle_1, \ldots, \langle\Theta\rangle_n$, which can no longer be seen as constants outside the initial layer.

This short-range behavior in the bit inclination θ has a repercussion on the borehole inclination Θ, which also displays a fast and local variation (Fig. 6.1b). On the intermediate range, this behavior is replicated further along the borehole with a delay corresponding to the distances from the bit to the stabilizers. For example, the borehole curvature in Figure 5.2a presents a boundary layer at $\xi = 0$, which induces a similar behavior at $\xi = 1$, $\xi = 1 + \varkappa_2$, and $\xi = 1 + \varkappa_2 + \varkappa_3$.

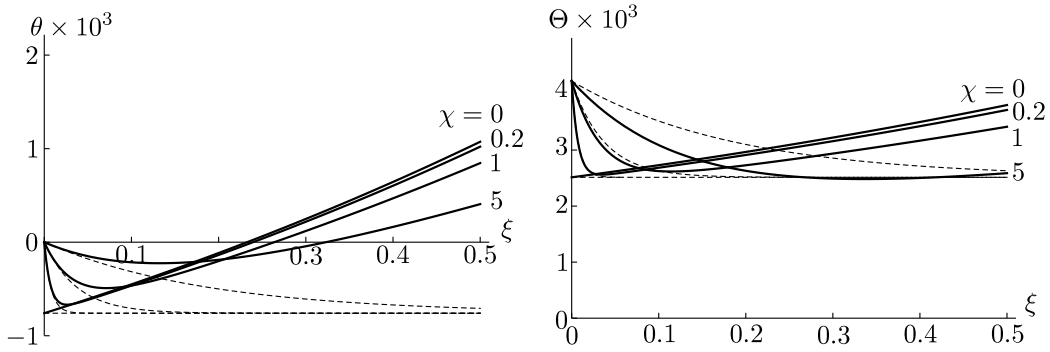

(a) Bit inclination.

(b) Borehole inclination.

Figure 6.1: 2D simulations for various magnitudes of the angular steering resistance χ. The numerical solutions are in solid lines and the inner solutions in dashed lines. The borehole and the BHA are initially straight and vertical. At $\xi = 0$, a constant RSS force is imposed. The system parameters are the same as in Section 5.2: $\varkappa_2 = 2$, $\varkappa_3 = 4.285$, $\Lambda \simeq 0.29$, $\eta = 25$, $\varpi = 0$, $\Upsilon \simeq 6.3 \times 10^{-3}$, $\Pi = 4.08 \times 10^{-2}$, $\Gamma_2 = 5 \times 10^{-3}$, and $\Gamma_3 = 0$.

The drilling model is constructed with the bit/rock interface laws collapsed onto a point so that the model resolution is at least of the order of the bit dimension, $O(b/\lambda_1)$. Hence, speaking about a boundary layer is only relevant when its dimensions are larger than the model resolution. It is usually not the case and the boundary layer should rather be interpreted as a jump discontinuity in θ at the scale of the model. (The bit/rock interaction laws are derived after assuming the bit kinematics to be stationary. In the boundary layer, this assumption fails and the validity of these interface laws is questionable.)

These conclusions can be generalized to the 3D problem with $\varpi \neq 0$ and to other cases for which $\chi\Pi \to 0$. For example, as the stiffness of the BHA is increased, $EI \to \infty$, a similar behavior is observed (Figs. 5.5, 5.6, and 5.7).

6.2 Long-Range Asymptotes and Equilibrium

After assuming convergence of the intermediate dynamics, the long-range evolution is associated with situations for which all the forces acting on the BHA are quasi-constant when measured in a reference system attached to the BHA. These forces only vary significantly on a length of borehole at least an order of magnitude larger than the length of the BHA. As suggested by (5.2), they are (i) forces proportional to the borehole curvature, (ii) the distributed weight $\Upsilon \sin\langle\Theta\rangle$, and (iii) the RSS force. On the long range, the slowly-varying inclination $\langle\Theta\rangle$ is interpreted as the averaged borehole inclination on the length of the BHA.

This quasi-invariance of the loading has two implications. First, the averaged motion of the BHA axis appears to be that of a rigid body since the averaged deformed configuration of the BHA remains almost unchanged on a length of borehole equivalent to the length of the BHA. Second, the penetration variables, which are associated with the advancement of the borehole, are quasi-stationary. The solutions that meet these conditions are boreholes with slowly-varying curvature components given by (5.2). The existence of such solutions evidently requires that the rock has homogeneous and isotropic properties and the RSS force and weight on bit are constant.

The long-range asymptotes are characterized by four geometric parameters. At the length scale of the BHA, the borehole axis is described by the components κ_{2s} and κ_{3s} of the quasi-constant curvature vector $\boldsymbol{\kappa}_s$ along the axes $\boldsymbol{I}_2$ and $\boldsymbol{I}_3$ (Fig. 6.2). The description is completed by the tilt angles ψ_{2s} and ψ_{3s}, proxies for the borehole cross-sectional area. These variables depend on the orientation of the BHA measured by the averaged inclination $\langle\Theta\rangle$ and azimuth $\langle\Phi\rangle$. The general expressions for the state variables are locally given by

$$\begin{aligned} \Theta &= \langle\Theta\rangle + \kappa_{2s}\xi, & \Phi &= \frac{\kappa_{3s}\xi}{\sin\langle\Theta\rangle}, \\ \theta &= \langle\Theta\rangle + \kappa_{2s}\xi + \psi_{2s}, & \phi &= \frac{\kappa_{3s}\xi + \psi_{3s}}{\sin\langle\Theta\rangle}. \end{aligned} \tag{6.4}$$

These expressions are valid as long as the departure of Θ from $\langle\Theta\rangle$ remains small. (The azimuthal direction is defined up to a constant which is set here to zero.) The mathematical model (4.7) of a directional drilling system constrained to propagate along a trajectory (6.4) yields a set of four algebraic equations in terms of the geometric parameters of the long-range solutions.

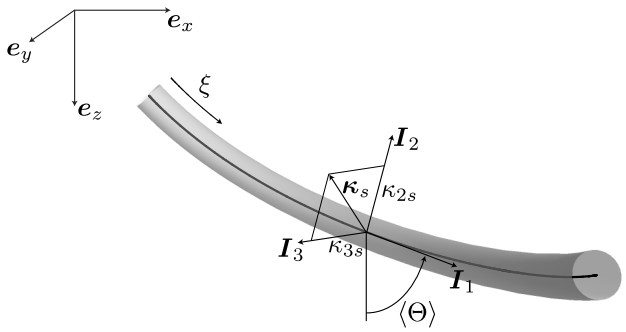

Figure 6.2: A borehole with a quasi-constant curvature vector $\boldsymbol{\kappa}_s$ when measured in the local BHA basis $(\boldsymbol{I}_1, \boldsymbol{I}_2, \boldsymbol{I}_3)$.

At the limit, the system reaches equilibrium if the borehole inclination converges, that is, if $\kappa_{2s} \to 0$. The equilibrium borehole trajectories are thus helices defined by a constant inclination Θ_∞ and constant curvature κ_∞ (Fig. 6.3). The plane $(\boldsymbol{I}_1, \boldsymbol{I}_3)$ is the plane in which the helix is curving, the so-called osculating plane. It contains the osculating circle defined locally as the best second order approximation of the helix and thus has the same radius of curvature $1/|\kappa_\infty|$ as the borehole. Formally, the curvature κ_∞ of the borehole is defined as

$$\kappa_\infty = \sin\Theta_\infty \frac{\mathrm{d}\Phi}{\mathrm{d}\xi}. \tag{6.5}$$

Hence, the general expressions for the state variables at equilibrium are now given by

$$\begin{aligned} \Theta &= \Theta_\infty, & \Phi &= \frac{\kappa_\infty \xi}{\sin\Theta_s}, \\ \theta &= \Theta_\infty + \psi_{2\infty}, & \phi &= \frac{\kappa_\infty \xi + \psi_{3\infty}}{\sin\Theta_\infty}. \end{aligned} \tag{6.6}$$

The equilibrium solutions degenerate into straight boreholes if $\kappa_\infty = 0$ and into a horizontal circular boreholes if $\Theta_\infty = \pi/2$.

To our knowledge, the general class of helical stationary solutions has only been studied by Perneder and Detournay (2013c), although solutions exist for the particular cases of straight boreholes (Lubinski and Woods, 1953; Bradley, 1975; Perneder and Detournay, 2013a) and circular boreholes in a vertical plane (Murphey and Cheatham, 1966; Fischer, 1974; Birades and Fenoul, 1986; Jogi et al., 1988; Pastusek et al., 2005; Downton, 2007). The straight borehole solutions are a particular case of helical boreholes and the latter circular boreholes in a vertical plane are a particular case of long-range asymptotes for which the azimuthal direction is constant.

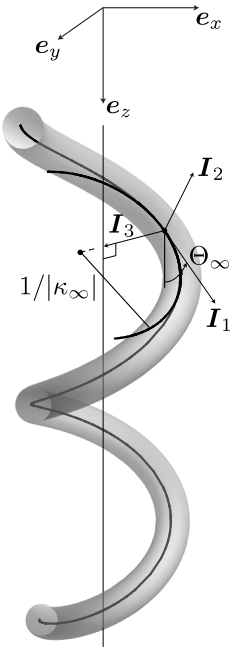

Figure 6.3: A right-handed helical borehole propagating downward. The axis of the borehole is characterized by its inclination $\Theta_\infty \in [0, \pi]$ and signed curvature κ_∞.

6.2.1 Solutions

Enforcing the system (4.7) to propagate according to the asymptotic evolution (6.4) provides a set of equations that can be solved for the geometric parameters describing the long-range solutions. Without loss of generality, the derivation is exemplified for $\varpi = 0$. Replacing Θ, Φ, θ, and ϕ in (4.11) by their expressions in (6.4) yields

$$\begin{aligned}
\eta\Pi\psi_{2s} &= \mathcal{F}_b\psi_{2s} + \frac{1}{2}\left[\mathcal{F}_b + \sum_{i=1}^{n-1}\mathcal{F}_i\left(\varkappa_i + \varkappa_{i+1}\right)\right]\kappa_{2s} + \mathcal{F}_w\Upsilon\sin\langle\Theta\rangle + \mathcal{F}_r\Gamma_2,\\
-\chi\Pi\kappa_{2s} &= \mathcal{M}_b\psi_{2s} + \frac{1}{2}\left[\mathcal{M}_b + \sum_{i=1}^{n-1}\mathcal{M}_i\left(\varkappa_i + \varkappa_{i+1}\right)\right]\kappa_{2s} + \mathcal{M}_w\Upsilon\sin\langle\Theta\rangle + \mathcal{M}_r\Gamma_2,\\
\eta\Pi\psi_{3s} &= \mathcal{F}_b\psi_{3s} + \frac{1}{2}\left[\mathcal{F}_b + \sum_{i=1}^{n-1}\mathcal{F}_i\left(\varkappa_i + \varkappa_{i+1}\right)\right]\kappa_{3s} + \mathcal{F}_r\Gamma_3,\\
-\chi\Pi\kappa_{3s} &= \mathcal{M}_b\psi_{3s} + \frac{1}{2}\left[\mathcal{M}_b + \sum_{i=1}^{n-1}\mathcal{M}_i\left(\varkappa_i + \varkappa_{i+1}\right)\right]\kappa_{3s} + \mathcal{M}_r\Gamma_3.
\end{aligned} \tag{6.7}$$

The expressions are simplified and generalized for any number n of stabilizers by introducing the additional coefficients $\mathcal{F}_\kappa$ and $\mathcal{M}_\kappa$ given by

$$\mathcal{F}_\kappa = \frac{1}{2}\left[\mathcal{F}_b + \sum_{i=1}^{n-1} \mathcal{F}_i \left(\varkappa_i + \varkappa_{i+1}\right)\right],$$
$$\mathcal{M}_\kappa = \frac{1}{2}\left[\mathcal{M}_b + \sum_{i=1}^{n-1} \mathcal{M}_i \left(\varkappa_i + \varkappa_{i+1}\right)\right]. \tag{6.8}$$

These coefficients depend on the geometry of the BHA only. They measure the influence of a constant curvature of the borehole on the lateral force and moment transmitted to the bit. They are given in Appendix C.

The equilibrium solutions can be derived similarly, using (4.11) and (6.6). Alternatively, the helical parameters can be derived from the long-range solutions by solving for the borehole inclination Θ_∞ that causes vanishing of the curvature component κ_{2s}.

Long-Range Asymptotes. If the bit does not walk ($\varpi = 0$), the parameters of the long-range asymptotes are given by

$$\kappa_{2s} = -\frac{\mathcal{F}_r\mathcal{M}_b - \mathcal{F}_b\mathcal{M}_r + \mathcal{M}_r\eta\Pi}{\mathcal{F}_\kappa\mathcal{M}_b - (\mathcal{F}_b - \eta\Pi)(\mathcal{M}_\kappa + \chi\Pi)}\Gamma_2 - \frac{\mathcal{F}_w\mathcal{M}_b - \mathcal{F}_b\mathcal{M}_w + \mathcal{M}_w\eta\Pi}{\mathcal{F}_\kappa\mathcal{M}_b - (\mathcal{F}_b - \eta\Pi)(\mathcal{M}_\kappa + \chi\Pi)}\Upsilon\sin\langle\Theta\rangle,$$
$$\psi_{2s} = \frac{\mathcal{F}_r\mathcal{M}_\kappa - \mathcal{F}_\kappa\mathcal{M}_r + \mathcal{F}_r\chi\Pi}{\mathcal{F}_\kappa\mathcal{M}_b - (\mathcal{F}_b - \eta\Pi)(\mathcal{M}_\kappa + \chi\Pi)}\Gamma_2 + \frac{\mathcal{F}_w\mathcal{M}_\kappa - \mathcal{F}_\kappa\mathcal{M}_w + \mathcal{F}_w\chi\Pi}{\mathcal{F}_\kappa\mathcal{M}_b - (\mathcal{F}_b - \eta\Pi)(\mathcal{M}_\kappa + \chi\Pi)}\Upsilon\sin\langle\Theta\rangle,$$
$$\kappa_{3s} = -\frac{\mathcal{F}_r\mathcal{M}_b - \mathcal{F}_b\mathcal{M}_r + \mathcal{M}_r\eta\Pi}{\mathcal{F}_\kappa\mathcal{M}_b - (\mathcal{F}_b - \eta\Pi)(\mathcal{M}_\kappa + \chi\Pi)}\Gamma_3,$$
$$\psi_{3s} = \frac{\mathcal{F}_r\mathcal{M}_\kappa - \mathcal{F}_\kappa\mathcal{M}_r + \mathcal{F}_r\chi\Pi}{\mathcal{F}_\kappa\mathcal{M}_b - (\mathcal{F}_b - \eta\Pi)(\mathcal{M}_\kappa + \chi\Pi)}\Gamma_3. \tag{6.9}$$

The variables κ_{2s} and ψ_{2s} associated with the vertical plane $(\boldsymbol{I}_1, \boldsymbol{I}_2)$ depend linearly on the loading in this plane, i.e., the RSS force Γ_2 and weight $\Upsilon\sin\langle\Theta\rangle$, while the variables κ_{3s} and ψ_{3s} associated with the plane $(\boldsymbol{I}_1, \boldsymbol{I}_3)$ depend on Γ_3 only.

If the bit exhibits a walking tendency ($\varpi \neq 0$), the general expressions of the asymptotic parameters are linear expressions given by

$$\kappa_{2s} = \mathcal{S}^{\kappa_2}_{\Gamma_2}\Gamma_2 + \mathcal{S}^{\kappa_2}_{\Gamma_3}\Gamma_3 + \mathcal{S}^{\kappa_2}_{\Upsilon}\Upsilon\sin\langle\Theta\rangle,$$
$$\psi_{2s} = \mathcal{S}^{\psi_2}_{\Gamma_2}\Gamma_2 + \mathcal{S}^{\psi_2}_{\Gamma_3}\Gamma_3 + \mathcal{S}^{\psi_2}_{\Upsilon}\Upsilon\sin\langle\Theta\rangle,$$
$$\kappa_{3s} = \mathcal{S}^{\kappa_3}_{\Gamma_3}\Gamma_3 + \mathcal{S}^{\kappa_3}_{\Gamma_2}\Gamma_2 + \mathcal{S}^{\kappa_3}_{\Upsilon}\Upsilon\sin\langle\Theta\rangle,$$
$$\psi_{3s} = \mathcal{S}^{\psi_3}_{\Gamma_3}\Gamma_3 + \mathcal{S}^{\psi_3}_{\Gamma_2}\Gamma_2 + \mathcal{S}^{\psi_3}_{\Upsilon}\Upsilon\sin\langle\Theta\rangle. \tag{6.10}$$

The dimensionless coefficients $\mathcal{S}$ are given in Appendix E.1. They depend on the geometry of the BHA, on the walk angle ϖ, and on the dimensionless groups $\eta\Pi$ and $\chi\Pi$. Equations (6.10) reduce to (6.9) if $\varpi = 0$. The bit walk is responsible for a coupling of the response of the system in the planes $(\boldsymbol{I}_1, \boldsymbol{I}_2)$ and $(\boldsymbol{I}_1, \boldsymbol{I}_3)$. Hence, the solution parameters now depend on the components of the loads applied in both planes.

Equilibrium Solutions. If the bit presents a neutral walk tendency, the equilibrium variables for the helical steady-state are given by

$$\begin{aligned}
\Upsilon \sin\Theta_\infty &= -\frac{\mathcal{F}_r\mathcal{M}_b - \mathcal{F}_b\mathcal{M}_r + \mathcal{M}_r\eta\Pi}{\mathcal{F}_w\mathcal{M}_b - \mathcal{F}_b\mathcal{M}_w + \mathcal{M}_w\eta\Pi}\Gamma_2,\\
\psi_{2\infty} &= \frac{\mathcal{F}_r\mathcal{M}_w - \mathcal{F}_w\mathcal{M}_r}{\mathcal{F}_w\mathcal{M}_b - \mathcal{F}_b\mathcal{M}_w + \mathcal{M}_w\eta\Pi}\Gamma_2,\\
\kappa_\infty &= -\frac{\mathcal{F}_r\mathcal{M}_b - \mathcal{F}_b\mathcal{M}_r + \mathcal{M}_r\eta\Pi}{\mathcal{F}_\kappa\mathcal{M}_b - (\mathcal{F}_b - \eta\Pi)(\mathcal{M}_\kappa + \chi\Pi)}\Gamma_3,\\
\psi_{3\infty} &= \frac{\mathcal{F}_r\mathcal{M}_\kappa - \mathcal{F}_\kappa\mathcal{M}_r + \mathcal{F}_r\chi\Pi}{\mathcal{F}_\kappa\mathcal{M}_b - (\mathcal{F}_b - \eta\Pi)(\mathcal{M}_\kappa + \chi\Pi)}\Gamma_3.
\end{aligned} \tag{6.11}$$

Again, a neutral walk tendency causes the behavior of the directional drilling system in the vertical plane $(\boldsymbol{I}_1, \boldsymbol{I}_2)$ and in the osculating plane $(\boldsymbol{I}_1, \boldsymbol{I}_3)$ to be uncoupled. As a consequence, the expressions for κ_∞ and $\psi_{3\infty}$ are the same as κ_{3s} and ψ_{3s} in (6.9).

If the bit exhibits a walk tendency, the general expressions of the equilibrium parameters are given by

$$\begin{aligned}
\Upsilon \sin\Theta_\infty &= \mathcal{Q}_1^\Theta\Gamma_2 + \mathcal{Q}_2^\Theta(1-\cos\varpi)\Gamma_2 + \mathcal{Q}_3^\Theta\sin\varpi\,\Gamma_3,\\
\psi_{2\infty} &= \mathcal{Q}_1^{\psi 2}\Gamma_2 + \mathcal{Q}_2^{\psi 2}(1-\cos\varpi)\Gamma_2 + \mathcal{Q}_3^{\psi 2}\sin\varpi\,\Gamma_3,\\
\kappa_\infty &= \mathcal{Q}_1^\kappa\Gamma_3 + \mathcal{Q}_2^\kappa(1-\cos\varpi)\Gamma_3 + \mathcal{Q}_3^\kappa\sin\varpi\,\Gamma_2,\\
\psi_{3\infty} &= \mathcal{Q}_1^{\psi 3}\Gamma_3 + \mathcal{Q}_2^{\psi 3}(1-\cos\varpi)\Gamma_3 + \mathcal{Q}_3^{\psi 3}\sin\varpi\,\Gamma_2.
\end{aligned} \tag{6.12}$$

The dimensionless coefficients $\mathcal{Q}$ are given in Appendix E.2. As for the coefficients $\mathcal{S}$, they depend on the geometry of the BHA, on the walk angle ϖ, and on the dimensionless groups $\eta\Pi$ and $\chi\Pi$.

6.2.2 Analysis of Equilibrium Solutions

The asymptotic solutions given in (6.9) or (6.10) are always well defined and unique as long as the intermediate dynamics converges.

But depending on the magnitude of the expression for $\Upsilon \sin\Theta_\infty$ in (6.11) or (6.12), there exists either two distinct equilibrium solutions (a downward solution, $\Theta_\infty \in [0, \pi/2]$, and an upward solution, $\Theta_\infty \in [\pi/2, \pi]$) or none. They only exist if

$$0 \leq \frac{\mathcal{Q}_1^\Theta \Gamma_2 + \mathcal{Q}_2^\Theta \left(1 - \cos\varpi\right) \Gamma_2 + \mathcal{Q}_3^\Theta \sin\varpi \Gamma_3,}{\Upsilon} \leq 1. \tag{6.13}$$

Typically, if the magnitude of the RSS force is too large, the inclination of the borehole never stabilizes and keeps increasing or decreasing.

The long-range evolution and stationary solutions exhibit particular behaviors for specific sets of drilling parameters, specifically, for distinct values of $\eta\Pi$ that are functions of the BHA geometry. The study of these particular cases is enlightening because they have interesting physical interpretations, but also because these particular behaviors seem to have an important impact on the transient borehole propagation (see Chapter 7). They are first investigated for a neutral walk tendency of the bit, before being generalized to $\varpi \neq 0$.

Examples of application are given in Section 7.3.

No Bit Walk. The following three particular cases can be identified from the expressions of the geometric variables in (6.9) and (6.11).

If the dimensionless group $\eta\Pi$ is equal to

$$\eta\Pi|_{\not\Gamma} = \frac{\mathcal{F}_b \mathcal{M}_r - \mathcal{F}_r \mathcal{M}_b}{\mathcal{M}_r}, \tag{6.14}$$

the RSS no longer influences the long-range evolution but still affects the deformation of the BHA. The value $\eta\Pi|_{\not\Gamma}$ is only related to the geometry of the BHA, defined by the position of the stabilizers and the RSS. For $\eta\Pi = \eta\Pi|_{\not\Gamma}$, the helical solution (6.11) degenerates into a vertical borehole propagating downward or upward ($\sin\Theta_\infty = 0$ and $\kappa_\infty = 0$) since now only the weight of the BHA affects the solution. Similarly, the long-range asymptotes (6.9) degenerate into circular boreholes in a vertical plane ($\kappa_{3s} = 0$) with a curvature κ_{2s} proportional to the transversal weight $\Upsilon \sin\langle\Theta\rangle$ on the BHA.

The physical explanation behind this particular behavior is as follows. The RSS force affects the drilling direction by (i) inducing a lateral force on the bit and (ii) tilting the bit. When $\eta\Pi = \eta\Pi|_{\boldsymbol{\gamma}}$, this bit tilt translates, via the bit/rock interaction laws (4.1), into another lateral force on the bit that exactly balances this initial lateral force transmitted by the RSS. In other words, when $\eta\Pi = \eta\Pi|_{\boldsymbol{\gamma}}$, the influence of the bit tilt and bit lateral force induced by the RSS are opposite and neutralize each other. Figure 6.4 illustrates this Γ-independent behavior for a vertical borehole and for several magnitudes of the RSS force; the deflection of the BHA is proportional to Γ.

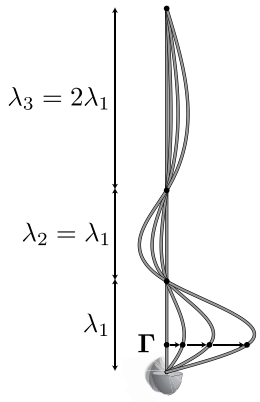

Figure 6.4: Exaggerated deformed configurations of a BHA with 3 stabilizers located at λ_1, $2\lambda_1$, and $4\lambda_1$, and for several magnitudes Γ of the RSS force. The RSS position is $\Lambda = 0.3$ and $\eta\Pi = \eta\Pi|_{\boldsymbol{\gamma}} \simeq 4.4$.

A second case is equivalent to the Γ-independent case but for the distributed weight Υ. If the drilling parameter $\eta\Pi$ is equal to

$$\eta\Pi|_{\boldsymbol{\Upsilon}} = \frac{\mathcal{F}_b\mathcal{M}_w - \mathcal{F}_w\mathcal{M}_b}{\mathcal{M}_w}, \tag{6.15}$$

the long-range borehole trajectories are independent of the weight Υ and thus of the inclination. Hence, helical stationary solutions do not exist unless $\Gamma_2 = 0$, in which case the equilibrium inclination Θ_∞ is undetermined as it can take any values between 0 and π.

The origin of this Υ-independent behavior is similar to the Γ-independent case: the effects on the borehole trajectory of the bit lateral force and bit tilt due to Υ counteract each other. As an example, Figure 6.5 sketches the deformed BHA in the plane $(\boldsymbol{I}_1, \boldsymbol{I}_2)$ for $\eta\Pi = \eta\Pi|_{\boldsymbol{\Upsilon}}$ and

$\Gamma_2 = 0$ after unfolding the helical borehole onto a flat surface. The deflection of the BHA is proportional to $\Upsilon \sin\Theta_\infty$.

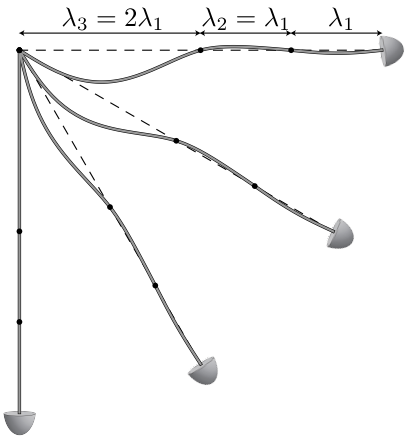

Figure 6.5: Exaggerated vertical deflection of a BHA with 3 stabilizers located at λ_1, $2\lambda_1$, and $4\lambda_1$, and for $\eta\Pi = \eta\Pi|_{\boldsymbol{\gamma}} \simeq 4.3$, so that the steady-state solution is Υ-independent. This plane view is obtained by unfolding the vertical cylinder containing the helical borehole.

A third particular behavior is associated with a specific position $\Lambda = \Lambda_*$ of the RSS force along the BHA. It is formally defined by the condition $\mathcal{F}_r\mathcal{M}_w - \mathcal{F}_w\mathcal{M}_r = 0$ so that this particular value Λ_* is only a function of the position of the stabilizers.

It impacts the helical solutions by vanishing the vertical bit tilt, $\psi_{2\infty} = 0$, so that the bit penetrates the rock formation along its axis of symmetry. As a consequence, the equilibrium inclination Θ_∞ is independent of the directional properties of the bit/rock interface laws, in particular of $\eta\Pi$, and is given by

$$\Upsilon \sin\Theta_\infty = -\frac{\mathcal{F}_r}{\mathcal{F}_w}\Gamma_2. \tag{6.16}$$

We denote this case as $\eta\Pi$-independent, although the stationary solutions are not entirely independent of $\eta\Pi$. Figure 6.6 illustrates the deflection of the BHA in the plane $(\boldsymbol{I}_1, \boldsymbol{I}_2)$ for helical borehole solutions with $\Lambda = \Lambda_*$.

Also, for this particular RSS position, $\eta\Pi|_{\boldsymbol{\gamma}} = \eta\Pi|_{\boldsymbol{\gamma}}$. Hence, under the conditions $\Lambda = \Lambda_*$ and $\eta\Pi = \eta\Pi|_{\boldsymbol{\gamma}} = \eta\Pi|_{\boldsymbol{\gamma}}$, the borehole geometries are independent of the RSS force Γ and weight Υ, and thus degenerate into straight boreholes.

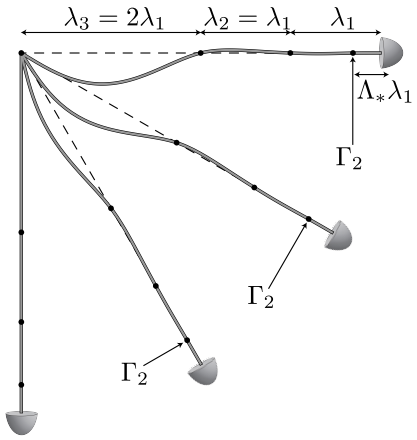

Figure 6.6: Exaggerated deformed configurations of a BHA with 3 stabilizers located at λ_1, $2\lambda_1$, and $4\lambda_1$ away from the bit. The RSS is positioned at $\Lambda = \Lambda_* \simeq 0.31$, so that $\psi_{2\infty} = 0$. This planar view is obtained by unfolding the vertical cylinder containing the helical borehole onto a flat surface.

Finally, the numerator $\mathcal{F}_r\mathcal{M}_\kappa - \mathcal{F}_\kappa\mathcal{M}_r + \mathcal{F}_r\chi\Pi$ in (6.9) and (6.11) is always negative and the denominator $\mathcal{F}_\kappa\mathcal{M}_b - (\mathcal{F}_b - \eta\Pi)(\mathcal{M}_\kappa + \chi\Pi)$ is always positive. Also, the numerator $\mathcal{F}_w\mathcal{M}_\kappa - \mathcal{F}_\kappa\mathcal{M}_w + \mathcal{F}_w\chi\Pi$ in the expression of ψ_{2s} in (6.9) may vanish but only in a very narrow strip in the space of drilling parameters; this case is not of practical relevance and is thus not investigated here.

With Bit Walk. The three particular cases identified in the absence of bit walk are now revisited.

Strictly speaking, the Γ-independent case does not exist if $\varpi \neq 0$: it is a feature of the system for a bit with a neutral walk tendency. Nevertheless, when $\eta\Pi = \eta\Pi|_{\mathcal{Y}}$ given in (6.14), the RSS force has a reduced influence on the stationary borehole geometry as $\mathcal{Q}_1^\Theta = \mathcal{Q}_1^\kappa = 0$.

The Υ-independent case still exists for the long-range solutions but for a specific value $\eta\Pi|_{\mathcal{X}}$ of $\eta\Pi$ different than (6.15): $\eta\Pi|_{\mathcal{X}}$ still depends on the geometry of the BHA but also on the walk angle ϖ. This particular value $\eta\Pi|_{\mathcal{X}}$ causes the system of equations derived from (4.7) and (6.6) to become singular when the RSS force $\mathbf{\Gamma}$ vanishes. The stationary solutions correspond

then to any helical borehole satisfying the condition

$$\kappa_\infty = \frac{\mathcal{F}_b\mathcal{M}_w - \mathcal{F}_w\mathcal{M}_b - \mathcal{M}_w\ \eta\Pi|_{\boldsymbol{\gamma}}\cos\varpi}{(\mathcal{M}_\kappa + \chi\Pi)\ \eta\Pi|_{\boldsymbol{\gamma}}\sin\varpi}\Upsilon\sin\Theta_\infty. \tag{6.17}$$

For the specific position $\Lambda = \Lambda_*$ of the RSS the helical borehole inclination Θ_∞ is again given by equation (6.16); that is Θ_∞ does not depend on the parameter $\eta\Pi$ nor on the bit walk angle ϖ. Also, the parameters $\psi_{2\infty}$, κ_∞, and $\psi_{3\infty}$ in (6.12) depend only on the horizontal RSS force Γ_3, not on Γ_2.

Influence of $\chi\Pi$ and Rigidity. The influence of $\chi\Pi$ on the long-range and stationary solutions can be quantified by $\chi\Pi/\mathcal{M}_\kappa$ ($\chi\Pi$ enters the expressions for the equilibrium parameters as the sum $\mathcal{M}_\kappa + \chi\Pi$). The coefficient $\mathcal{M}_\kappa$ measuring the influence of the borehole curvature is always of order $O(1)$, while $\chi\Pi$ is generally of order $O(10^{-2})$. The angular steering resistance χ has thus in general a negligible influence on the long-range evolution.

The long-range and equilibrium solutions degenerate into straight boreholes for $EI \to \infty$, if the BHA has 2 or more stabilizers. After rescaling and taking the limit $\Upsilon \to 0$, the expressions of the curvatures and tilts given in (6.10) and (6.12) vanish. But the limit of the stationary borehole inclination Θ_∞ in (6.12) is well defined; this contradicts the fact that the rigid solution is no longer influenced by the gravity and any straight borehole should be in principle a stationary solution. The reason is that the straight solutions for the rigid case become marginally stable or simply unstable if the BHA has more than one stabilizer.

6.3 Stability and Rate of Convergence

The convergence of the solutions is investigated on the intermediate and long ranges. On the intermediate range, this analysis is concerned with the transient behavior arising from the delayed influence of the borehole geometry (cf. the secular terms in the evolution equations). When unstable, this transient evolution induces oscillations in the borehole trajectory. On the long range, the stability of the helical equilibrium solutions is studied.

Borehole oscillations have been observed on the field (Millheim, 1977; Amara, 1985; Pastusek and Brackin, 2003). Three types of oscillations are described: (i) rippling oscillations, which are

sinusoidal oscillations of the borehole, (ii) spiraling oscillations when the borehole is corkscrewing, (iii) and hour-glassing, which is a cyclic enlargement of the borehole. They are a danger for the drilling operations: an excessive tortuosity of the borehole impairs the transmission of axial force and torque to the bit and jeopardizes the completion of the well. Pastusek and Brackin (2003) states that the wave length of these oscillations is often observed to be about the distance between the bit and the first contact point of the BHA with the borehole. Frequently, this wave length is smaller than the distance between successive points of measurement of the borehole geometry, so that they are not detected during drilling.

The stability analysis is based on the linearized version of the evolution equations about an equilibrium, from which a characteristic equation is derived (Hale, 1977). The stability of the equilibrium is related to the location of the roots of this characteristic equation in the complex plane; they need to be in the left-half plane for the solution to be stable. For the sake of simplicity, this section mainly treats the case of a neutral walk tendency; but its conclusions can be generalized to the general case with $\varpi \neq 0$.

The eigenvalue based approach is implemented using the software package DDE-BIFTOOL for MATLAB, which is used as a numerical root finder of the characteristic equations (Engelborghs et al., 2001, 2002).

6.3.1 Theoretical Background

Many of the results on the stability of ordinary differential equations are similar for DDE (Bellman and Cooke, 1963; Hale, 1977; Stepan, 1989; Gu et al., 2003; Michiels and Niculescu, 2007).

The general system (4.7) is first converted into a system of first order delay differential equations by introducing the additional state variables $\langle\Theta\rangle_1, \ldots, \langle\Theta\rangle_n$ and $\langle\Phi\rangle_1, \ldots, \langle\Phi\rangle_n$. It is then linearized about an equilibrium. If the equilibrium of this linearized system is asymptotically stable, then the equilibrium of the non-linear system (4.7) is likewise asymptotically stable (Stepan, 1989).

Hence, the rest of this section focuses on the stability of linear retarded delay differential equations (RDDE) of the form

$$\boldsymbol{x}'(\xi) = A_0 \boldsymbol{x}(\xi) + \sum_{i=1}^{n} A_i \boldsymbol{x}(\xi - \xi_i), \tag{6.18}$$

where $\boldsymbol{x}(\xi)$ is a vector of state variables and A_i, $i = 0, \ldots, n$ are real matrices.

The corresponding characteristic equation is given by

$$Q(\alpha) = \det\left[\alpha I - A_0 - \sum_{i=1}^{n} A_i e^{-\alpha\xi_i}\right] = 0. \tag{6.19}$$

It is a transcendental equation, meaning that it possesses an infinite number of roots. It can be shown that the roots of the characteristic equation verify (Michiels and Niculescu, 2007)

$$|\alpha| \leq \|A_0\|_2 + \sum_{i=1}^{n} \|A_i\|_2 e^{-\Re(\alpha)\xi_i}. \tag{6.20}$$

There exists a number $\gamma \in \mathbb{R}$ such that all the roots are in the half-plane $\{\alpha \in \mathbb{C} : \Re(\alpha) < \gamma\}$. Also, there are only a finite number of roots in any vertical strip $\{\alpha \in \mathbb{C} : \alpha_1 < \Re(\alpha) < \alpha_2\}$ of the complex plane, with α_1, $\alpha_2 \in \mathbb{R}$ and $\alpha_1 < \alpha_2$.

The null solution of (6.18) is exponentially stable if and only if all the characteristic roots are located in the open left half-plane. Furthermore, the solution to the linear RDDE (6.18) possesses the following modal expansion. For any $\zeta \in \mathbb{R}$ such that the characteristic function $Q(\alpha) \neq 0$ for all $\alpha \in \mathbb{C}$ on the line $\Re(\alpha) = \zeta$, a solution $x(\xi)$ to (6.18) can be approximated by

$$x(\xi) = \sum_{k=1}^{l} p_k(\xi) e^{\alpha_k \xi} + o\left(e^{\zeta\xi}\right), \quad \text{for } \xi \to \infty, \tag{6.21}$$

where $\alpha_1, \ldots, \alpha_l$ are the (finitely many) characteristic roots with real parts exceeding ζ, and $p_k(\xi)$ are vector valued polynomial of degree less than or equal to $m_k - 1$, with m_k being the multiplicity of α_k as a root of the characteristic equation (Michiels and Niculescu, 2007).

For RDDE, the position in the complex plane of the characteristic roots is continuously dependent on the variations of the matrices $A_0, \ldots, A_n$ and delays ξ_i. Hence, a point in the parameter space associated with a loss or acquisition of stability corresponds to having characteristic roots on the imaginary axis.

The stability of neutral delay differential equations (NDDE) and delay difference equations (respectively governing the 1-stabilizer and 2-stabilizer rigid systems) do not share the same properties as RDDE. In particular, the spectrum of the characteristic equation for linear NDDE or linear delay difference equations is not continuously dependent on the delays ξ_i.

6.3.2 Intermediate-Range vs Long-Range Stability

Examples of spectra are given in Figure 6.7. The shaded area corresponds to the region of the complex plane defined by (6.20) and in which the characteristic roots live. It ensures that roots with large imaginary parts are stable. Two distinct roots of the spectrum appear to be important.

The first root, α_0, characterizes the stability of the equilibrium solutions. Under normal drilling conditions, α_0 is close to the origin of the complex plane and $|\Re(\alpha_0)|$ has the same order of magnitude as Υ, that is $O(10^{-3})$. The rest of the spectrum governs the transient behavior. In particular, the right-most root α_1 of the spectrum after discarding α_0, controls the stability and rate of convergence of the solution toward the intermediate asymptotes. These conclusions can be justified as follows.

At the intermediate scale, the influence of the weight is quasi-constant. The convergence toward a long-range asymptote can thus be investigated under the assumption that $\Upsilon \sin \langle\Theta\rangle_1 = \Upsilon \sin \langle\Theta\rangle$ in (4.11) is constant. For this purpose, it is thus enough to study the homogeneous linear differential equation

$$\begin{aligned}\chi \Pi \Theta'(\xi) = &-\mathcal{M}_b \left[\Theta(\xi) - \langle\Theta\rangle_1\right] + \frac{\chi}{\eta}\mathcal{F}_b \left[\Theta(\xi) - \Theta(\xi_1)\right] \\ &+ \sum_{i=1}^{n-1} \left[\frac{\mathcal{F}_b\mathcal{M}_i - \mathcal{F}_i\mathcal{M}_b - \mathcal{M}_i\eta\Pi}{\eta\Pi}\right] \left(\langle\Theta\rangle_i - \langle\Theta\rangle_{i+1}\right) \\ &- \frac{\chi}{\eta}\sum_{i=1}^{n-1} \mathcal{F}_i \left(\frac{\Theta(\xi_{i-1}) - \Theta(\xi_i)}{\varkappa_i} - \frac{\Theta(\xi_i) - \Theta(\xi_{i+1})}{\varkappa_{i+1}}\right), \end{aligned} \tag{6.22}$$

obtained from (4.12). The corresponding characteristic equation $Q(\alpha)$ possesses a root α_0 at the origin, a consequence of the steady-state of (6.22) being defined up to a constant inclination. Hence, the rate of exponential convergence (or divergence) toward a quasi-constant curvature solution is controlled by the right-most root α_1 of the spectrum. (In practice, since equation (6.22) is brought into a system of DDE by introducing n additional state variables $\langle\Theta\rangle_1, \ldots, \langle\Theta\rangle_n$, the spectrum has n additional characteristic roots at the origin.)

Also, the convergence of the borehole inclination Θ toward a quasi-constant curvature solution is a sufficient condition for the convergence of the system. In other words, if the evolution of the inclination Θ governed by (6.22) is stable, the other state variables θ, Φ, and ϕ also

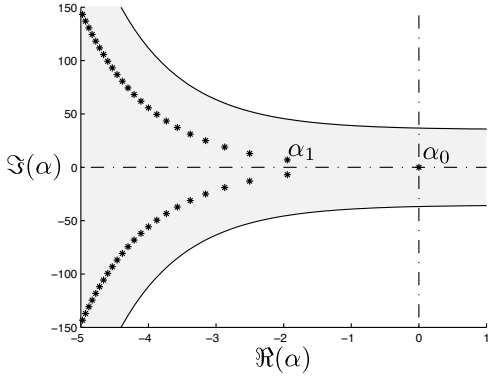

(a) Spectrum for a 1-stabilizer BHA. The RSS force to have $\Theta_\infty = 45°$ is $\Gamma = 3.1 \times 10^{-3}$. The real parts of the right-most roots are $\Re(\alpha_0) = -0.0028$ and $\Re(\alpha_1) = -1.95$.

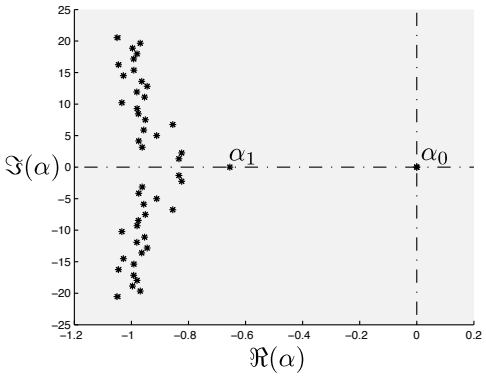

(b) Spectrum for a 3-stabilizer BHA with $\varkappa_2 = 2$, $\varkappa_3 = 4.285$. The RSS force to have $\Theta_\infty = 45°$ is $\Gamma = 4.2 \times 10^{-3}$. The real parts of the right-most roots are $\Re(\alpha_0) = -0.0028$ and $\Re(\alpha_1) = -0.655$. Only the 51 roots with the largest real parts are shown here.

Figure 6.7: Spectra of the characteristic equation for equilibrium solutions with inclination $\Theta_\infty = 45°$. These examples consider a 1-stabilizer and a 3-stabilizer BHA; the system parameters are the same as the simulations in Section 5.2: $\eta = 25$, $\chi = 1$, $\varpi = 0$, $\Pi = 4.08 \times 10^{-2}$, $\Upsilon = 6.3 \times 10^{-3}$, and $\Lambda = 0.29$. The RSS force is chosen so that the equilibrium inclination (of the downward solution) is $\Theta_\infty = 45°$. The shaded region is defined by (6.20); its boundaries do not appear in Figure 6.7b.

converges to a long-range asymptote. The convergence of θ is ensured as $\mathcal{M}_b \geq 1$ in (4.11b); also the stability properties of equations (4.11c) and (4.11d) governing Φ and ϕ are the same as for (4.11a) and (4.11b).

On the long range, the borehole inclination can no longer be approximated as constant and the weight Υ has a non-linear influence on the system. Nevertheless, this nonlinear effect is weak, a consequence of $\Upsilon \ll 1$. Thus, it only perturbs the spectrum of the characteristic equation and the root α_0 is slightly shifted. Provided that all the other roots remain in the left-hand side of the complex plane, it is α_0 that determines the stability of the stationary solutions. Alternatively, the stability of the equilibrium solutions could be assessed using (5.2) governing the large-range dynamics.

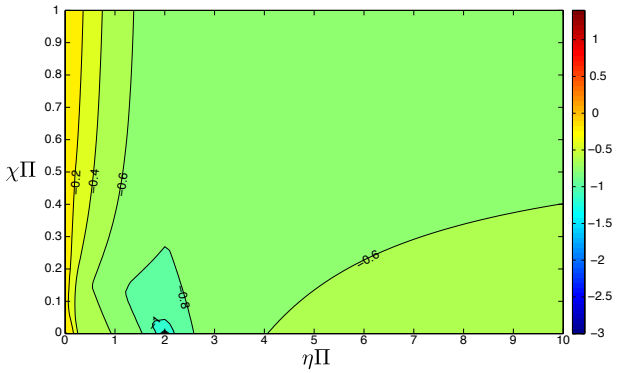

(a) $\varkappa_2 = 2$ and $\varkappa_3 = 4.285$.

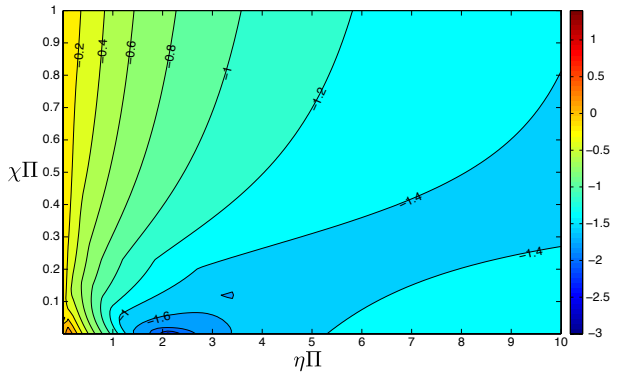

(b) $\varkappa_2 = 1$ and $\varkappa_3 = 1$.

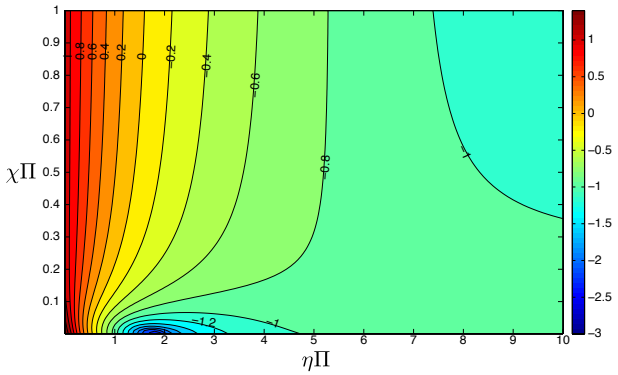

(c) $\varkappa_2 = 0.5$ and $\varkappa_3 = 0.5$.

Figure 6.8: Real part of the right-most root $\Re(\alpha_1)$ as a function of the dimensionless groups $\eta\Pi$ and $\chi\Pi$, and for different geometries of the BHA. The ranges of $\eta\Pi$ and $\chi\Pi$ are purposely large; in practice $\eta\Pi$ is of order of $O(1)$ and $\chi\Pi$ is at most of the order of $O(10^{-1})$.

6.3.3 Convergence on the Intermediate Range

If $\varpi = 0$, the parameters controlling the rate of convergence toward a large-range asymptote are the dimensionless groups $\eta\Pi$ and $\chi\Pi$ arising from the bit/rock interface laws, and the positions of the stabilizers, measured by $\varkappa_1, \ldots, \varkappa_n$ (Fig. 6.8).

The general trend shows that decreasing the rigidity of the BHA improves the rate of convergence. This can be achieved by decreasing the bending stiffness EI or by increasing the distances between stabilizers. Roughly speaking, decreasing the constraints on the BHA decreases the delayed feedback of the borehole geometry on the system and improves its stability. This observation advocates for the use of flexible elements that are often placed between the first and the second stabilizer. A bit with a strong tendency to drill along its principal axis tends to increase the rate of convergence compared to an aggressive bit. Hence, for this purpose, drill bits with long passive gauges tend to drill a smoother borehole. Finally, a sweet spot in the parametric space seems to systematically appear at $\eta\Pi \simeq 2$ and $\chi\Pi \ll 1$, independently of the geometry of the BHA (numerical investigations for 2-stabilizer BHA confirm this tendency). We did not find an explanation that justifies this observation.

The imaginary parts of the characteristic roots measure the frequency associated with each oscillation mode. For the dominant modes, $\Im(\alpha) = O(1)$ so that the borehole oscillations are expected to have a wave length of the order of the distance from the bit to the first stabilizer. In general, the modal frequencies increase if the distances $\varkappa_i$ between stabilizers decrease.

The spectrum of the characteristic equation does not drastically change with the bit walk angle ϖ, especially in view that ϖ is usually of the order of $O(10^\circ)$. Figure 6.9 illustrates this influence for a continuous variation of ϖ. The spectrum does not depend on the sign of ϖ. The rate of convergence is usually reduced by increasing the walk angle ϖ.

Finally, Figure 6.10 illustrates the strong dependence of the spectrum with respect to the delay $1 + \varkappa_2$ for the delay difference equation (4.19) governing the 2-stabilizer stiff case. For $\varkappa_2 = 2$, the roots are distributed along the lines $\Re(\alpha) = -\log 2$ and $\Re(\alpha) = 0$ and their imaginary parts are multiples of π.

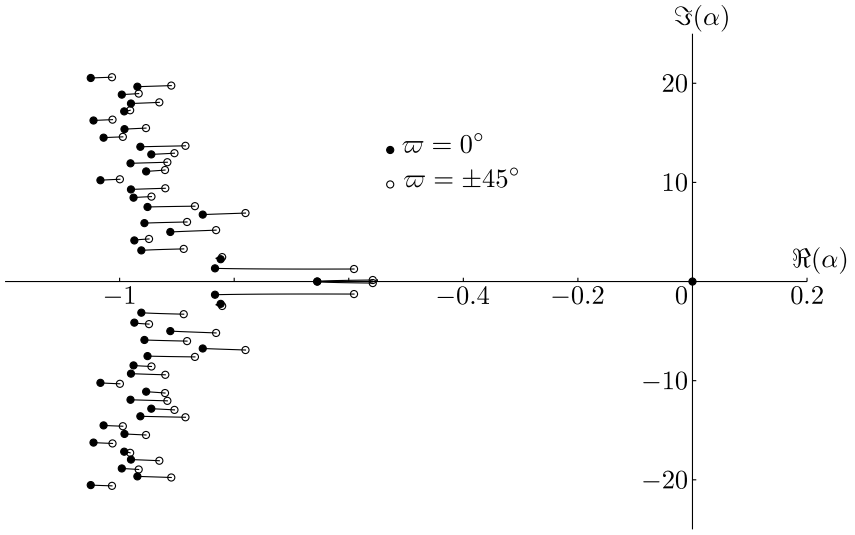

Figure 6.9: Shift of the characteristic roots for a continuous variation of ϖ from $\varpi = 0°$ to $\varpi = \pm 45°$. The system parameters are $\eta = 25$, $\chi = 1$, $\varpi = 0$, $\Pi = 4.08 \times 10^{-2}$, $\varkappa_2 = 2$, $\varkappa_3 = 4.285$, $\Upsilon = 6.3 \times 10^{-3}$, $\Lambda = 0.29$, and $\Theta_\infty = 45°$; the initial spectrum for $\varpi = 0°$ is the same as in Figure 6.7b.

6.3.4 Stability of Stationary Solutions

When they exist, two stationary solutions are associated with a given set of drilling parameters: a downward solution $\Theta_\infty \in [0, \pi/2]$ and an upward one $\Theta_\infty \in [\pi/2, \pi]$. Always, one of them is stable and the second one unstable (Fig. 6.11). But, whether it is the downward or upward equilibrium which is stable depends on the value of $\eta\Pi$ with respect to $\eta\Pi|_{\boldsymbol{\chi}}$, which has been defined in Section 6.2.2 as the particular value of $\eta\Pi$ for which the equilibrium is independent of the weight Υ. For a continuous change of $\eta\Pi$ with all other parameters being kept constant, $\Re(\alpha_0)$ changes sign for $\eta\Pi = \eta\Pi|_{\boldsymbol{\chi}}$. It is first observed that for this particular value $\eta\Pi|_{\boldsymbol{\chi}}$, the equilibrium solutions are marginally stable. Furthermore, for $\eta\Pi < \eta\Pi|_{\boldsymbol{\chi}}$ the downward solutions are stable, while for $\eta\Pi > \eta\Pi|_{\boldsymbol{\chi}}$ the upward ones are stable. The reason is that $\eta\Pi|_{\boldsymbol{\chi}}$ is the value of $\eta\Pi$ for which the influence of the gravity on the system is reversed; it is associated with a change of drilling regime (see Section 7.2.2).

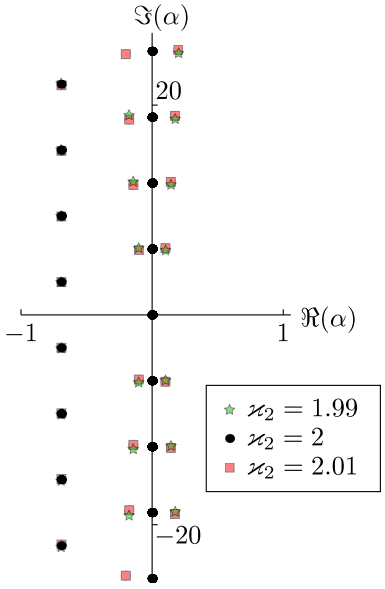

Figure 6.10: Spectrum for the stiff 2-stabilizer case for three BHA geometries.

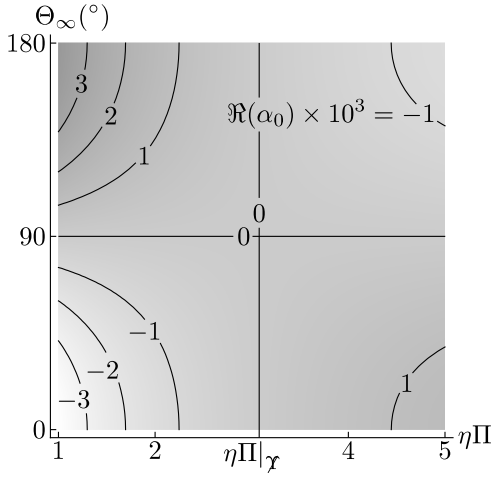

Figure 6.11: Magnitude of $\Re(\alpha_0)$ as a function of $\eta\Pi$ and the equilibrium inclination Θ_∞. The system parameters are $\varpi = 0$, $\chi\Pi = 4.08 \times 10^{-2}$, $\varkappa_2 = 2$, and $\varkappa_3 = 4.285$.

Chapter 7

Applications

The following applications illustrate the discussions and results from Chapters 5 and 6. The main outcome of this chapter is the identification of different drilling regimes. The transitions between these regimes is characterized by the particular values $\eta\Pi|_{\mathcal{Y}}$ and $\eta\Pi|_{\mathcal{X}}$ of $\eta\Pi$ identified in Section 6.2.2. The directional response of the system to the external loads $\mathbf{\Gamma}$ and Υ will appear to be predominantly controlled by the dimensionless group $\eta\Pi$ and the geometry of the BHA.

7.1 Drilling Parameters

Table 7.1 provides a compilation of relevant information concerning bit sizes, characteristics of the BHA, and properties of push-the-bit RSS used for directional drilling operations. These data are given as an indication of the order of magnitude for the system parameters that can be encountered in practice as they may vary greatly depending on the application. They are organized according to the RSS outer diameter, which ranges from $4^3/_4$ to $9^1/_2$ inches (according to the convention followed by the industry). For BHA equipped with a push-the-bit RSS, the distance λ_1 between the bit and the first stabilizer usually varies between 3 to 5 m. The RSS is located close to the bit so that the RSS lateral force is generated within 0.5 to 1 m from the bit.

When the BHA is not equipped with a RSS, the location of the stabilizers alone is used to

influence the directional tendency of the apparatus. In this case, the length λ_1 may range from 1 m up to 20 m (Millheim, 1979). Depending on the positions of the stabilizers, drillers dub the BHA as having a dropping, holding, or building tendency, whether it is expected to decrease, hold, or increase the inclination of the borehole, respectively.

The corresponding dimensionless parameters are listed in Table 7.2. The maximum cutting component of the weight on bit, $\Pi_{\max}$, has been assessed on the assumption that the bit is "sharp," i.e., $G_1 = 0$. The threshold contact force G_1 depends on the bluntness of the bit, the bit size, and the rock strength. Everything else being the same, G_1 scales with the bit size. Experimental investigations in sandstone (Detournay et al., 2008) suggest values for G_1 of order $O\,(10\,\mathrm{kN})$ for moderately blunt $6^1/_2$ PDC bits ($a = 8.3$ cm).

RSS diameter	$4^3/_4$"	$6^3/_4$"	$8^1/_4$"	$9^1/_2$"
$a_{\min}$ (cm)	7.5	10.8	15.6	15.6
$a_{\max}$ (cm)	8.6	12.5	18.7	23.2
w (kN/m)	0.88	1.29	2.21	3.8
EI (MNm^2)	2	8.4	18.7	33
λ_1 (m)	3.5	3.8	3.8	3.8
λ_2 (m)	7	8	8	9.2
$\lvert\hat{F}_1\rvert_{\max}$ (kN)	100	250	400	450
$\lvert C\rvert_{\max}$ (kNm)	7	20	45	68
$\breve{F}_{\max}$ (kN)	10	18.6	32	40
$K_{\max}$ (km^{-1})	8	3.7	3.7	3.7

Table 7.1: Approximate system parameters for different BHA sizes; the number on the first row is the RSS outer diameter in inches. The radii $a_{\min}$ and $a_{\max}$ are the minimum and maximum radii of the bit, $\lvert\hat{F}_1\rvert_{\max}$ and $\lvert C\rvert_{\max}$ are the maximum weight on the bit and torque allowed by the apparatus, and $\breve{F}_{\max}$ is the maximum magnitude of the lateral force that can be generated by the RSS. The quantity $K_{\max}$ is the maximum curvature of the borehole that is allowed when drilling with a RSS of a certain size.

RSS diameter	$4^3/_4$"	$6^3/_4$"	$8^1/_4$"	$9^1/_2$"
$\Upsilon \times 10^3$	6.27	2.77	2.13	2.09
$\Gamma_{\max} \times 10^2$	2.03	1.06	0.82	0.58
$\Pi_{\max} \times 10$	1.82	1.42	1.00	0.64
$\varkappa_2$	2	2.11	2.11	2.42
Λ	0.29	0.26	0.26	0.26

Table 7.2: Suggested dimensionless parameters for a "sharp" bit ($G_1 = 0$).

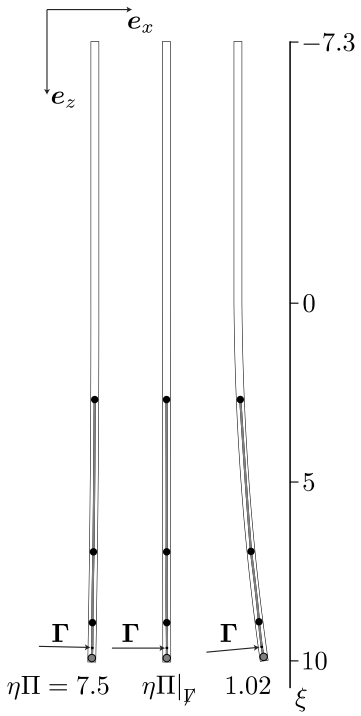

Figure 7.1: Borehole and BHA geometryies for various values of Π, which are selected such that $\eta\Pi$ is smaller, equal, and larger than $\eta\Pi|_{\mathcal{Y}}$. The borehole and BHA are initially vertical and at $\xi = 0$ a constant RSS force is imposed. For $\eta\Pi = 7.5$ the borehole slightly drifts to the left. The parameters are $\varkappa_2 = 2$, $\varkappa_3 = 4.285$, $\eta = 25$, $\chi = 1$, $\varpi = 0$, $\Gamma = 2.03 \times 10^{-2}$. The axis ξ is the projected length of the borehole. The borehole and BHA diameters are not up to scale and the deformation of the BHA is magnified.

7.2 Simulations

7.2.1 RSS Force

In view of (4.12), the efficiency of the RSS can be quantified by the gain g given by

$$g = \frac{\mathcal{F}_b\mathcal{M}_r - \mathcal{F}_r\mathcal{M}_b - \mathcal{M}_r\eta\Pi}{\eta\Pi}, \tag{7.1}$$

which depends on $\eta\Pi$ and the geometry of the BHA. For the specific value $\eta\Pi = \eta\Pi|_{\mathcal{Y}}$ given in (6.14), the gain vanishes; it is positive if $\eta\Pi < \eta\Pi|_{\mathcal{Y}}$ and negative otherwise. Figure 7.1 illustrates the influence of $\mathbf{\Gamma}$ on a vertical borehole path, for which the influence of the weight Υ is negligible. When $\eta\Pi < \eta\Pi|_{\mathcal{Y}}$, the borehole propagates in the direction of the RSS force. In

most cases, the system actually evolves in this regime and drillers expect the borehole to evolve accordingly. But for large values of $\eta\Pi$, this tendency is reversed.

From this point of view, $\eta\Pi$ should remain small. This can be achieved using an aggressive bit (η small) or limiting the weight on bit. The design of the BHA, in particular the position of the stabilizers and RSS, can also increase the gain (7.1); it is the case if Λ is small, that is if the RSS is close to the bit.

The switch between these two tendencies can be explained as the consequence of the competition between two processes (Fig. 7.2). The first one is dominated by the lateral force transmitted to the bit and the borehole propagates in the direction of this force (or close to this direction if $\varpi \neq 0$ but remains small); this regime is associated with small values of $\eta\Pi$. The second one is controlled by the orientation of the bit and is a consequence of the bit having a strong propensity to drill along its axis. It is thus dominated by the bit tilt and occurs for large values of $\eta\Pi$.

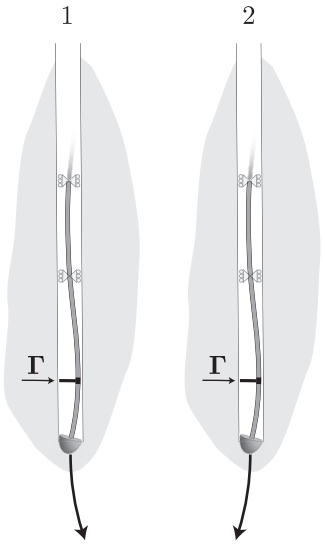

Figure 7.2: Sketches of two drilling regimes which are respectively dominated by the lateral force transmitted to the bit and the tilt of the bit.

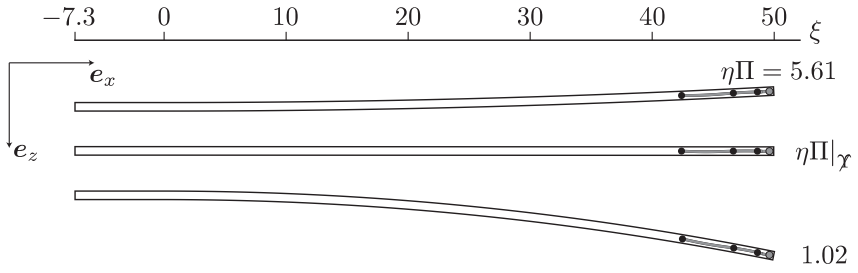

Figure 7.3: Borehole and BHA geometries for various values of Π, which are selected such that $\eta\Pi$ is smaller, equal, and larger than $\eta\Pi|_{\curlywedge}$. The borehole and BHA are initially horizontal; the simulation starts at $\xi = 0$. No force is imposed at the RSS, $\Gamma = 0$, and the other parameters are $\varkappa_2 = 2$, $\varkappa_3 = 4.285$, $\eta = 25$, $\chi = 1$, $\varpi = 0$, $\Upsilon \simeq 6.3 \times 10^{-3}$. The axis ξ is the projected length of the borehole. The borehole and BHA diameters are not up to scale and the deformation of the BHA is magnified.

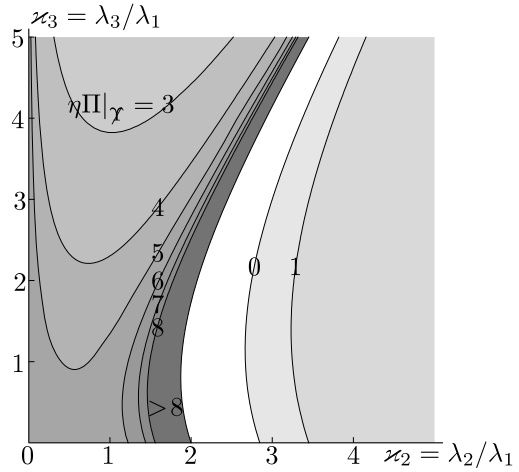

Figure 7.4: Particular value $\eta\Pi|_{\curlywedge}$ as a function of the geometry of a 3-stabilizer BHA.

7.2.2 Distributed Weight

For $\eta\Pi = \eta\Pi|_{\curlywedge}$, it was observed that the stationary solutions and long-range asymptotes are not influenced by gravity. As for the RSS force, $\eta\Pi|_{\curlywedge}$ corresponds to a change of drilling regime: for $\eta\Pi < \eta\Pi|_{\curlywedge}$ the gravity tends to decrease the borehole inclination and for $\eta\Pi > \eta\Pi|_{\curlywedge}$ it tends to increase the inclination.

Figure 7.3 illustrates this behavior. No force is imposed at the RSS and the active weight on

bit Π is varied, while all the other drilling parameters are maintained constant. The phenomena responsible for this change of behavior are similar as the ones described in Figure 7.2: for $\eta\Pi$ small, the system is force-dominated and for $\eta\Pi$ large, it is tilt-dominated.

Figure 7.4 illustrates the dependence of the geometry of a 3-stabilizer BHA defined by $\varkappa_2$ and $\varkappa_3$ on the particular value $\eta\Pi|_{\boldsymbol{\gamma}}$. For some BHA geometries, $\eta\Pi|_{\boldsymbol{\gamma}}$ is not defined (white region) and the Υ-independent case cannot be achieved.

7.2.3 Borehole Oscillations

It seems that in the majority of cases with normal drilling conditions, the system is stable. Perhaps one of the main risks of obtaining trajectory instabilities is when the axial force is not transmitted to the bit properly so that Π is abnormally small. Moreover, these risks are increased if the bit has an aggressive gauge (η small). Figure 7.5 illustrates the influence of Π on the borehole tortuosity.

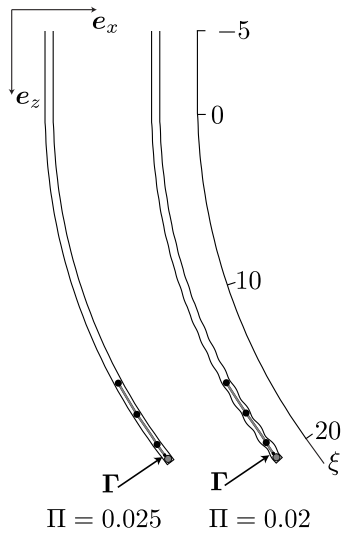

Figure 7.5: Evolution of the borehole and BHA geometry. The borehole and BHA are initially vertical; the simulation starts at $\xi = 0$. The system parameters are $\varkappa_2 = 2$, $\varkappa_3 = 2$, $\eta = 5$, $\chi = 0.1$, $\varpi = 0$, and $\Upsilon \simeq 6.3 \times 10^{-3}$. The borehole and BHA diameters are not up to scale.

7.3 Long-Range Solutions

In addition to providing orders of magnitude for the parameters of the long-range and stationary solutions, the purpose of these examples is to illustrate the influence of the particular values $\eta\Pi|_{\Upsilon}$ and $\eta\Pi|_{\chi}$ on these solutions.

We consider the same $4^3/4$" push-the-bit system as in Section 5.2 . The lateral and angular steering resistances are respectively selected to be $\eta = 25$ and $\chi = 1$ and if $G_1 = 10\,\mathrm{kN}$. The other drilling parameters are $\varkappa_2 = 2$, $\varkappa_3 = 4.285$, $\Upsilon \simeq 6.3 \times 10^{-3}$, $\Gamma_{\max} \simeq 2 \times 10^{-2}$, and $\Lambda \simeq 0.29$.

For this BHA geometry, the Γ-independent case corresponds to $\eta\Pi|_{\Upsilon} = 4.4$ (weight on bit given by $|\hat{F}_1| = 96\,\mathrm{kN}$) and the Υ-independent case to $\eta\Pi|_{\chi} = 3.1$ ($|\hat{F}_1| = 70\,\mathrm{kN}$).

The long-range and equilibrium solutions are represented in the (Γ_2, Γ_3)-space (Figs. 7.6 and 7.7). They are computed for three different magnitudes of the weight on bit:

1. $|\hat{F}_1| = 30\,\mathrm{kN}$, so that $\eta\Pi = 1.02$ and $\eta\Pi < \eta\Pi|_{\chi}$;
2. $|\hat{F}_1| = 85\,\mathrm{kN}$, so that $\eta\Pi = 3.83$ and $\eta\Pi|_{\chi} < \eta\Pi < \eta\Pi|_{\Upsilon}$;
3. $|\hat{F}_1| = 120\,\mathrm{kN}$, so that $\eta\Pi = 5.61$ and $\eta\Pi|_{\Upsilon} < \eta\Pi$.

For each value of $\eta\Pi$, the influence of the bit walk is also investigated by first considering zero bit walk ($\varpi = 0°$) and then a left walk tendency ($\varpi = -15°$).

7.3.1 Helical solutions

Helical solutions only exist in the grayed area delimited by the circle defined by $|\mathbf{\Gamma}| = \Gamma_{\max}$ and the lines corresponding to $\sin\Theta_\infty = 0$ and $\sin\Theta_\infty = 1$ (Fig. 7.6). Two helical solutions are associated with each point of this solution space: one propagating downward, $\Theta_\infty < \pi/2$, and the other one propagating upward, $\Theta_\infty > \pi/2$.

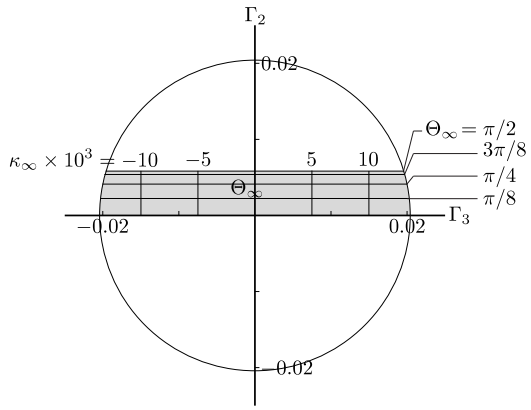

(a) $\eta\Pi = 1.02 < \eta\Pi|_{\gamma}$, $\varpi = 0°$.

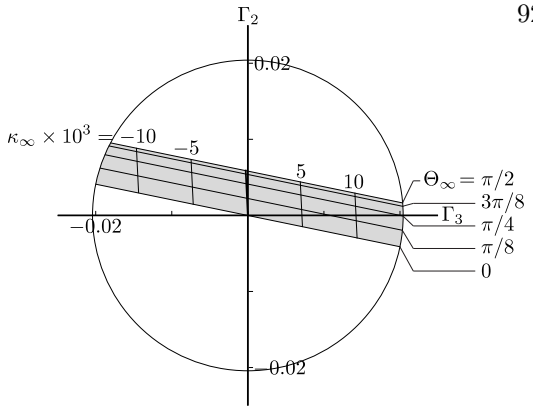

(b) $\eta\Pi = 1.02 < \eta\Pi|_{\gamma}$, $\varpi = -15°$.

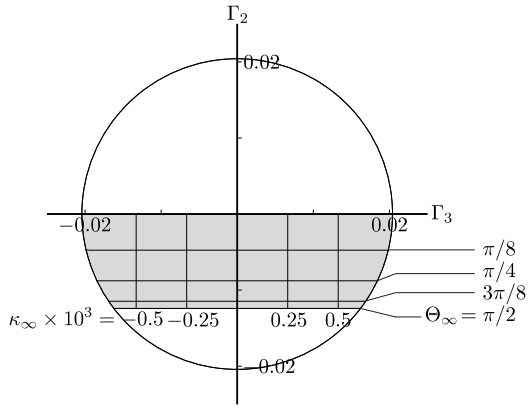

(c) $\eta\Pi|_{\gamma} < \eta\Pi = 3.83 < \eta\Pi|_{\bar{\gamma}}$, $\varpi = 0°$.

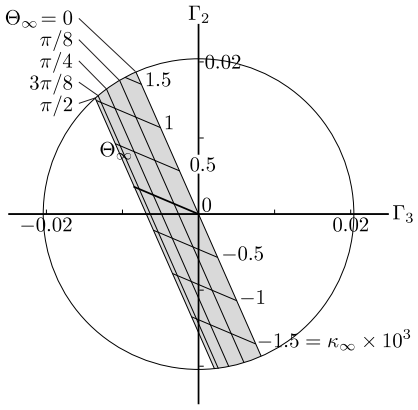

(d) $\eta\Pi|_{\gamma} < \eta\Pi = 3.83 < \eta\Pi|_{\bar{\gamma}}$, $\varpi = -15°$.

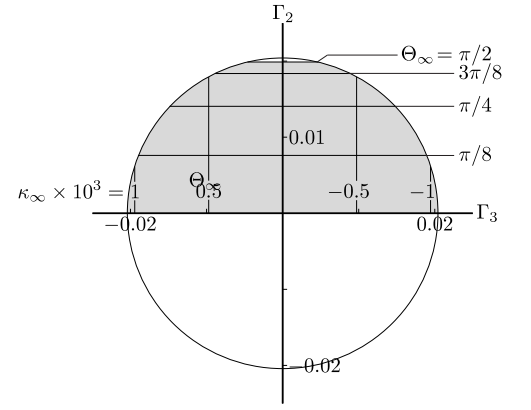

(e) $\eta\Pi = 5.61 > \eta\Pi|_{\bar{\gamma}}$, $\varpi = 0°$.

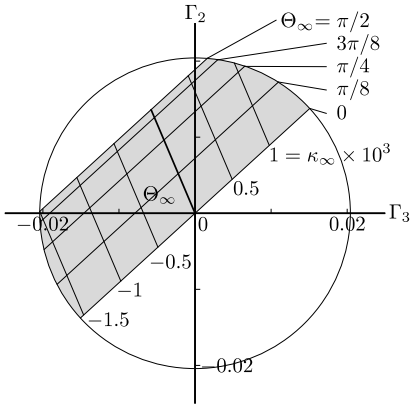

(f) $\eta\Pi = 5.61 > \eta\Pi|_{\bar{\gamma}}$, $\varpi = -15°$.

Figure 7.6: The region of helical solutions is represented in the (Γ_2, Γ_3)-space for three values of $\eta\Pi$ and for the walk angles $\varpi = 0°$ and $\varpi = -15°$. A point in this (Γ_2, Γ_3)-space represents the RSS force when looking in the direction of propagation of the borehole.

Two sets of straight lines are represented; they respectively correspond to steady-state solutions of same inclination Θ_∞ and curvature κ_∞ (the equilibrium inclination is given for the downward solutions only). When the bit has a neutral walk tendency, the lines of equal inclination are parallel to the Γ_3-axis, while the lines of equal curvature are parallel to the Γ_2-axis (Figs. 7.6a, 7.6c, and 7.6e). This is no longer the case when the bit has a tendency to walk ($\varpi \neq 0$) as the inclination and curvature now depend on both components Γ_2 and Γ_3 of the RSS force (Figs. 7.6b, 7.6d, and 7.6f).

For $\eta\Pi = 1.02 < \eta\Pi|_{\Upsilon}$ and $\varpi = 0$, steady-state solutions only exist if $\Gamma_2 > 0$, that is, if the component Γ_2 of the RSS force is directed upward (Fig. 7.6a). Also in this case, the curvature of the borehole has the same sign as Γ_3, meaning that, in the osculating plane, the borehole bends in the direction of the RSS force.

For $\eta\Pi|_{\Upsilon} < \eta\Pi = 3.83 < \eta\Pi|_{\bar{\Upsilon}}$ and $\varpi = 0$, the influence of the weight Υ on the directional drilling tendency is inverted with respect to the previous case. In order to counter this change of tendency, the sign of Γ_2 required to have steady-state changes and is negative (Fig. 7.6c).

Finally, for $\eta\Pi = 5.61 > \eta\Pi|_{\bar{\Upsilon}}$ and $\varpi = 0$, the influence of the RSS force $\mathbf{\Gamma}$ on the system is inverted and is opposite to the previous examples with $\eta\Pi < \eta\Pi|_{\bar{\Upsilon}}$. Now the system tends to propagate in a direction opposite to the RSS force. Hence, steady-state solutions exist only for $\Gamma_2 > 0$ and the sign of the curvature of the borehole is now opposite to the sign of Γ_3 (Fig. 7.6e).

The influence of the bit walk on the steady-state geometry of the borehole is significant (Figs. 7.6b, 7.6d, and 7.6f). First, the region of solutions in the (Γ_2, Γ_3)-space is affected. Second, the range of equilibrium curvatures that can be achieved changes; this is particularly evident in Figure 7.6d.

7.3.2 Long-Range Asymptotes

The long-range asymptotes are associated with a quasi-constant averaged inclination $\langle\Theta\rangle$ of the BHA. Here, this inclination is set to $\langle\Theta\rangle = 45°$. The only restriction on these solutions is that $|\mathbf{\Gamma}| \leq \Gamma_{\max}$ and a unique quasi-stationary solution is associated with each point in the circle represented in the (Γ_2, Γ_3)-space (Fig. 7.7).

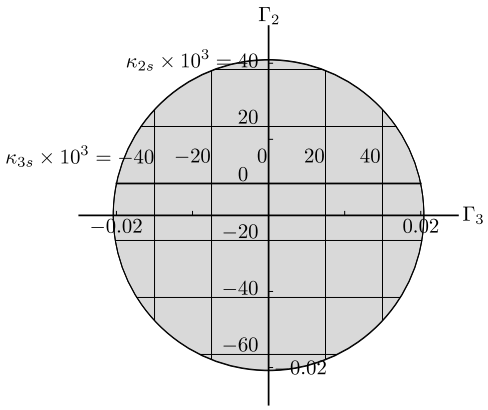

(a) $\eta\Pi = 1.02 < \eta\Pi|_{\boldsymbol{\gamma}}$, $\varpi = 0°$.

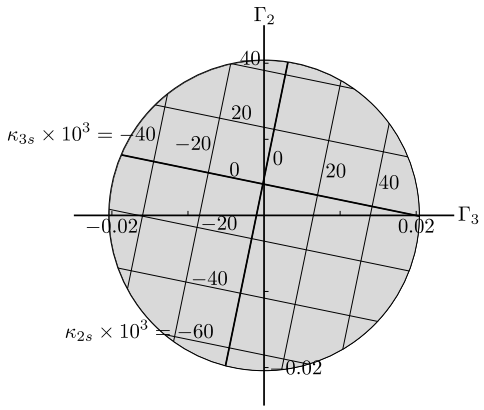

(b) $\eta\Pi = 1.02 < \eta\Pi|_{\boldsymbol{\gamma}}$, $\varpi = -15°$.

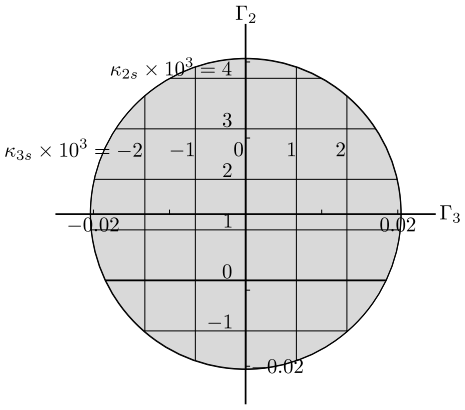

(c) $\eta\Pi|_{\boldsymbol{\gamma}} < \eta\Pi = 3.83 < \eta\Pi|_{\boldsymbol{\gamma}'}$, $\varpi = 0°$.

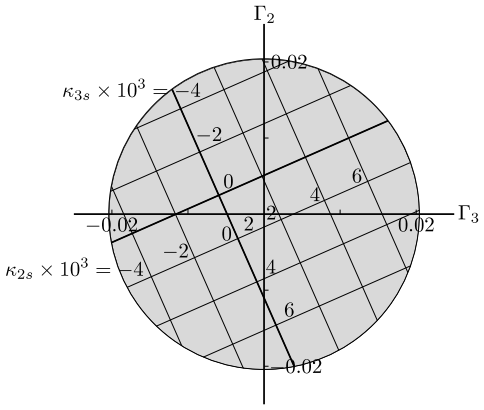

(d) $\eta\Pi|_{\boldsymbol{\gamma}} < \eta\Pi = 3.83 < \eta\Pi|_{\boldsymbol{\gamma}'}$, $\varpi = -15°$.

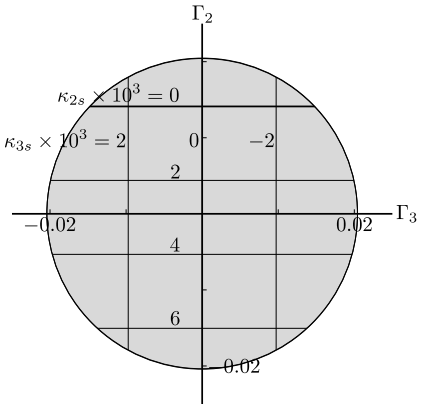

(e) $\eta\Pi = 5.61 > \eta\Pi|_{\boldsymbol{\gamma}'}$, $\varpi = 0°$.

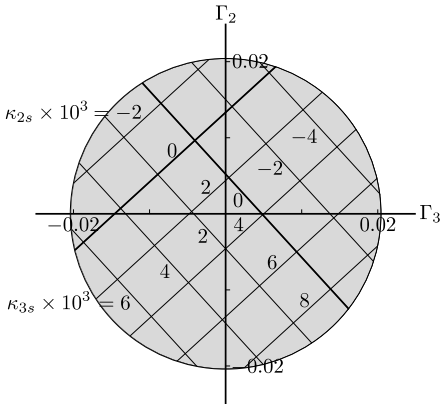

(f) $\eta\Pi = 5.61 > \eta\Pi|_{\boldsymbol{\gamma}'}$, $\varpi = -15°$.

Figure 7.7: The quasi-constant curvature solutions are represented in the (Γ_2, Γ_3)-space for three values of $\eta\Pi$ and for the walk angles $\varpi = 0°$ and $\varpi = -15°$.

As for the helical solutions, two sets of straight lines are represented corresponding to solutions of equal curvatures κ_{2s} and κ_{3s}. For a neutral walk tendency, the κ_{2s}- and κ_{3s}-lines are orthogonal to the Γ_2- and Γ_3-axes, respectively (Figs. 7.7a, 7.7c, and 7.7e). This is no longer the case when the bit has a tendency to walk (Figs. 7.7b, 7.7d, and 7.7f).

The observations made for the helical solutions are similar for the long-range solutions. The Υ-independent case, $\eta\Pi = \eta\Pi|_{\boldsymbol{\Upsilon}}$, corresponds to a switch in the influence of the weight. As a consequence, the line $\kappa_{2s} = 0$ is above the Γ_3-axis for $\eta\Pi < \eta\Pi|_{\boldsymbol{\Upsilon}}$ (Fig. 7.7a) but below the Γ_3-axis for $\eta\Pi > \eta\Pi|_{\boldsymbol{\Upsilon}}$ (Fig. 7.7c). Also, as suggested in Figures 7.7a, 7.7c, and 7.7e, the borehole is bending in the direction of the RSS force when $\eta\Pi < \eta\Pi|_{\boldsymbol{\Upsilon}}$ and $\varpi = 0$; this behavior is reversed for $\eta\Pi > \eta\Pi|_{\boldsymbol{\Upsilon}}$.

7.3.3 Comparison with Simulations

Finally, the long-range evolution are compared with the simulations from Section 5.2.4 (Fig. 7.8). The long-range asymptote perfectly matches the simulation (Fig. 7.8a). The rate of convergence of the intermediate dynamics is fast (Figs. 7.8b, 7.8c, and 7.8d). For this example, $\lambda_1 = 3.5\,\mathrm{m}$, thus, after a length of borehole of about 17.5 m, the system can be considered to evolve along the quasi-constant curvature trajectory for any practical purpose.

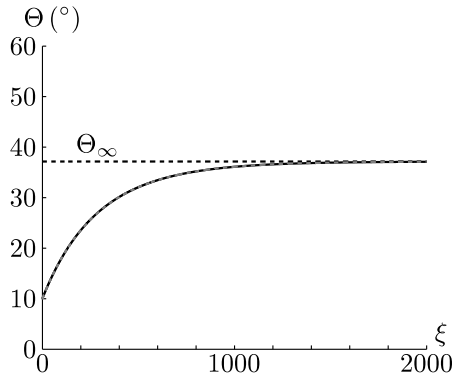

(a) Long-range evolution of the borehole inclination. The long-range asymptote overlaps the simulation.

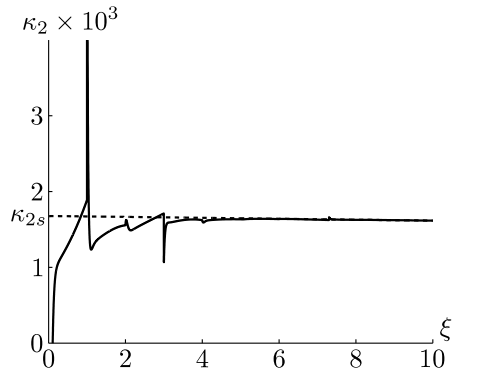

(b) Medium-range evolution of the component of the curvature in the vertical plane of the borehole.

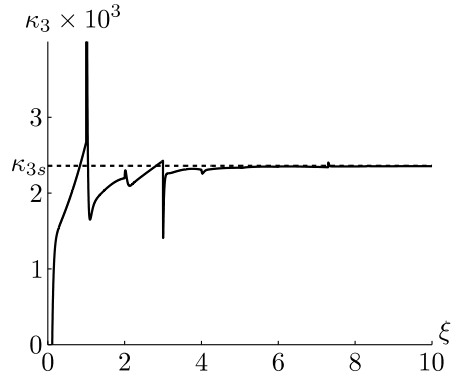

(c) Medium-range evolution of the component of the curvature in the azimuthal direction.

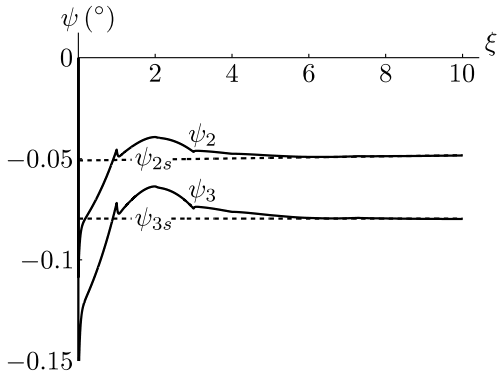

(d) Medium-range evolution of the bit tilt angles ψ_2 and ψ_3.

Figure 7.8: Comparison between the 3D simulation (solid lines) and the stationary and long-range solutions (dashed lines). The system parameters are the same as in Section 5.2; they are $\varkappa_2 = 2$, $\varkappa_3 = 4.285$, $\Lambda \simeq 0.29$, $\eta = 25$, $\chi = 1$, $\varpi = -15°$, $\Upsilon \simeq 6.3 \times 10^{-3}$, $\Pi = 4.08 \times 10^{-2}$, $\Gamma_2 = 3.54 \times 10^{-3}$, and $\Gamma_3 = 3.54 \times 10^{-3}$.

Chapter 8

Conclusions

8.1 Contributions

This research has led to the development of a dynamical model for the 3D evolution of the bit trajectory of a directional drilling system. It incorporates interface laws describing the interaction of the bit with the rock formation, a mechanical model of the BHA, and relationships relating the kinematics of the bit to the evolution of the borehole geometry.

The mathematical formulation of the model yields a set of functional differential equations. The history-dependent nature of these equations is a consequence of the delayed influence of the borehole geometry on the deformation of the BHA and thus on the bit trajectory. The model parameters reduce to the dimensionless groups $\eta\Pi$ and $\chi\Pi$, the walk angle ϖ, and geometric parameters measuring the positions of the RSS and stabilizers along the BHA.

Three length scales are identified in the response.

On the short range, the bit and borehole can experience fast variations in their orientation. This local behavior is mainly controlled by the dimensionless group $\chi\Pi$, a measure of the system resistance against a change in bit orientation. It appears that these fast variations usually occur on a length scale of the order or smaller than the model resolution, which is given by the dimensions of the bit. They can thus rather be interpreted as discontinuities in the solution.

On the medium range, the system evolution is dominated by the delayed influence of the

geometry of the borehole. In general, the transient behavior due to this secular effect quickly smooths out and the solution converges to a quasi-constant curvature borehole. This convergence occurs on a length of borehole of the order of 10 times the distance bit to first stabilizer.

The long-range behavior corresponds to a slow variation of the borehole curvature as a consequence of the nonlinear influence of the BHA weight. In some cases, the solution converges to a constant inclination and the borehole follows a helical path. Typically, the length of borehole required to reach equilibrium is of the order of 1000 times the distance between the bit and the first stabilizer.

The dimensionless group $\chi\Pi$ has been introduced to measure the resistance against a change of bit orientation. It appears that the system response is weakly influenced by this parameter. Hence, the angular steering resistance χ can generally be set to zero, except for long-gauged bits.

The dimensionless group $\eta\Pi$ depends on properties of the bit and rock formation and on characteristic parameters of the BHA. It measures the system resistance against a tilt of the bit with respect to the borehole axis. This parameter $\eta\Pi$ and the geometry of the BHA appears to be the primordial variables governing the directional response.

As $\eta\Pi$ is varied, the directional tendency changes. In particular, if $\eta\Pi$ is small, the drilling direction is dominated by the lateral force transmitted to the bit; if $\eta\Pi$ is large, it is dominated by the bit tilt. The transition between these two regimes depends on the geometry of the BHA.

Oscillations in the borehole trajectory are instigated by the retarded influence of the borehole geometry on the drilling direction. In general, they are observed to be reduced if $\eta\Pi$ is large and for flexible BHA.

8.2 Future Work

In its current state, the model can in principle be used to design a robust model-based controller for the RSS. Such a controller should aim at directing the borehole in the desired direction but also reduce the borehole tortuosity.

Some aspects of the problem have been overlooked.

The points of the BHA contacting the borehole wall were supposed to be known and located

at the bit and stabilizers. But, the stabilizers are never perfectly centered in the borehole. In fact, they are often undergauged, that is, they have a diameter slightly smaller than the bit. In this case, the stabilizers may or may not contact the borehole. Contacts can also appear along the BHA somewhere else than at a stabilizer. Moreover, the RSS uses a set of pads to push on the side of the borehole and thus was modeled as inducing a lateral force on the BHA. But in practice these pads have a limited extension. If they reach their maximum length, the imposed force condition at the RSS becomes an imposed displacement with respect to the borehole axis. Incorporating these considerations in the model of the BHA requires to solve for the contact pattern of the BHA with the borehole wall and the BHA problem becomes intrinsically nonlinear (Denoël and Detournay, 2011).

The bit/rock interaction was modeled for a bit drilling an isotropic and homogeneous rock formation and was reduced to linear relationships. Such perfect conditions are rarely met on the field. Revised interface laws can account for the rock anisotropy or for a sudden change of rock stratum. In addition, experimental investigations suggest that the bit tilt has a nonlinear influence on the interface laws, possibly due to a geometric effect of the bit gauge contacting the hole bottom (Pastusek et al., 2005).

Directional drilling data are hardly available in the literature. It seems that the industry is not keen on releasing complete results of directional drilling campaigns. Moreover, experimental investigations in a laboratory environment seems unrealistic, especially at a university. The model should thus be validated by a joint effort with the industry.

Bibliography

Aadnoy, B. S. and Andersen, K. (1998). Friction analysis for long-reach wells. In *IADC/SPE Drilling Conference*, number IADC/SPE 39391, pages 819–834, Dallas, Texas.

Aadnoy, B. S. and Huusgaard, P. P. (2002). Analytical models for design of wellpath and BHA. In *IADC/SPE Asia Pacific Drilling Technology*, number IADC/SPE 77220, pages 1–13, Jakarta, Indonesia.

Aarrestad, T. V. and Blikra, H. (1994). Torque and drag: Key factors in extended-reach drilling. In *IADC/SPE Drilling Conference*, number IADC/SPE 27491, pages 547–552, Dallas, Texas.

Almenara, J. R. and Detournay, E. (1992). Cutting experiments in sandstones with blunt PDC cutters. In *Isrm Symposium: Eurock 92*, pages 215–220. British Geotechnical Soc C/O Inst Civil Engineers, London.

Amara, M. H. (1985). Use of drillstring models and data bases for the scientific control of vertical and directional hole paths. In *SPE/IADC Drilling Conference*, number SPE/IADC 13495, New Orleans, Louisiana.

Antman, S. (2005). *Nonlinear Problems of Elasticity*, volume 107. Springer Verlag.

Bai, J. (1986). An exact solution for bottomhole assembly analysis. In *37th Annual Technical Meeting of the Petroleum Society of CIM*, Calgary, Alberta.

Barton, S., Clarke, A., Perez, D. G., and Peach, S. (2007). Unique pivot stabilizer geometry advances directional efficiency and borehole quality with a specific-rotary steerable system. In

SPE/IADC Drilling Conference, number SPE/IADC 105493, pages 1–18, Amsterdam, The Netherlands.

Bellman, R. and Cooke, K. L. (1963). *Differential-Difference Equations*, volume 6. Elsevier.

Birades, M. (1986). ORPHEE 3D: Static and dynamic tridimensional BHA computer models. In *61st Annual Technical Conference and Exhibition of the Society of Petroleum Engineers*, number SPE 15466, pages 1–12, New Orleans, Louisiana.

Birades, M. and Fenoul, R. (1986). ORPHEE 2D: A microcomputer program for prediction of bottomhole assembly trajectory. In *Symposium on Petroleum Industry Application of Microcomputers of the Society of Petroleum Engineers*, number SPE 15285, pages 31–38, Silver Creek, Colorado.

Birades, M. and Fenoul, R. (1988). A microcomputer program for prediction of bottomhole assembly trajectory. *SPE Drilling Engineering*, 3(SPE 15285):167–172.

Boualleg, R., Sellami, H., Menand, S., and Simon, C. (2006). Effect of formations anisotropy on directional tendencies of drilling systems. In *IADC/SPE Drilling Conference*, number IADC/SPE 98865, pages 1–10, Miami, Florida.

Bradley, W. B. (1975). Factors affecting the control of borehole angle in straight and directional wells. *Journal of Petroleum Technology*, 27(SPE 5070):679–688.

Brantly, J. E. (1971). *History of Oil Well Drilling*. Book Division, Gulf Publishing Company.

Brett, J. F., Gray, J. A., Bell, R. K., and Dunbar, M. E. (1986). A method of modeling the directional behavior of bottomhole assemblies including those with bent subs and downhole motors. In *IADC/SPE Drilling Conference*, number IADC/SPE 14767, pages 365–376, Dallas, Texas.

Brochure (2012). The thrill to drill. International Continental Scientific Drilling Program.

Brown, E. T., Green, S. J., and Sinha, K. P. (1981). The influence of rock anisotropy on hole deviation in rotary drilling–a review. *International Journal of Rock Mechanics and Mining Sciences*, 18(5):387–401.

Callas, N. P. (1981). Predicting borehole trajectories. *Oil & Gas Journal*, 79(34):129–133.

Callas, N. P. and Callas, R. L. (1980). Stabilizer placement–3. boundary value problem is solved. *Oil & Gas Journal*, 78(50):62–66.

Capelushnikov, M. (1930). Why holes go crooked in drilling. *World Petroleum*, pages 191–194.

Chandra, U. (1986). Basic concepts in static BHA analysis for directional drilling. In *SPE Annual Technical Conference and Exhibition*, number SPE 15467, New Orleans, Louisiana.

Cheatham, C. A. and Loeb, D. A. (1985). Effects of field wear on PDC bit performance. In *SPE/IADC Drilling Conference*, number SPE/IADC 13464, pages 359–364, New Orleans, Louisiana.

Cheatham, Jr., J. B. and Daniels, W. H. (1979). A study of factors influencing the drillability of shales: Single-cutter experiments with STRATAPAX drill blanks. *Journal of Energy Resources Technology*, 101(3):189–195.

Cheatham, Jr., J. B. and Ho, C. Y. (1981). A theoretical model for directional drilling tendency of a drill bit in anisotropic rock. Technical report, Rice University, Houston, Texas.

Chen, D. C.-K. and Wu, M. (2008). State-of-the-art BHA program produces unprecedented results. In *International Petroleum Technology Conference*, Kuala Lumpur, Malaysia.

Chen, S. L. and Geradin, M. (1993). Three dimensional modelling of PDC bit/formation interaction. Technical report, University of Liège.

Clark, D. A. and Walker, B. H. (1985). Comparison of laboratory and field data for a PDC bit. In *SPE/IADC Drilling Conference*, number SPE/IADC 13459, pages 323–330, New Orleans, Louisiana.

Close, U. (1939). More oil from crooked wells. *Scientific American*, 161(2):84–87.

Dagrain, F., Detournay, E., and Richard, T. (2001). Influence of cutter geometry in rock cutting. In *Rock Mechanics in the National Interest, Vols 1 and 2*, pages 927–933. A. A. Balkema.

Deliac, E. P. (1986). *Optimisation Des Machines D'Abattage a Pics*. PhD thesis, Université Pierre et Marie Curie, Paris, France.

Denoël, V. and Detournay, E. (2011). Eulerian formulation of constrained elastica. *International Journal of Solids and Structures*, 48(3):625–636.

Detournay, E. (2007). Mathematical model of the near-bit region of an advancing drilling system (confidential). Technical Report SLB-BM-07-1, Schlumberger.

Detournay, E. (2010). Modeling challenges in directional drilling. Keynote Lecture, 9th HSTAM Congress on Mechanics, Limassol, Cyprus.

Detournay, E. and Atkinson, C. (2000). Influence of pore pressure on the drilling response in low-permeability shear-dilatant rocks. *International Journal of Rock Mechanics and Mining Sciences*, 37(7):1091–1101.

Detournay, E. and Defourny, P. (1992). A phenomenological model for the drilling action of drag bits. *International Journal of Rock Mechanics and Mining Sciences & Geomechanics Abstracts*, 29(1):13–23.

Detournay, E. and Perneder, L. (2011). Dynamical model of a propagating borehole. In *Proceedings of the 7th EUROMECH Nonlinear Oscillations Conference (ENOC)*, Rome, Italy.

Detournay, E., Richard, T., and Shepherd, M. (2008). Drilling response of drag bits: Theory and experiment. *International Journal of Rock Mechanics and Mining Sciences*, 45(8):1347–1360.

Downton, G. C. (2007). Directional drilling system response and stability. In *16th IEEE International Conference on Control Applications*, pages 1543–1550, Singapore.

Downton, G. C., Hendricks, A., Klausen, T. S., and Pafitis, D. (2000). New directions in rotary steerable drilling. *Oilfield Review*, 12(1):18–29.

Eastman, H. J. (1937). The art of oil well surveying and controlled directional drilling. In *2nd World Petroleum Congress*, pages 933–942, Paris, France.

Engelborghs, K., Luzyanina, T., and Roose, D. (2002). Numerical bifurcation analysis of delay differential equations using DDE-BIFTOOL. *ACM Trans. Math. Softw. (TOMS)*, 28(1):1–21.

Engelborghs, K., Luzyanina, T., and Samaey, G. (2001). DDE-BIFTOOL v. 2.00: a Matlab package for bifurcation analysis of delay differential equations. Technical Report TW-330, Department of Computer Science, K.U.Leuven, Leuven, Belgium.

Ernst, S., Pastusek, P., and Lutes, P. (2007). Effects of RPM and ROP on PDC bit steerability. In *SPE/IADC Drilling Conference*, number SPE/IADC 105594, pages 1–11, Amsterdam, The Netherlands.

ExxonMobil (2011). Sakhalin-1 project drills world's longest extended-reach well (press release).

Fairhurst, C. and Lacabanne, W. D. (1957). Hard rock drilling techniques. *Mine and Quarry Engineering*, 23:157–161.

Faÿ, H. (1993). Practical evaluation of rock-bit wear while drilling. *SPE drilling & completion*, 8(2):99–104.

Fischer, F. J. (1974). Analysis of drillstring in curved boreholes. In *49th Annual Fall Meeting of the Society of Petroleum Engineers of AIME*, number SPE 5071, Houston, Texas.

Franca, L. F. P. (2010). Drilling action of roller-cone bits: Modeling and experimental validation. *Journal of Energy Resources Technology*, 132(4).

Gerbaud, L., Menand, S., and Sellami, H. (2006). PDC bits: All comes from the cutter/rock interaction. In *IADC/SPE Drilling Conference*, number IADC/SPE 98988, Miami, Florida.

Germay, C., van de Wouw, N., Nijmeijer, H., and Sepulchre, R. (2009). Nonlinear drillstring dynamics analysis. *SIAM Journal on Applied Dynamical Systems*, 8(2):527–553.

Glowka, D. A. (1989). Use of single-cutter data in the analysis of PDC bit designs: Part 1–development of a PDC cutting force model. *Journal of Petroleum Technology*, 41(8):797–799, 844–849.

Gray, K. E., Armstrong, F., and Gatlin, C. (1962). Two-dimensional study of rock breakage in drag-bit drilling at atmospheric pressure. *Journal of Petroleum Technology*, 14(1):93–98.

Gu, K., Kharitonov, V. L., and Chen, J. (2003). *Stability of Time-Delay Systems*. Birkhauser.

Hale, J. K. (1977). *Theory of Functional Differential Equations*. Applied Mathematical Sciences (vol. 3). Springer Verlag, New York.

Hinch, E. J. (1991). *Perturbation Methods*. Cambridge University Press.

Ho, H.-S. (1986). General formulation of drillstring under large deformation and its use in BHA analysis. In *SPE Annual Technical Conference and Exhibition*, number SPE 15562, New Orleans, Louisiana.

Ho, H.-S. (1987). Prediction of drilling trajectory in directional wells via a new rock-bit interaction model. In *SPE Annual Technology Conference and Exhibition*, number SPE 16658, pages 83–95, Dallas, Texas.

Ho, H.-S. (1988). An improved modeling program for computing the torque and drag in directional and deep wells. In *SPE Annual Technical Conference and Exhibition*, number SPE 18047, pages 407–418, Houston, Texas.

Ho, H.-S. (1989). *U.S. Patent No. 4,804,051.* Washington, DC: U.S. Patent and Trademark Office.

Ho, H.-S. (1995). *U.S. Patent No. 5,456,141.* Washington, DC: U.S. Patent and Trademark Office.

Ho, H.-S. (1997). *U.S. Patent No. 5,608,162.* Washington, DC: U.S. Patent and Trademark Office.

Huang, H. and Detournay, E. (2008). Intrinsic length scales in tool-rock interaction. *International Journal of Geomechanics*, 8(1):39–44.

Huang, H., Lecampion, B., and Detournay, E. (2012). Discrete element modeling of tool-rock interaction I: Rock cutting. *International Journal for Numerical and Analytical Methods in Geomechanics*.

Hughes, J. D. (1935). Value of oil-well surveying and applications of controlled directional drilling. *Drilling and Production Practice*.

Inglis, T. A. (1987). *Directional Drilling*. Petroleum Engineering and Development Studies (vol. 2). Graham & Trotman.

Jogi, P. N., Burgess, T. M., and Bowling, J. P. (1988). Predicting the build/drop tendency of rotary drilling assemblies. *SPE Drilling Engineering*, 3(2):177–186.

Kashikar, S. (2005). New frontiers in directional drilling. *Middle East & Asia Reservoir Review*, 6:24–43.

Kopey, B. (2007). Development of drilling technics from ancient ages to modern times. In *12th IFToMM World Congress*, Besançon, France.

Kou, S. Q., Lindqvist, P.-A., Tang, C. A., and Xu, X. H. (1999). Numerical simulation of the cutting of inhomogeneous rocks. *International Journal of Rock Mechanics and Mining Sciences*, 36(5):711–717.

Kozlovsky, Y. A. (1984). The world's deepest well. *Scientific American*, 251(6):98–104.

Lahee, F. H. (1929). Problem of crooked holes. *Bulletin of the American Association of Petroleum Geologists*, 13(9):1095–1162.

Lasserre, C. (1994). Rock friction apparatus: Réalisation de tests de coupe sur roches à l'aide d'un outil PDC. Technical report, Institut en Sciences et Technologies Géophysique et Géotechniques, Université Pierre et Marie Curie, Paris, France.

Liu, H. (2002). Numerical modelling of the rock fracture process under mechanical loading. Licentiate thesis, Luleå University of Technology, Luleå, Sweden.

Lubinski, A. and Woods, H. B. (1953). Factors affecting the angle of inclination and dog-legging in rotary bore holes. In *Drilling and Production Practice*, pages 222–250, Tulsa, U.S.A. American Petroleum Institute.

MacDonald, G. C. and Lubinski, A. (1951). Straight-hole drilling in crooked-hole country. In *Spring Meeting of the Mid-Continent District, Division of Production*, Amarillo, Texas.

Maouche, Z. (1999). *Contribution à l'Amélioration de la Prédiction en Inclinaison des Systèmes de Forage Rotary Couplage Garniture-Outil de Forage*. PhD thesis, Ecole Nationale Supérieure des Mines de Paris, Paris, France.

Menand, S. (2001). *Analyse et Validation d'un Modèle de Comportement Directionnel des Outils de Forage Monoblocs PDC*. PhD thesis, Ecole Nationale Supérieure des Mines de Paris.

Menand, S., Sellami, H., Simon, C., Besson, A., and Da Silva, N. (2002). How the bit profile and gages affect the well trajectory. In *IADC/SPE Drilling Conference*, number SPE 74459, Dallas, Texas.

Menand, S., Sellami, H., Tijani, M., Stab, O., Dupuis, D., and Simon, C. (2006). Advancements in 3D drillstring mechanics: From the bit to the topdrive. In *IADC/SPE Drilling Conference*, number IADC/SPE 98965, Miami, Florida.

Menand, S., Simon, C., Gaombalet, J., Macresy, L., Gerbaud, L., Ben Hamida, M., Amghar, Y., Denoix, H., Cuiller, B., and Sinardet, H. (2012). PDC bit steerability modeling and testing for push-the-bit and point-the-bit RSS. In *IADC/SPE Drilling Conference and Exhibition*, San Diego, California.

Michiels, W. and Niculescu, S.-I. (2007). *Stability and Stabilization of Time-Delay Systems: An Eigenvalue-Based Approach*. Advances in Design and Control. Society for Industrial and Applied Mathematics.

Millheim, K. K. (1977). The effect of hole curvature on the trajectory of a borehole. In *SPE Annual Fall Technical Conference and Exhibition*, number SPE 6779, Denver, Colorado.

Millheim, K. K. (1979). Behavior of multiple-stabilizer bottom-hole assemblies. *Oil and Gas Journal*, 77(1):59–64.

Millheim, K. K. (1982). Computer simulation of the directional drilling process. In *International Petroleum Exhibition and Technical Symposium*, number SPE 9990, pages 483–496, Beijing, China.

Millheim, K. K., Jordan, S., and Ritter, C. J. (1978). Bottom-hole assembly analysis using finite-element method. *Journal of Petroleum Technology*, 30(SPE 6057):265–274.

Millheim, K. K. and Warren, T. M. (1978). Side cutting characteristics of rock bits and stabilizers while drilling. In *SPE Annual Fall Technical Conference and Exhibition*, number SPE 7518, Houston, Texas.

Miska, S., Luo, F., and Chaharlang, S. (1988). A new approach to the analysis of bottom hole assembly performance. In *Eleventh Annual Energy-Source Technology Conference and Exhibit*, pages 211–220, New Orleans, Louisiana.

Moon, F. C. (2007). *The machines of Leonardo Da Vinci and Franz Reuleaux: Kinematics of Machines from the Renaissance to the 20th Century*. Springer Verlag.

Moor, W. D. (1977). Ingenuity sparks drilling history. *Oil and Gas Journal*, 75(35):159–177.

Muller, F. G. D. (1924). Much trouble caused by crooked holes. *The Oil Weekly*.

Murphey, C. E. and Cheatham, Jr., J. B. (1966). Hole deviation and drill string behavior. *Society of Petroleum Engineers Journal*, 6(SPE 1259):44–54.

Neubert, M. (1997). *Richtungsregelung beim Tiefbohren*. PhD thesis, Institut für Technische Mechanik, Technische Universität Braunschweig, Germany.

Neubert, M. and Heisig, G. (1996). Mathematical description of the directional drilling process and simulation of directional control algorithm. *Zeitschrift für angewandte Mathematik und Mechanik*, 76:361–362.

Norris, J. A., Dykstra, M. W., Beuershausen, C. C., Fincher, R. W., and Ohanian, M. P. (1998). Development and successful application of unique steerable PDC bits. In *IADC/SPE Drilling Conference*, number IADC/SPE 39308, pages 153–166, Dallas, Texas.

Palmov, V. A. and Vetyukov, Y. M. (2002). Model for the bit-rock interaction analysis. In *Fifth International Workshop on Nondestructive Testing and Computer Simulations in Science and Engineering*, volume 4627, pages 243–248.

Pastusek, P. and Brackin, V. (2003). A model for borehole oscillations. In *SPE Annual Technical Conference and Exhibition*, number SPE 84448, Denver, Colorado.

Pastusek, P., Brackin, V., and Lutes, P. (2005). A fundamental model for prediction of hole curvature and build rates with steerable bottomhole assemblies. In *SPE Annual Technical Conference and Exhibition*, number SPE 95546, Dallas, Texas.

Pastusek, P. E., Cooley, C. H., Sinor, L. A., and Anderson, M. (1992). Directional and stability characteristics of anti-whirl bits with non-axisymmetric loading. In *SPE Annual Technical Conference and Exhibition*, number SPE 24614, Washington, DC.

Perneder, L. and Detournay, E. (2013a). Equilibrium inclinations of straight boreholes. *SPE Journal, in press*, (SPE 160335).

Perneder, L. and Detournay, E. (2013b). Stability of bit trajectory in rotary drilling. *SIAM Journal of Applied Mathematics, in preparation*.

Perneder, L. and Detournay, E. (2013c). Steady-state solutions of a propagating borehole. *International Journal of Solids and Structures, in press*.

Perneder, L., Detournay, E., and Downton, G. C. (2012). Bit/rock interface laws in directional drilling. *International Journal of Rock Mechanics and Mining Sciences*, 51:81–90.

Rafie, S. (1988). Mechanistic approach in designing BHA's and forecasting wellbore position. In *IADC/SPE Drilling Conference*, number IADC/SPE 17196, pages 161–170, Dallas, Texas.

Rafie, S., Ho, H.-S., and Chandra, U. (1986). Applications of a BHA analysis program in directional drilling. In *IADC/SPE Drilling Conference*, number IADC/SPE 14765, pages 345–354, Dallas, Texas.

Rashidi, B., Hareland, G., and Nygaard, R. (2008). Real-time drill bit wear prediction by combining rock energy and drilling real-time drill bit wear prediction by combining rock energy and drilling strength concepts. In *Abu Dhabi International Petroleum Exhibition and Conference*, number SPE 117109, Abu Dhabi, UAE.

Richard, T., Germay, C., and Detournay, E. (2007). A simplified model to explore the root cause of stick-slip vibrations in drilling systems with drag bits. *Journal of Sound and Vibration*, 305(3):432–456.

Sellami, H., Fairhurst, C., Deliac, E., and Delbast, B. (1989). The role of in-situ rock stresses and mud pressure on the penetration rate of PDC bits. In *ISRM International Symposium*, pages 769–777, Pau, France.

Simon, C. (1996). *Modélisation du Comportement Directionnel des Outils de Forage Monoblocs en Formations Anisotropes*. PhD thesis, Ecole Nationale Supérieure des Mines de Paris, Paris, France.

Sinor, L. A., Powers, J. R., and Warren, T. M. (1998). The effect of PDC cutter density, back rake, size, and speed on performance. In *IADC/SPE Drilling Conference*, number IADC/SPE 39306, pages 131–139, Dallas, Texas.

Stepan, G. (1989). *Retarded Dynamical Systems: Stability and Characteristic Functions*. Longman Scientific & Technical.

Studer, R., Simon, C., Genevois, J.-M., and Menand, S. (2007). Learning curve benefits resulting from the use of a unique BHA directional behaviour drilling performances post-analysis. In *SPE Annual Technical Conference and Exhibition*, number SPE 110432, Anaheim, California.

Teale, R. (1965). The concept of specific energy in rock drilling. *International Journal of Rock Mechanics and Mining Science & Geomechanics Abstracts*, 2(1):57–73.

Voinov, O. V. and Reutov, V. A. (1991). Drill bit operation in an anisotropic rock. *Soviet Mining Science*, 27(2):138–146.

Waughman, R. J., Kenner, J. V., and Moore, R. A. (2002). Real-time specific energy monitoring reveals drilling inefficiency and enhances the understanding of when to pull worn PDC bits. In *IADC/SPE Drilling Conference*, number IADC/SPE 74520, Dallas, Texas.

Weaver, D. K. (1946). Practical aspects of directional drilling. In *Twenty-sixth Annual Meeting*, Chicago, Illinois.

Williamson, J. S. and Lubinski, A. (1986). Predicting bottomhole assembly performance. In *IADC/SPE Drilling Conference*, number SPE 14764, pages 337–341, Dallas, Texas.

Woods, H. B. and Lubinski, A. (1955). Use of stabilizers in controlling hole deviation. In *Spring Meeting of the Mid-Continent District, Division of Production*, Amarillo, Texas.

Appendix A

Interface Laws for a Cylindrical Bit

The procedure described in Section 3.3 is used to derive the bit/rock interface laws for the toy problem of a cylindrical bit of radius a and height $2b$ (Fig. A.1). The reference point of the bit is placed at the geometric center of the cylinder and the bit kinematics is limited to a planar trajectory ($d_3 = 0$ and $\varphi_2 = 0$).

The *bit face* refers to the base of the cylinder and is the set of points with cylindrical coordinates $\{(r, \omega, -b),\ 0 \leq r \leq a,\ 0 \leq \omega < 2\pi\}$. The *bit gauge* is the side of the cylinder and is defined by $\{(a, \omega, z),\ 0 \leq \omega < 2\pi,\ -b \leq z \leq b\}$. The equivalent blade can be decomposed into an equivalent blade for the bit face and another one for the bit gauge. Their properties are assumed constant on their length: λ_f, ζ_f, ζ'_f, ζ''_f, p_{f*} for the bit face and λ_g, ζ_g, ζ'_g, ζ''_g, p_{g*} for the bit gauge.

The bit is assumed to maintain a steady motion, meaning that the penetration variables d_1, d_2, and φ_3 are constant along the trajectory of the bit. Consequently, the bit tilt ψ_2 in the plane of the bit trajectory is also constant and can be approximated by $\psi_2 \simeq -d_2/d_1$ as a consequence of (3.20) and (3.21). The axial penetration d_1 is supposed to be much larger than d_2 and $a\varphi_3$, so that all the bit face penetrates the rock. The trajectories characterized by constant penetrations are straight lines if $\varphi_3 = 0$ and circular trajectories of radius $R = d/\varphi_3$ if $\varphi_3 \neq 0$. The sign of the radius is given by the sign of φ_3.

The magnitudes of the penetration parameters are such that the cutting process takes place

in Regime II on the bit face and in Regime I on the bit gauge, i.e., $p > p_{f*}$ for the face and $p < p_{g*}$ for the gauge.

The incremental normal displacement δu_n for a point of the bit face is given by

$$\delta u_n = \delta \boldsymbol{u}.\hat{\boldsymbol{i}}_1 = d_1 - r\cos\omega\varphi_3 \tag{A.1}$$

and is always positive. For the gauge, it is given by

$$\delta u_n = (d_2 - z\varphi_3)\cos\omega, \tag{A.2}$$

which can be positive or negative. Contrary to the bit face, the gauge does not interact everywhere with the rock. For a curved borehole, an outer and inner side of the gauge are naturally defined. The part of the gauge interacting with the rock depends on the tilt ψ_2 (ψ_3 is here set to zero as the trajectory of the bit is planar) and on the ratio between the bit height and the borehole radius of curvature:

$$\psi_* = 2b/R. \tag{A.3}$$

There are four interaction configurations, denoted C1-C4, which depend on the relative values of ψ_2 and ψ_* (the criteria given below assume that $\varphi_3 > 0$). These configurations are characterized by different patterns of contact between the bit gauge and the rock: C1 ($\psi_2 \geq \psi_*/2$), all of the outer side of the gauge penetrates the rock; C2 ($\psi_2 \in [0, \psi_*/2]$), both sides of the gauge are in partial contact with the rock; C3 ($\psi_2 \in [-\psi_*/2, 0]$), the inner side is partially in contact with the rock; and C4 ($\psi_2 \leq -\psi_*/2$), all of the inner side of the gauge penetrates the rock (Fig. A.2).

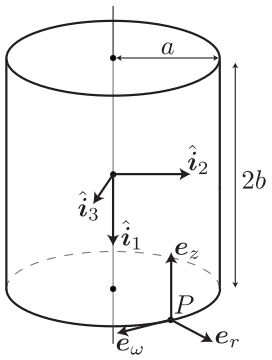

Figure A.1: A cylindrical bit with its reference point at its geometric center. Cylindrical basis $(\boldsymbol{e}_r, \boldsymbol{e}_\omega, \boldsymbol{e}_z)$ is represented at a point P of the bit.

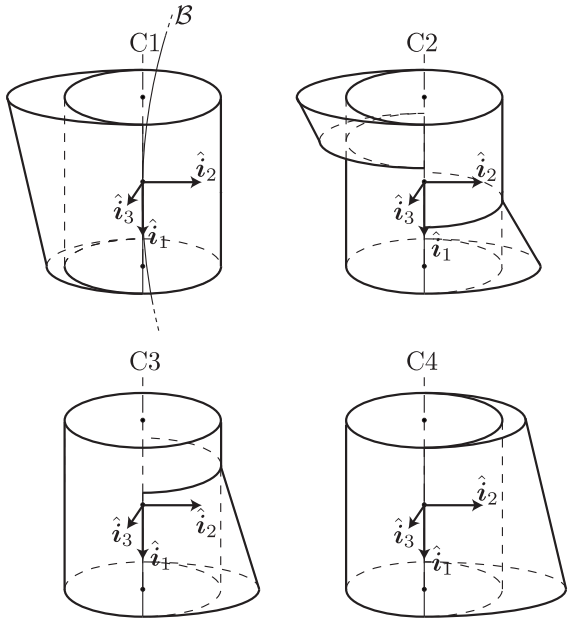

Figure A.2: Surfaces delimited by the penetration p of the bit gauge in the four interaction configurations of the gauge for the case $\varphi_3 > 0$. C1: the outer side of gauge penetrates the rock; C2: both sides of the gauge are in partial contact with the rock; C3: the inner side of the gauge is in partial contact with the rock; C4 the inner side of the gauge penetrates the rock.

The penetration p is equal to the incremental normal displacement on the interaction surfaces, while it is equal to zero elsewhere. Note that, if the trajectory is a straight line, $\psi_* = 0$ and the gauge can interact with the borehole only in the first and fourth configurations.

Once the penetration p is known everywhere on the cutting profile, the force densities f_n, f_ω given by the single cutter laws can be integrated and averaged over one revolution. Finally, the bit/rock interaction laws can be written as

$$\begin{bmatrix} \hat{F}_1/\varepsilon a^2 \\ \hat{F}_2/\varepsilon a^2 \\ \hat{F}_3/\varepsilon a^2 \\ \hat{M}_2/\varepsilon a^3 \\ \hat{M}_3/\varepsilon a^3 \end{bmatrix} = - \begin{bmatrix} \frac{\lambda_f}{a}\frac{\sigma}{\varepsilon} \\ 0 \\ 0 \\ 0 \\ 0 \end{bmatrix} - \begin{bmatrix} \zeta_f & 0 & 0 \\ 0 & \frac{1}{2}\zeta_g'\nu\Psi_1 & -\frac{1}{2}\zeta_g'\nu^2\Psi_2 \\ 0 & \frac{1}{2}\zeta_g''\nu\Psi_1 & -\frac{1}{4} - \frac{1}{2}\zeta_g''\nu^2\Psi_2 \\ 0 & \frac{1}{2}\zeta_g''\nu^2\Psi_2 & \frac{1}{4}\nu - \frac{1}{6}\zeta_g''\nu^3\Psi_3 \\ 0 & -\frac{1}{2}\zeta_g'\nu^2\Psi_2 & \frac{1}{6}\zeta_f + \frac{1}{6}\zeta_g'\nu^3\Psi_3 \end{bmatrix} \begin{bmatrix} d_1/a \\ d_2/a \\ \varphi_3 \end{bmatrix}, \tag{A.4}$$

where $\nu = b/a$ is the slenderness of the bit and Ψ_1, Ψ_2, Ψ_3 are continuous functions of the ratio ψ_2/ψ_*, which depend on the gauge/rock interaction surface configuration. For configurations

C1 and C4 (when one side of the gauge is in full contact with the rock), $\Psi_1 = \Psi_3 = 1$ and $\Psi_2 = 0$, but for configurations C2 and C3, Ψ_1, Ψ_2, Ψ_3 are given below. Always, $0 < \Psi_i \leq 1$, $i = 1, 2, 3$.

Configuration C2 ($0 \leq \psi_2 \leq \psi_*/2$, $\varphi_3 > 0$):

$$\begin{aligned}
\Psi_1 &= \frac{1}{2} + \frac{\psi_2}{\psi_*}, \\
\Psi_2 &= -\frac{1}{4}\frac{\psi_2\left(-3\psi_2 + 2\psi_*\right)}{\psi_*^2}, \\
\Psi_3 &= \frac{1}{2} + \frac{2\psi_2\left(14\psi_2^2 - 12\psi_2\psi_* + 3\psi_*^2\right)}{\psi_*^3}.
\end{aligned} \tag{A.5}$$

Configuration C3 ($-\psi_*/2 \leq \psi_2 \leq 0$, $\varphi_3 > 0$):

$$\begin{aligned}
\Psi_1 &= \frac{1}{2} - \frac{\psi_2}{\psi_*}, \\
\Psi_2 &= -\frac{1}{4} + \left(\frac{\psi_2}{\psi_*}\right)^2, \\
\Psi_3 &= \frac{1}{2} - 4\left(\frac{\psi_2}{\psi_*}\right)^3.
\end{aligned} \tag{A.6}$$

Assuming that the interaction occurs in configuration C1 or C4, the expressions for the lateral and angular steering resistances for a cylindrical bit are respectively given by

$$\begin{aligned}
\eta &= \frac{\nu}{2}\frac{\sqrt{\left(\zeta_g'\right)^2 + \left(\zeta_g''\right)^2}}{\zeta_f}, \\
\chi &= \frac{a^2}{6\lambda_1^2}\left(1 + \frac{\nu^3\zeta_g'}{\zeta_f}\right).
\end{aligned} \tag{A.7}$$

Typically, ζ_g' and ζ_g'' are one to two orders of magnitude larger than ζ_f (Detournay and Defourny, 1992; Detournay et al., 2008).

Appendix B

Upper Boundary of the BHA

The BHA model runs from the bit to the n^{th} stabilizer, which is modeled as a simple support, that is, a no moment boundary condition. The rest of the drilling structure is replaced by a torque and axial force. This appendix tries to justify this assumption by investigating the influence on the bit of a moment at this last stabilizer. It appears that if the number of stabilizers is large enough, this influence is small. On this ground, it will be argued that taking into account the first 3 or 4 stabilizers is sufficient to model the directional tendency of the system. These results also justify the no moment boundary condition at the n^{th} stabilizer.

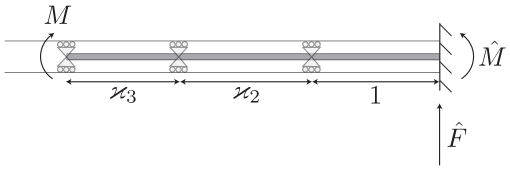

Figure B.1: Toy model of the BHA with three stabilizers.

Consider a BHA in a straight borehole with a fixed boundary condition at the bit (Fig. B.1). A moment M is imposed at the last stabilizer and the reaction moment $\hat{M}$ at the bit is computed as a function of the BHA geometry and for different numbers n of stabilizers. No other load is acting on the BHA.

For example, the simulations in Section 5.2 consider a 3-stabilizer BHA with $\varkappa_2 = 2$, $\varkappa_3 = 4.285$. In this case, $\hat{M} = -0.066M$.

The general expressions are:

- for 1 stabilizer,

$$\hat{M} = -\frac{M}{2};$$

- for 2 stabilizers,

$$\hat{M} = \frac{\varkappa_2}{3 + 4\varkappa_2} M;$$

- for 3 stabilizers,

$$\hat{M} = -\frac{\varkappa_2 \varkappa_3}{6\varkappa_2^2 + (8\varkappa_3 + 6)\,\varkappa_2 + 6\varkappa_3} M;$$

- for 4 stabilizers,

$$\hat{M} = \frac{\varkappa_2 \varkappa_3 \varkappa_4}{12\,(\varkappa_3 + \varkappa_4)\,\varkappa_2^2 + 4\left[3\varkappa_3^2 + (4\varkappa_4 + 3)\,\varkappa_3 + 3\varkappa_4\right]\varkappa_2 + 3\varkappa_3\,(3\varkappa_3 + 4\varkappa_4)} M.$$

Appendix C

Influence Coefficients

The influence coefficients $\mathcal{F}$ and $\mathcal{M}$ depend only on the geometry of the BHA, i.e., on the n parameters Λ and $\varkappa_i = \lambda_i/\lambda_1$, $i = 2, \ldots, n$. They are given in (C.1), (C.2), and (C.3) for BHA with 1, 2, and 3 stabilizers, respectively. Some of these coefficients always have the same sign independently of the geometry of the BHA,

$$\begin{array}{llll} \mathcal{F}_b \leq -1, & \mathcal{F}_r < 0, & \mathcal{F}_1 > 0, & \mathcal{F}_2 < 0, \\ \mathcal{M}_b \geq 1, & \mathcal{M}_r > 0, & \mathcal{M}_1 < 0, & \mathcal{M}_2 > 0. \end{array}$$

1-stabilizer BHA

$$\begin{aligned} \mathcal{F}_b &= -1, \\ \mathcal{F}_w &= \frac{5}{8}, \\ \mathcal{F}_r &= -\frac{2 - 3\Lambda^2 + \Lambda^3}{2}, \\ \mathcal{M}_b &= 1, \\ \mathcal{M}_w &= -\frac{1}{8}, \\ \mathcal{M}_r &= \frac{\Lambda\left(2 - 3\Lambda + \Lambda^2\right)}{2}. \end{aligned} \tag{C.1}$$

2-stabilizer BHA

$$
\begin{aligned}
\mathcal{F}_b &= -\frac{6+4\varkappa_2}{3+4\varkappa_2},\\
\mathcal{F}_w &= \frac{6+10\varkappa_2-3\varkappa_2^3}{12+16\varkappa_2},\\
\mathcal{F}_r &= \frac{-3-4\varkappa_2+\Lambda^2\left(9+6\varkappa_2\right)-2\Lambda^3\left(3+\varkappa_2\right)}{3+4\varkappa_2},\\
\mathcal{F}_1 &= \frac{6}{3+4\varkappa_2},\\
\mathcal{M}_b &= \frac{4\left(1+\varkappa_2\right)}{3+4\varkappa_2},\\
\mathcal{M}_w &= \frac{-1-2\varkappa_2+\varkappa_2^3}{12+16\varkappa_2},\\
\mathcal{M}_r &= \frac{\Lambda\left(1-\Lambda\right)\left[3+4\varkappa_2-\Lambda\left(3+2\varkappa_2\right)\right]}{3+4\varkappa_2},\\
\mathcal{M}_1 &= -\frac{2}{3+4\varkappa_2}.
\end{aligned}
\tag{C.2}
$$

3-stabilizer BHA

$$
\begin{aligned}
\mathcal{F}_b &= -\frac{6\varkappa_3+\left(6+4\varkappa_3\right)\varkappa_2+3\varkappa_2^2}{3\varkappa_3+\left(3+4\varkappa_3\right)\varkappa_2+3\varkappa_2^2},\\
\mathcal{F}_w &= \frac{12\varkappa_3+\left(12+20\varkappa_3+3\varkappa_3^3\right)\varkappa_2+15\varkappa_2^2-6\varkappa_3\varkappa_2^3-3\varkappa_2^4}{8\left[3\varkappa_3+\left(3+4\varkappa_3\right)\varkappa_2+3\varkappa_2^2\right]},\\
\mathcal{F}_r &= \left(1-\Lambda\right)\left[6\left(-1-\Lambda+2\Lambda^2\right)\varkappa_3\right.\\
&\quad +2\left(-3-4\varkappa_3-\Lambda\left(3+4\varkappa_3\right)+2\Lambda^2\left(3+\varkappa_3\right)\right)\varkappa_2\\
&\quad \left.+3\left(-2-2\Lambda+\Lambda^2\right)\varkappa_2^2\right]\\
&\quad /\left[6\varkappa_3+\left(6+8\varkappa_3\right)\varkappa_2+6\varkappa_2^2\right],\\
\mathcal{F}_1 &= \frac{6\left(\varkappa_2+\varkappa_3\right)}{3\varkappa_3+\left(3+4\varkappa_3\right)\varkappa_2+3\varkappa_2^2},\\
\mathcal{F}_2 &= -\frac{3\varkappa_2}{3\varkappa_3+\left(3+4\varkappa_3\right)\varkappa_2+3\varkappa_2^2},
\end{aligned}
$$

$$
\begin{aligned}
\mathcal{M}_b &= \frac{4\varkappa_3 + 4\left(1+\varkappa_3\right)\varkappa_2 + 3\varkappa_2^2}{3\varkappa_3 + \left(3+4\varkappa_3\right)\varkappa_2 + 3\varkappa_2^2}, \\
\mathcal{M}_w &= \left[-2\varkappa_3 - \left(2+4\varkappa_3+\varkappa_3^3\right)\varkappa_2\right. \\
&\quad \left. -3\varkappa_2^2 + 2\varkappa_3\varkappa_2^3 + \varkappa_2^4\right] \\
&\quad /8\left[3\varkappa_3 + \left(3+4\varkappa_3\right)\varkappa_2 + 3\varkappa_2^2\right], \\
\mathcal{M}_r &= -\Lambda\left(1-\Lambda\right)\left[-6\left(1-\Lambda\right)\varkappa_3 - 3\left(2-\Lambda\right)\varkappa_2^2\right. \\
&\quad \left. -\left(6+8\varkappa_3-\left(6+4\varkappa_3\right)\Lambda\right)\varkappa_2\right] \\
&\quad /\left[6\varkappa_3 + \left(6+8\varkappa_3\right)\varkappa_2 + 6\varkappa_2^2\right], \\
\mathcal{M}_1 &= -\frac{2\left(\varkappa_2+\varkappa_3\right)}{3\varkappa_3 + \left(3+4\varkappa_3\right)\varkappa_2 + 3\varkappa_2^2}, \\
\mathcal{M}_2 &= \frac{\varkappa_2}{3\varkappa_3 + \left(3+4\varkappa_3\right)\varkappa_2 + 3\varkappa_2^2}.
\end{aligned} \tag{C.3}
$$

Influence Coefficients for the Borehole Curvature

For a 1-stabilizer BHA,

$$
\begin{aligned}
\mathcal{F}_\kappa &= -\frac{1}{2}, \\
\mathcal{M}_\kappa &= \frac{1}{2}.
\end{aligned} \tag{C.4}
$$

For a 2-stabilizer BHA,

$$
\begin{aligned}
\mathcal{F}_\kappa &= \frac{\varkappa_2}{3+4\varkappa_2}, \\
\mathcal{M}_\kappa &= \frac{1+\varkappa_2}{3+4\varkappa_2}.
\end{aligned} \tag{C.5}
$$

For a 3-stabilizer BHA,

$$
\begin{aligned}
\mathcal{F}_\kappa &= -\frac{\varkappa_2\varkappa_3}{6\varkappa_3 + \left(8\varkappa_3+6\right)\varkappa_2 + 6\varkappa_2^2}, \\
\mathcal{M}_\kappa &= \frac{2\varkappa_3 + \left(3\varkappa_3+2\right)\varkappa_2 + 2\varkappa_2^2}{6\varkappa_3 + \left(8\varkappa_3+6\right)\varkappa_2 + 6\varkappa_2^2}.
\end{aligned} \tag{C.6}
$$

As for the other coefficients $\mathcal{F}$ and $\mathcal{M}$, they depend only on the geometry of the BHA. The coefficient $\mathcal{M}_\kappa$ is always positive. The coefficient $\mathcal{F}_\kappa$ changes sign for every additional stabilizer: for a BHA with one stabilizer it is negative, for 2 stabilizers it is positive, and so on.

Appendix D

Bit Forces in Two Different Bases

On the one hand, the bit force $\hat{\boldsymbol{F}}$ is decomposed in the bit basis $\left(\hat{\boldsymbol{i}}_1, \hat{\boldsymbol{i}}_2, \hat{\boldsymbol{i}}_3\right)$ when deriving the bit/rock interface laws (3.17). In this basis, its components are denoted $\hat{F}_1$, $\hat{F}_2$, $\hat{F}_3$. On the other hand, the model of the BHA decomposes $\hat{\boldsymbol{F}}$ with respect to the chord $\mathcal{C}_1$ defining the undeformed configuration of the BHA (Fig. 3.7). This second set of components is different than the first one and is denoted $\hat{F}_1^{\mathcal{C}}$, $\hat{F}_2^{\mathcal{C}}$, $\hat{F}_3^{\mathcal{C}}$.

The relation between these different sets of forces is derived for a borehole evolving in a vertical plane. The generalization to the 3D case follows the same derivation. The angle between the bit principal axis $\hat{\boldsymbol{i}}_1$ and the chord $\mathcal{C}_1$ is $\hat{\theta} - \langle\Theta\rangle_1$ (Fig. D.1). Hence,

$$\left\{ \begin{array}{c} \hat{F}_1^{\mathcal{C}} \\ \hat{F}_2^{\mathcal{C}} \end{array} \right\} = \left[\begin{array}{cc} \cos\left(\hat{\theta} - \langle\Theta\rangle_1\right) & -\sin\left(\hat{\theta} - \langle\Theta\rangle_1\right) \\ \sin\left(\hat{\theta} - \langle\Theta\rangle_1\right) & \cos\left(\hat{\theta} - \langle\Theta\rangle_1\right) \end{array} \right] \left\{ \begin{array}{c} \hat{F}_1 \\ \hat{F}_2 \end{array} \right\}. \tag{D.1}$$

These expressions are further simplified after considering that $\hat{\theta} - \langle\Theta\rangle_1$ is always a small angle and $\hat{F}_1 \gg \hat{F}_2$, so that

$$\begin{aligned} \hat{F}_1^{\mathcal{C}} &= \hat{F}_1, \\ \hat{F}_2^{\mathcal{C}} &= \hat{F}_2 + \left(\hat{\theta} - \langle\Theta\rangle_1\right) \hat{F}_1. \end{aligned} \tag{D.2}$$

Taking this last expression into consideration does not change the nature of the evolution equations. For a borehole constrained to propagate in a vertical plane with $\varpi = 0$, the borehole

inclination is then governed by

$$\begin{aligned}\chi\Pi\Theta'(\xi) = &-\mathcal{M}_b\left[\Theta(\xi) - \langle\Theta\rangle_1\right] + \frac{\chi}{\eta}\left(\mathcal{F}_b - \Pi_t\right)\left[\Theta(\xi) - \Theta(\xi-1)\right] \\ &+ \sum_{i=1}^{n-1}\left[\frac{\mathcal{F}_b\mathcal{M}_i - \mathcal{F}_i\mathcal{M}_b - \mathcal{M}_i\eta\Pi - \mathcal{M}_i\Pi_t}{\eta\Pi}\right]\left(\langle\Theta\rangle_i - \langle\Theta\rangle_{i+1}\right) \\ &- \frac{\chi}{\eta}\sum_{i=1}^{n-1}\mathcal{F}_i\left(\frac{\Theta(\xi_{i-1}) - \Theta(\xi_i)}{\varkappa_i} - \frac{\Theta(\xi_i) - \Theta(\xi_{i+1})}{\varkappa_{i+1}}\right) \\ &+ \frac{\mathcal{F}_b\mathcal{M}_w - \mathcal{F}_w\mathcal{M}_b - \mathcal{M}_w\eta\Pi - \mathcal{M}_w\Pi_t}{\eta\Pi}\Upsilon\sin\langle\Theta\rangle_1 \\ &- \frac{\chi}{\eta}\mathcal{F}_w\Upsilon\left[\Theta(\xi) - \Theta(\xi_1)\right]\cos\langle\Theta\rangle_1 \\ &+ \frac{\mathcal{F}_b\mathcal{M}_r - \mathcal{F}_r\mathcal{M}_b - \mathcal{M}_r\eta\Pi - \mathcal{M}_r\Pi_t}{\eta\Pi}\Gamma_2 - \frac{\chi}{\eta}\mathcal{F}_r\Gamma_2', \end{aligned} \tag{D.3}$$

which is similar to (4.12). The total scaled weight on bit Π_t is given by $\Pi_t = -\hat{F}_1/F_*$. As for Π, it is of the order of $O(10^{-2})$, and unless η is small, it appears not to have a strong influence on the borehole evolution.

The same procedure can be extended to the 3D model or to the moment $\hat{\boldsymbol{M}}$ and torque $\hat{\boldsymbol{C}}$ on the bit.

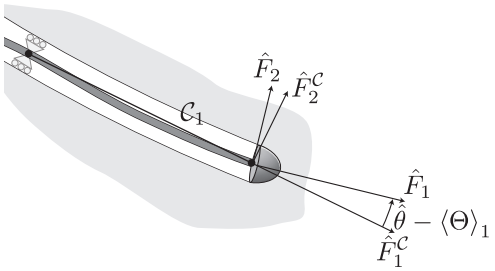

Figure D.1: Components of the bit force $\hat{\boldsymbol{F}}$ with respect to the bit basis and to the chord $\mathcal{C}_1$.

Appendix E

Coefficients for the Long-Range and Equilibrium Solutions

E.1 Long-Range Asymptotes

In the expression (6.10), the coefficients $\mathcal{S}$ of the steady-state parameters are given by

$$
\begin{aligned}
\mathcal{S}_{\Gamma_2}^{\kappa_2} = &\left\{-\mathcal{M}_r\left[-\mathcal{F}_b\mathcal{M}_b\mathcal{F}_\kappa + \mathcal{F}_b^2\left(\mathcal{M}_\kappa + \chi\Pi\right) + \eta\Pi^2\left(\mathcal{M}_\kappa + \chi\Pi\right)\right]\right. \\
&+ \mathcal{M}_b\mathcal{F}_r\left[\mathcal{F}_b\mathcal{M}_\kappa - \mathcal{F}_\kappa\mathcal{M}_b + \mathcal{F}_b\chi\Pi\right] \\
&\left.-\eta\Pi\left[\mathcal{M}_b\mathcal{M}_r\mathcal{F}_\kappa + \left(\mathcal{M}_b\mathcal{F}_r - 2\mathcal{F}_b\mathcal{M}_r\right)\left(\mathcal{M}_\kappa + \chi\Pi\right)\right]\cos\varpi\right\}/\mathcal{R}, \\
\mathcal{S}_{\Gamma_3}^{\kappa_2} = &\frac{\eta\Pi\mathcal{M}_b\left(\mathcal{F}_r\mathcal{M}_\kappa - \mathcal{F}_\kappa\mathcal{M}_r + \mathcal{F}_r\chi\Pi\right)\sin\varpi}{\mathcal{R}}, \\
\mathcal{S}_{\Upsilon}^{\kappa_2} = &\left\{-\mathcal{M}_w\left[-\mathcal{F}_b\mathcal{M}_b\mathcal{F}_\kappa + \mathcal{F}_b^2\left(\mathcal{M}_\kappa + \chi\Pi\right) + \eta\Pi^2\left(\mathcal{M}_\kappa + \chi\Pi\right)\right]\right. \\
&+ \mathcal{M}_b\mathcal{F}_w\left[\mathcal{F}_b\mathcal{M}_\kappa - \mathcal{F}_\kappa\mathcal{M}_b + \mathcal{F}_b\chi\Pi\right] \\
&\left.-\eta\Pi\left[\mathcal{M}_b\mathcal{M}_w\mathcal{F}_\kappa + \left(\mathcal{M}_b\mathcal{F}_w - 2\mathcal{F}_b\mathcal{M}_w\right)\left(\mathcal{M}_\kappa + \chi\Pi\right)\right]\cos\varpi\right\}/\mathcal{R},
\end{aligned}
$$

$$
\begin{aligned}
\mathcal{S}^{\psi_2}_{\Gamma_2} &= -\left(\mathcal{F}_\kappa\mathcal{M}_r - \mathcal{F}_r\mathcal{M}_\kappa - \mathcal{F}_r\chi\Pi\right)\left[\mathcal{F}_\kappa\mathcal{M}_b - \mathcal{F}_b\mathcal{M}_\kappa - \mathcal{F}_b\chi\Pi + \eta\Pi\left(\mathcal{M}_\kappa + \chi\Pi\right)\cos\varpi\right]/\mathcal{R},\\
\mathcal{S}^{\psi_2}_{\Gamma_3} &= -\frac{\eta\Pi\left(\mathcal{M}_\kappa + \chi\Pi\right)\left(\mathcal{F}_r\mathcal{M}_\kappa - \mathcal{F}_\kappa\mathcal{M}_r + \mathcal{F}_r\chi\Pi\right)\sin\varpi}{\mathcal{R}},\\
\mathcal{S}^{\psi_2}_{\Upsilon} &= -\left(\mathcal{F}_\kappa\mathcal{M}_w - \mathcal{F}_w\mathcal{M}_\kappa - \mathcal{F}_w\chi\Pi\right)\left[\mathcal{F}_\kappa\mathcal{M}_b - \mathcal{F}_b\mathcal{M}_\kappa - \mathcal{F}_b\chi\Pi + \eta\Pi\left(\mathcal{M}_\kappa + \chi\Pi\right)\cos\varpi\right]/\mathcal{R},\\
\mathcal{S}^{\kappa_3}_{\Gamma_3} &= \mathcal{S}^{\kappa_3}_{\Gamma_2},\\
\mathcal{S}^{\kappa_3}_{\Gamma_2} &= -\mathcal{S}^{\kappa_3}_{\Gamma_3},\\
\mathcal{S}^{\kappa_3}_{\Upsilon} &= \frac{\eta\Pi\mathcal{M}_b\left(\mathcal{F}_\kappa\mathcal{M}_w - \mathcal{F}_w\mathcal{M}_\kappa - \mathcal{F}_w\chi\Pi\right)\sin\varpi}{\mathcal{R}},\\
\mathcal{S}^{\psi_3}_{\Gamma_3} &= \mathcal{S}^{\psi_2}_{\Gamma_2},\\
\mathcal{S}^{\psi_3}_{\Gamma_2} &= -\mathcal{S}^{\psi_2}_{\Gamma_3},\\
\mathcal{S}^{\psi_3}_{\Upsilon} &= \frac{\eta\Pi\left(\mathcal{M}_\kappa + \chi\Pi\right)\left(\mathcal{F}_w\mathcal{M}_\kappa - \mathcal{F}_\kappa\mathcal{M}_w + \mathcal{F}_w\chi\Pi\right)\sin\varpi}{\mathcal{R}},
\end{aligned}
\tag{E.1}
$$

where the denominator is given by

$$
\begin{aligned}
\mathcal{R} = &\left(\mathcal{F}_b^2 + \eta\Pi^2\right)\left(\mathcal{M}_\kappa + \chi\Pi\right)^2 - 2\mathcal{F}_b\mathcal{M}_b\mathcal{F}_\kappa\left(\mathcal{M}_\kappa + \chi\Pi\right) + \mathcal{M}_b^2\mathcal{F}_\kappa^2\\
&- 2\eta\Pi\left(\mathcal{M}_\kappa + \chi\Pi\right)\left(\mathcal{F}_b\mathcal{M}_\kappa - \mathcal{F}_\kappa\mathcal{M}_b + \mathcal{F}_b\chi\Pi\right)\cos\varpi.
\end{aligned}
\tag{E.2}
$$

E.2 Equilibrium Solutions

The coefficients $\mathcal{S}$, in the general expression (6.12) of the steady-state parameters, are given by

$$
\begin{aligned}
\mathcal{Q}^{\Theta}_1 &= -\frac{\left(\mathcal{F}_r\mathcal{M}_b - \mathcal{F}_b\mathcal{M}_r + \mathcal{M}_r\eta\Pi\right)\left[\mathcal{F}_\kappa\mathcal{M}_b - \left(\mathcal{F}_b - \eta\Pi\right)\left(\mathcal{M}_\kappa + \chi\Pi\right)\right]}{\mathcal{R}},\\
\mathcal{Q}^{\Theta}_2 &= \frac{\eta\Pi\left[\mathcal{F}_\kappa\mathcal{M}_b\mathcal{M}_r + \left(\mathcal{F}_r\mathcal{M}_b - 2\mathcal{F}_b\mathcal{M}_r\right)\left(\mathcal{M}_\kappa + \chi\Pi\right)\right]}{\mathcal{R}},\\
\mathcal{Q}^{\Theta}_3 &= \frac{\eta\Pi\mathcal{M}_b\left(\mathcal{F}_r\mathcal{M}_\kappa - \mathcal{F}_\kappa\mathcal{M}_r + \mathcal{F}_r\chi\Pi\right)}{\mathcal{R}},\\
\mathcal{Q}^{\psi_2}_1 &= \frac{\left(\mathcal{F}_r\mathcal{M}_w - \mathcal{F}_w\mathcal{M}_r\right)\left[\mathcal{F}_\kappa\mathcal{M}_b - \left(\mathcal{F}_b - \eta\Pi\right)\left(\mathcal{M}_\kappa + \chi\Pi\right)\right]}{\mathcal{R}},\\
\mathcal{Q}^{\psi_2}_2 &= -\frac{\eta\Pi\left(\mathcal{F}_r\mathcal{M}_w - \mathcal{F}_w\mathcal{M}_r\right)\left(\mathcal{M}_\kappa + \chi\Pi\right)}{\mathcal{R}},\\
\mathcal{Q}^{\psi_2}_3 &= -\frac{\eta\Pi\mathcal{M}_w\left(\mathcal{F}_r\mathcal{M}_\kappa - \mathcal{F}_\kappa\mathcal{M}_r + \mathcal{F}_r\chi\Pi\right)}{\mathcal{R}},
\end{aligned}
$$

$$
\begin{aligned}
\mathcal{Q}_1^{\kappa} &= -\frac{\left(\mathcal{F}_r\mathcal{M}_b - \mathcal{F}_b\mathcal{M}_r + \mathcal{M}_r\eta\Pi\right)\left(\mathcal{F}_w\mathcal{M}_b - \mathcal{F}_b\mathcal{M}_w + \mathcal{M}_w\eta\Pi\right)}{\mathcal{R}},\\
\mathcal{Q}_2^{\kappa} &= \frac{\eta\Pi\left(\mathcal{F}_r\mathcal{M}_b\mathcal{M}_w + \mathcal{F}_w\mathcal{M}_b\mathcal{M}_r - 2\mathcal{F}_b\mathcal{M}_r\mathcal{M}_w\right)}{\mathcal{R}},\\
\mathcal{Q}_3^{\kappa} &= -\frac{\eta\Pi\mathcal{M}_b\left(\mathcal{F}_r\mathcal{M}_w - \mathcal{F}_w\mathcal{M}_r\right)}{\mathcal{R}},\\
\mathcal{Q}_1^{\psi_3} &= \frac{\left(\mathcal{F}_w\mathcal{M}_b - \mathcal{F}_b\mathcal{M}_w + \mathcal{M}_w\eta\Pi\right)\left(\mathcal{F}_r\mathcal{M}_\kappa - \mathcal{F}_\kappa\mathcal{M}_r + \mathcal{F}_r\chi\Pi\right)}{\mathcal{R}},\\
\mathcal{Q}_2^{\psi_3} &= -\frac{\eta\Pi\mathcal{M}_w\left(\mathcal{F}_r\mathcal{M}_\kappa - \mathcal{F}_\kappa\mathcal{M}_r + \mathcal{F}_r\chi\Pi\right)}{\mathcal{R}},\\
\mathcal{Q}_3^{\psi_3} &= \frac{\eta\Pi\left(\mathcal{M}_\kappa + \chi\Pi\right)\left(\mathcal{F}_r\mathcal{M}_w - \mathcal{F}_w\mathcal{M}_r\right)}{\mathcal{R}},
\end{aligned}
\tag{E.3}
$$

where the denominator is given by

$$
\begin{aligned}
\mathcal{R} = &\left(\mathcal{F}_w\mathcal{M}_b - \mathcal{F}_b\mathcal{M}_w + \mathcal{M}_w\eta\Pi\right)\left[\mathcal{F}_\kappa\mathcal{M}_b - \left(\mathcal{F}_b - \eta\Pi\right)\left(\mathcal{M}_\kappa + \chi\Pi\right)\right]\\
&- \eta\Pi\left[\mathcal{F}_\kappa\mathcal{M}_b\mathcal{M}_w + \left(\mathcal{F}_w\mathcal{M}_b - 2\mathcal{F}_b\mathcal{M}_w\right)\left(\mathcal{M}_\kappa + \chi\Pi\right)\right]\left(1 - \cos\varpi\right).
\end{aligned}
\tag{E.4}
$$